You may also like:

SERS-Based Advanced Diagnostics for Infectious Diseases

Artificial Intelligence and Spectroscopic Techniques for Gemology Applications

International Organizing Committee of the FAPM-2019:

Part III

Appendices

Appendix A

Review of angular momentum commutators

The customary starting point for the quantum theory of angular momentum is the commutation formula for the Cartesian components of the angular momentum operator $\mathbf{J}$,

$$\mathbf{J}_i\mathbf{J}_j - \mathbf{J}_j\mathbf{J}_i = i\varepsilon_{ijk}\mathbf{J}_k \tag{A.1}$$

where

$$\varepsilon_{ijk} = \begin{cases} +1 & i, j, k \text{ in cyclic order} \\ -1 & i, j, k \text{ not in cyclic order} \\ 0 & \text{if any indices equal} \end{cases} \tag{A.2}$$

The above commutator property usually defines the angular momentum operator. Coordinate transformations leave the angular momentum operator definition invariant. The conservation law for angular momentum is fundamental. The definition of angular momentum, equation (A.1), is, of course, invariant under specifically spatial translations and rotations. Furthermore, equation (A.1) is invariant under coordinate inversion and time reversal.

Van Vleck's reversed angular momentum method starts with equation (A.1) but then utilizes change of sign of i for angular momentum when a transformation of coordinates to a system attached to a rotating molecule is made,

$$\mathbf{J}_{i'}\mathbf{J}_{j'} - \mathbf{J}_{j'}\mathbf{J}_{i'} = -i\varepsilon_{i'j'k'}\mathbf{J}_{k'}. \tag{A.3}$$

Here, the primed index denotes a rotated coordinate. This equation containing the reversed sign of i is known as Klein's [1] anomalous commutation formula.

Two approaches are debated in this book, namely an operator and an algebraic approach [2], without utilizing Klein's anomalous commutation formula. Each approach begins with the standard commutator formula (equation (A.1)). The operator approach is included in the text, the algebraic approach is discussed in detail in this appendix. In principle, equation (A.3) can be utilized in building angular momentum theory. However, in analogy to the distinction between

right- and left-handed coordinate systems, different signs occur. We only use the *standard* sign as indicated in equation (A.1) in computation of a molecular diatomic spectrum [3], i.e., without resorting to use of Klein's anomaly and Van Vleck's reversed angular momentum method.

Here, the reversal of the sign in equation (A.1) is briefly investigated for a unitary and an anti-unitary transformation. The Euler rotation matrix is a real, unitary matrix (see equation (A.5)). The determinate of the Euler rotation matrix is +1 meaning that the sign of vectors is preserved under rotations. A spatial rotation of coordinates is a proper transformation. Conversely, the inversion or parity operator constitutes an improper rotation—this transformation cannot be described exclusively in terms of the Euler angles. However, angular momentum is a pseudo or axial vector, preserving the sign of $\mathbf{J}$ under improper rotations. The parity operator is also unitary and equation (A.1) is preserved by the parity operator. Time reversal (time inversion or reversal of motion) changes the sign of $\mathbf{J}$ and it complex-conjugates the imaginary unit due to time reversal being anti-unitary. Thus, equation (A.1) is invariant under time reversal. As shown in texts (e.g., Messiah [4]), the time reversal operator has been designed to be anti-unitary, consequently preserving the sign of i in commutation formulae.

An algebraic approach reveals that the commutator equation equation (A.1) remains invariant when proper rotation of coordinates is applied. Standard Cartesian coordinates are employed in the particular representation of the rotation matrix, the use of spherical polar coordinates would yield the same results. The laboratory referenced $\mathbf{J}$ is transformed to the rotated coordinate system by application of the rotation matrix $\mathbf{D}(\alpha\beta\gamma)$,

$$\mathbf{J}' = \mathbf{D}(\alpha\beta\gamma)\mathbf{J}, \tag{A.4}$$

where α, β, and γ are the Euler angles and $\mathbf{D}(\alpha\beta\gamma)$ is an orthogonal matrix whose determinant is +1, Goldstein [5],

$$\mathbf{D}(\alpha\beta\gamma) = \begin{pmatrix} \cos\alpha\cos\beta\cos\gamma - \sin\alpha\sin\gamma & \sin\alpha\cos\beta\cos\gamma + \cos\alpha\sin\gamma & -\sin\beta\cos\gamma \\ -\cos\alpha\cos\beta\sin\gamma - \sin\alpha\cos\gamma & -\sin\alpha\cos\beta\sin\gamma + \cos\alpha\cos\gamma & \sin\beta\sin\gamma \\ \cos\alpha\sin\beta & \sin\alpha\sin\beta & \cos\beta \end{pmatrix}. \tag{A.5}$$

The Euler angles and the matrix $\mathbf{D}(\alpha\beta\gamma)$ used here are those normally used in quantum mechanics, such as by Messiah [4], Davydov [6], Goldstein [5], Rose [7], Brink and Satchler [8], Tinkham [9], Gottfried [10], Baym [11], and Shore and Menzel [12]. This same set of Euler angles is also used by some authors of books on the theory of diatomic spectra, such as Judd [13] and Mizushima [14]. Evaluation of the angular momentum commutation formulae in the rotated system of coordinates gives

$$\mathbf{J}_{i'}\mathbf{J}_{j'} - \mathbf{J}_{j'}\mathbf{J}_{i'} = i\varepsilon_{i'j'k'}\mathbf{J}_{k'}. \tag{A.6}$$

This result is obtained from equations (A.1), (A.4), and (A.5). The calculation is simplified somewhat if one notes that for an orthogonal matrix the cofactors, i.e., signed minor determinants, are equal to the corresponding matrix elements of $\mathbf{D}(\alpha\beta\gamma)$ labeled m_{ij}, i.e., m_{ij} is its own cofactor. For example,

$$J_{x'}J_{y'} - J_{y'}J_{x'} = i\Big[(m_{12}m_{23} - m_{13}m_{22})(J_yJ_z - J_zJ_y)$$
$$+ (m_{13}m_{21} - m_{11}m_{23})(J_xJ_z - J_zJ_x) \tag{A.7}$$
$$+ (m_{11}m_{22} - m_{12}m_{21})(J_xJ_y - J_yJ_x) \Big],$$

and since

$$m_{12}m_{23} - m_{13}m_{22} = m_{31},$$
$$m_{13}m_{21} - m_{11}m_{23} = - m_{32}, \tag{A.8}$$
$$m_{11}m_{22} - m_{12}m_{21} = m_{33},$$

the right-hand side of equation (A.6) reduces to $iJ_{z'}$.

The review of Klein's [1] anomalous formula concludes that reversal of the sign of the sign is not required in diatomic molecular spectroscopy. The anomalous sign in the angular momentum commutators does not reveal a novel aspect of the nature of diatomic molecules. It is noteworthy that the anomalous commutation formula remains today a time-honored tradition in the theory of molecular spectra, as evidenced in several references [10–22]. Klein's anomalous commutators are means by which matrix elements of various operators in the molecular Hamiltonian are obtained, in particular those expressed in terms of angular momentum raising and lowering operators.

References

[1] Klein O 1929 *Zur Frage der Quantelung des asymmetrischen Kreisels* **58** 730
[2] Parigger C G and Hornkohl J O 2010 *Int. Rev. At. Mol. Phys.* **1** 25
[3] Hornkohl J O and Parigger C G 1996 *Am. J. Phys.* **64** 623
[4] Messiah A 1964 *Quantum Mechanics* (Amsterdam: North-Holland)
[5] Goldstein H, Poole C P and Safko J L 2001 *Classical Mechanics* 3rd edn (Reading, MA: Addison-Wesley)
[6] Davydov A S 1965 *Quantum Mechanics* (Oxford: Pergamon)
[7] Rose M E 1995 *Elementary Theory of Angular Momentum* (Mineola, NY: Dover)
[8] Brink D M and Satchler G R 1968 *Angular Momentum* (Oxford: Oxford University Press)
[9] Tinkham M 1964 *Group Theory and Quantum Mechanics* (New York: McGraw-Hill)
[10] Gottfried K 1989 *Quantum Mechanics* (Reading: Addison-Wesley)
[11] Baym G 1969 *Lectures on Quantum Mechanics* (London: Benjamin/Cummings)
[12] Shore B W and Menzel D H 1968 *Principles of Atomic Spectra* (Reading: Addison-Wesley)
[13] Judd B 1975 *Angular Momentum Theory for Diatomic Molecules* (New York: Academic)
[14] Mizushima M 1975 *The Theory of Rotating Diatomic Molecules* (New York: Wiley)
[15] Van Vleck J H 1951 The coupling of angular momentum vectors in molecules *Rev. Mod. Phys.* **23** 213
[16] Freed K F 1966 *J. Chem. Phys.* **45** 4214
[17] Kovács I 1969 *Rotational Structure in the Spectra of Diatomic Molecules* (New York: American Elsevier)
[18] Hougen J T 2001 *The Calculation of Rotational Energy Levels and Rotational Line Intensities in Diatomic Molecules* (Gaithersburg, MD: National Institute of Standards and Technology) http://physics.nist.gov/DiatomicCalculations. Originally published as *The Calculation of*

Rotational Energy Levels and Rotational Line Intensities in Diatomic Molecules, J. T. Hougen, NBS Monograph 115 (1970)

[19] Miller T A, Carrington A and Levy D H 1970 *Adv. Chem. Phys.* **18** 149

[20] Brown J M and Carrington A 2003 *Rotational Spectroscopy of Diatomic Molecules* (Cambridge: Cambridge University Press)

[21] Lefebvre-Brion H and Field R W 2004 *The Spectra and Dynamics of Diatomic Molecules* (New York: Elsevier/Academic)

[22] Bunker P R and Jensen P 1998 *Molecular Symmetry and Spectroscopy* 2nd edn (Ottawa: NRC))

Appendix B

Effects of raising and lowering operators

This appendix addresses details of the effects of raising and lowering operators on standard states $|JM\rangle$ and on elements of the rotation matrix $D_{M\Omega}^{J*}(\boldsymbol{\alpha\beta\gamma})$ [1]. The angular momentum raising and lowering operators have the following effects on the standard $|JM\rangle$ states,

$$J_{\pm}|JM\rangle = C_{\pm}(J, M)\,|J, M \pm 1\rangle, \tag{B.1}$$

where

$$\begin{aligned} C_{\pm}(J, M) &= \sqrt{J(J + 1) - M(M \pm 1)} \\ &= \sqrt{(J \mp M)(J \pm M - 1)}. \end{aligned} \tag{B.2}$$

This general equation is, of course, applicable to the diatomic molecule. However, as a result of approximation, one deals with approximate diatomic eigenfunctions. Contained in Van Vleck's method is his discovery that the above standard results are not directly applicable to approximate diatomic eigenfunctions. Typically, two magnetic quantum numbers occur for approximate diatomic eigenfunctions, M and Ω in Hund's case (*a*) or M_N and Λ in case (*b*).

In modern notation, approximate diatomic angular momentum states are represented by elements of the rotation matrix, $D_{M\Omega}^{J*}(\alpha\beta\gamma)$, which carry two magnetic quantum numbers, one more than allowed by the nature of angular momentum. Only $\mathbf{J}^2$ and one of its components, by usual convention J_z, commute with the Hamiltonian. It will be important in our approach to find the effects of the raising and lowering operators on elements of the rotation matrix while applying standard theory.

The rotated raising operator, J_+',

$$J_+' = J_{x'} + iJ_{y'}, \tag{B.3}$$

lowers the Ω quantum number on Hund's case (*a*) states; see, for example, Van Vleck [2], Judd [3], Mizushima [4], Freed [5], Kovacs [6], Hougen [7], Carrington *et al* [8],

Zare *et al* [9], Brown and Howard [10], and Lefebvre-Brion and Field [11]. Similarly, the rotated raising operator N'_+ lowers the Λ quantum number on case (*b*) kets. Agreement between eigenvalues of Hamiltonian matrices built using these results and experimentally measured term values has firmly established their correctness. Klein's anomalous commutators are often referenced in debating the reason why J'_+ lowers Ω and why N'_+ lowers Λ. However, of interest will be the following equation

$$J'_\pm \, D^{J*}_{M\Omega}(\alpha\beta\gamma) = -C_\mp(J, \, \Omega) \, D^{J*}_{M, \, \Omega\mp1}(\alpha\beta\gamma), \tag{B.4}$$

which will be derived below. Note that J'_+ lowers Ω, that J'_- raises Ω, and that an unexpected minus sign occurs.

The nature of angular momentum does not allow M and Ω both to be rigorously *good* quantum numbers. This is equivalent to stating that J_z and $J_{z'}$ do not commute. According to definition of angular momentum, J_z does not commute with J_x or J_y, but it is, perhaps, not obvious that J_z and $J_{z'}$ fail to commute. One can easily show, Gottfried [12], that

$$[J_z, \, J_{z'}] = i \sin(\beta)J_\beta \tag{B.5}$$

$$= i \sin(\beta)[-\sin(\alpha)J_x + \cos(\alpha)J_y]. \tag{B.6}$$

where $J_\beta = \partial/\partial\beta$ is the angular momentum operator for rotation about the first intermediate *y*-axis. In general, J_z and $J_{z'}$ do not commute. Thus, $D^{J*}_{M, \, \Omega}(\alpha\beta\gamma)$ cannot represent a state of angular momentum of a molecule or any other system. The rotation matrix connects two different states of angular momentum.

B.1 Angular momentum operators

Angular momentum operator representations in terms of Euler angles are elaborated. A rotation provides a particularly simple way of expressing a component of angular momentum. The three Euler rotations give the following three components:

$$J_\alpha = -i\frac{\partial}{\partial\alpha} = J_z, \tag{B.7}$$

$$J_\beta = -i\frac{\partial}{\partial\beta}, \tag{B.8}$$

$$J_\gamma = -i\frac{\partial}{\partial\gamma} = J_{z'}. \tag{B.9}$$

Each of these operators is referenced to a different coordinate system, i.e., $J_\alpha = J_z$ in the laboratory system, $J_\beta = J_{y_1}$ in the first intermediate system, and $J_\gamma = J_{z'}$ in the fully rotated system. Applying the first Euler rotation to the vector operator **J** results in

$$\begin{pmatrix} J_{x_1} \\ J_{y_1} \\ J_{z_1} \end{pmatrix} = \begin{pmatrix} \cos\alpha & \sin\alpha & 0 \\ -\sin\alpha & \cos\alpha & 0 \\ 0 & 0 & 1 \end{pmatrix} \begin{pmatrix} J_x \\ J_y \\ J_z \end{pmatrix}. \tag{B.10}$$

From this one finds

$$J_{y_1} = J_\beta = -\sin\alpha\, J_x + \cos\alpha\, J_y, \tag{B.11}$$

giving J_β in terms of the laboratory coordinates of $\mathbf{J}$. Similarly, using the full rotation matrix, equation (A.4), one can express J_γ in laboratory coordinate system,

$$\mathbf{J}' = D(\alpha\beta\gamma)\mathbf{J}, \tag{B.12}$$

$$J_{z'} = J_\gamma = \cos\alpha\sin\beta\, J_x + \sin\alpha\sin\beta\, J_y + \cos\beta\, J_\alpha, \tag{B.13}$$

where the substitution $J_z = J_\alpha$ has been made. Equations (B.11) and (B.13) can be inverted for J_x and J_y:

$$J_x = -i\left(-\cos\alpha\cot\beta\frac{\partial}{\partial\alpha} - \sin\alpha\frac{\partial}{\partial\beta} + \frac{\cos\alpha}{\sin\beta}\frac{\partial}{\partial\gamma}\right), \tag{B.14}$$

$$J_y = -i\left(-\sin\alpha\cot\beta\frac{\partial}{\partial\alpha} + \cos\alpha\frac{\partial}{\partial\beta} + \frac{\sin\alpha}{\sin\beta}\frac{\partial}{\partial\gamma}\right), \tag{B.15}$$

$$J_z = -i\frac{\partial}{\partial\gamma}. \tag{B.16}$$

The method in obtaining these results included evaluation of J_β and J_γ in terms of the laboratory components of $\mathbf{J}$. Similarly, $J_{x'}$, $J_{y'}$, and $J_{z'}$ can be obtained by expressing J_α and J_β in terms of the components of $\mathbf{J}'$. The inverse of the full rotation matrix is applied to the rotated vector $\mathbf{J}'$,

$$\mathbf{J} = D^{-1}(\alpha\beta\gamma)\mathbf{J}' = D^\dagger(\alpha\beta\gamma)\mathbf{J}', \tag{B.17}$$

to find J_α in terms of the rotated coordinates of $\mathbf{J}$,

$$J_z = J_\alpha = -\sin\beta\cos\gamma\, J_{x'} + \sin\beta\sin\gamma\, J_{y'} + \cos\beta\, J_\gamma. \tag{B.18}$$

The Euler β-rotation is taken about the first intermediate y-axis meaning that the first intermediate and second intermediate y-axes coincide. Thus, J_β can be evaluated in fully rotated coordinates by applying the inverse of the γ rotation matrix to $\mathbf{J}'$,

$$\begin{pmatrix} J_{x_2} \\ J_{y_2} \\ J_{z_2} \end{pmatrix} = \begin{pmatrix} \cos\gamma & -\sin\gamma & 0 \\ \sin\gamma & \cos\gamma & 0 \\ 0 & 0 & 1 \end{pmatrix} \begin{pmatrix} J_{x'} \\ J_{y'} \\ J_{z'} \end{pmatrix}. \tag{B.19}$$

$J_{y_2} = J_{y_1} = J_\beta$; therefore, we find

$$J_\beta = \sin \gamma\ J_{x'} + \cos \gamma\ J_{y'}. \tag{B.20}$$

The two equations in two unknowns are inverted as before. We find for $J_{x'}$ and $J_{y'}$

$$J_{x'} = -i\left(\cos \gamma \cot \beta \frac{\partial}{\partial \gamma} + \sin \gamma \frac{\partial}{\partial \beta} - \frac{\cos \gamma}{\sin \beta} \frac{\partial}{\partial \alpha}\right), \tag{B.21}$$

$$J_{y'} = -i\left(-\sin \gamma \cot \beta \frac{\partial}{\partial \gamma} + \cos \gamma \frac{\partial}{\partial \beta} + \frac{\sin \gamma}{\sin \beta} \frac{\partial}{\partial \alpha}\right), \tag{B.22}$$

$$J_{z'} = -i\frac{\partial}{\partial \gamma}. \tag{B.23}$$

The raising and lowering operators are then constructed using the results above,

$$J_+ = -ie^{i\alpha}\left(-\cot \beta \frac{\partial}{\partial \alpha} + i\frac{\partial}{\partial \beta} + \frac{1}{\sin \beta} \frac{\partial}{\partial \gamma}\right), \tag{B.24}$$

$$J_- = -ie^{-i\alpha}\left(-\cot \beta \frac{\partial}{\partial \alpha} - i\frac{\partial}{\partial \beta} + \frac{1}{\sin \beta} \frac{\partial}{\partial \gamma}\right), \tag{B.25}$$

$$J_{+'} = -ie^{-i\gamma}\left(\cot \beta \frac{\partial}{\partial \gamma} + i\frac{\partial}{\partial \beta} - \frac{1}{\sin \beta} \frac{\partial}{\partial \alpha}\right), \tag{B.26}$$

$$J_{-'} = -ie^{i\gamma}\left(\cot \beta \frac{\partial}{\partial \gamma} - i\frac{\partial}{\partial \beta} - \frac{1}{\sin \beta} \frac{\partial}{\partial \alpha}\right). \tag{B.27}$$

These general results also apply to systems composed of any number of particles. A modification or better *simplification* is required for a system consisting of a single particle (or two particles, since the two-body reduction can always be applied to a system of two particles). The third Euler angle, γ, is superfluous for a single particle, i.e., $\partial/\partial\gamma = 0$. Choosing the first Euler angle to be azimuthal angle ϕ and the second Euler angle to be the polar angle θ, the equations (B.14)-(B.16)) reduce to the familiar textbook equations for the angular momentum operators of a single particle.

Comparison of equations (B.14)–(B.16)) with equations (B.14–B.16) shows that the components of angular momentum are changed by a coordinate transformation. However, the defining commutators for angular momentum in terms of its Cartesian components remain invariant, although the individual components differ. We note that equations (B.7), (B.24), and (B.25) agree with Judd's [3] equation (1.22), but (B.9), (B.26), and (B.27) differ in sign from Judd's equation (1.23), presumably due to the use of the anomalous commutator formula. It appears that Judd obtained his rotated operators in a manner which guaranteed they would obey Klein's anomalous commutation formula.

B.2 Angular momentum commutators and rotation matrix elements

General relations for commutators are typically obtained by applying the commutator to an abstract ket describing a physical state. Alternatively, in the Schrödinger representation, the commutators are obtained by applying differential operators to physical eigenfunctions. This appendix demonstrates how two anomalous results may occur when applying $[J_{x'}, J_{y'}]$ and $[J_y, J_{y'}]$ to the rotation matrix elements $D_{M\Omega}^{J*}(\alpha\beta\gamma)$.

The commutator $[J_{x'}, J_{y'}]$ is evaluated using

$$[J_{x'}, J_{y'}] = \left[\frac{1}{2}(J_+' + J_-'), \frac{1}{2i}(J_+' - J_-') \right] = -\frac{i}{2}[J_-', J_+'], \tag{B.28}$$

and equation (B.4) which for convenience is repeated here

$$J_\pm' \, D_{M\Omega}^{J*}(\alpha\beta\gamma) = -C_\mp(J, \Omega) \, D_{M, \Omega\mp1}^{J*}(\alpha\beta\gamma). \tag{B.29}$$

Successive application of the operators in the rotated frame of reference yields the intermediate result

$$-\frac{i}{2}[J_-', J_+']D_{M\Omega}^{J*}(\alpha\beta\gamma) = -\frac{i}{2}(C_+(J, \Omega - 1)C_-(J, \Omega) - C_-(J, \Omega + 1)C_+(J, \Omega))D_{M\Omega}^{J*}(\alpha\beta\gamma), \tag{B.30}$$

which after inserting (compare equation (B.2))

$$C_\pm(J, \Omega) = \sqrt{(J \mp \Omega)(J \pm \Omega + 1)}, \tag{B.31}$$

leads to

$$[J_{x'}, J_{y'}]D_{M\Omega}^{J*}(\alpha\beta\gamma) = -i\Omega D_{M\Omega}^{J*}(\alpha\beta\gamma). \tag{B.32}$$

It might be tempting to conclude anomalous commutator relations in the rotated molecular frame from this identity. However, the rotation matrix elements contain two quantum numbers M and Ω, one too many to represent a physical eigenfunction.

Similarly, $[J_y, J_{y'}]$ is evaluated using

$$[J_y, J_{y'}] = \left(-\frac{1}{4}[J_+, J_+'] - \frac{1}{4}[J_-, J_-'] + \frac{1}{4}[J_+, J_-'] + \frac{1}{4}[J_-, J_+'] \right), \tag{B.33}$$

and applying it to the rotation matrix elements $D_{M\Omega}^{J*}(\alpha\beta\gamma)$. Note $J_{y'}$ acts on Ω (see equations (B.29)) while J_y acts on M,

$$J_\pm \, D_{M\Omega}^{J*}(\alpha\beta\gamma) = C_\pm(J, M) \, D_{M\pm1, \Omega}^{J*}(\alpha\beta\gamma). \tag{B.34}$$

The intermediate step is given here

$$[J_y, J_{y'}]D_{M\Omega}^{J*}(\alpha\beta\gamma) =$$

$$+ \frac{1}{4}C_-(J, \Omega)J_+ D_{M\,\Omega-1}^{J*}(\alpha\beta\gamma) + \frac{1}{4}C_+(J, M)J'_+ D_{M+1\,\Omega}^{J*}(\alpha\beta\gamma)$$

$$+ \frac{1}{4}C_+(J, \Omega)J_- D_{M\,\Omega+1}^{J*}(\alpha\beta\gamma) + \frac{1}{4}C_-(J, M)J'_- D_{M-1\,\Omega}^{J*}(\alpha\beta\gamma) \quad \text{(B.35)}$$

$$- \frac{1}{4}C_+(J, \Omega)J_+ D_{M\,\Omega+1}^{J*}(\alpha\beta\gamma) - \frac{1}{4}C_+(J, M)J'_- D_{M+1\,\Omega}^{J*}(\alpha\beta\gamma)$$

$$- \frac{1}{4}C_-(J, \Omega)J_- D_{M\,\Omega-1}^{J*}(\alpha\beta\gamma) - \frac{1}{4}C_-(J, M)J'_+ D_{M-1\,\Omega}^{J*}(\alpha\beta\gamma),$$

which reduces to

$$[J_y, J_{y'}]D_{M\Omega}^{J*}(\alpha\beta\gamma) = 0. \quad \text{(B.36)}$$

Again, one might be tempted to infer from equation (B.36) a general commutator relation that also applies to angular momentum states.

References

[1] Parigger C G and Hornkohl J O 2010 *Int. Rev. At. Mol. Phys.* **1** 25

[2] Van Vleck J H 1951 The coupling of angular momentum vectors in molecules *Rev. Mod. Phys.* **23** 213

[3] Judd B 1975 *Angular Momentum Theory for Diatomic Molecules* (New York: Academic)

[4] Mizushima M 1975 *The Theory of Rotating Diatomic Molecules* (New York: Wiley)

[5] Freed K F 1966 *J. Chem. Phys.* **45** 4214

[6] Kovács I 1969 *Rotational Structure in the Spectra of Diatomic Molecules* (New York: American Elsevier)

[7] Hougen J T 2001 *The Calculation of Rotational Energy Levels and Rotational Line Intensities in Diatomic Molecules* (Gaithersburg, MD: National Institute of Standards and Technology) http://physics.nist.gov/DiatomicCalculations. Originally published as *The Calculation of Rotational Energy Levels and Rotational Line Intensities in Diatomic Molecules*, J. T. Hougen, NBS Monograph 115 (1970)

[8] Miller T A, Carrington A and Levy D H 1970 *Adv. Chem. Phys.* **18** 149

[9] Zare R N, Schmeltekopf A L, Harrop W J and Albritton D L 1973 *J. Mol. Spectrosc.* **46** 37

[10] Brown J M and Howard B J 1976 *Mol. Phys.* **31** 1517

[11] Lefebvre-Brion H and Field R W 2004 *The Spectra and Dynamics of Diatomic Molecules* (New York: Elsevier/Academic)

[12] Gottfried K 1989 *Quantum Mechanics* (Reading: Addison-Wesley)

Appendix C

Modified Boltzmann plots

This appendix elaborates on the use of Boltzmann plots [1] for diatomic molecular spectroscopy inferences of temperature from a measured emission spectra. The Boltzmann plot method evaluates temperature by finding the slope from a semilog graph of recorded spectral lines, e.g., the integrated line shape in determination of hydrogen excitation temperature in atomic spectroscopy. In molecular spectroscopy, usually there are many lines within a spectral resolution of the order of 0.1nm, which are typical for laser-plasma emission spectroscopy that uses resolving powers of the order of 5000. Consequently, a modified Boltzmann plot approach [2] is developed for analysis of measured molecular spectra.

C.1 Boltzmann plots

The formal approach starts with an equation containing an exponential,

$$f(x) = A\, e^{-\alpha\, x}, \tag{C.1}$$

one evaluates the logarithm of both sides, and puts the result into point-slope form for a straight line,

$$\begin{aligned} \ln[f(x)] &= -\,\alpha\, x + \ln A \\ y(x) &= \quad m\, x + b. \end{aligned} \tag{C.2}$$

In spectroscopy, spontaneous emission from a gas adheres to the spectral radiance, or frequently labeled 'intensity', originating from an upper level, u, to a lower level, l,

$$I_{ul} = \frac{64\,\pi^4\,(a_0 e)^2\,c\,C_{\mathrm{abs}}\,N_0}{3\,Q}\, C_{\tilde{\nu}}\,\tilde{\nu}_{ul}^4\,S_{ul}\,e^{-h\,c\,F_u/(k_B\,T)}. \tag{C.3}$$

The individual terms are listed below.

- $a_0\, e$: Bohr radius ×electronic charge.
- c, h, k_B: speed of light, Planck constant, Boltzmann constant.
- C_{abs}: absolute intensity calibration factor and $C_{\tilde{\nu}}$—relative spectral sensitivity calibration factor.
- N_0: number density, molecules / cm^3.
- Q: partition function of gas.
- $\tilde{\nu}$: wave number of spectral line produced by $u \to l$ transition.
- S_{ul}: electric dipole line strength.
- F_u: upper term value (i.e., energy eigenvalue divided by $h\,c$).
- T: absolute temperature.

The linearized spontaneous emission equation,

$$\ln\left(\frac{I_{ul}}{C_{\tilde{\nu}}\,\tilde{\nu}^4\,S_{ul}}\right) = -\frac{h\,c}{k_B\,T}\,F_u - \ln\left(\frac{64\,\pi^4\,(a_0 e)^2\,c\,C_{\text{abs}}\,N_0}{3\,Q}\right), \qquad (C.4)$$
$$= \; y \quad m \quad x \;+\; b,$$

is solved to find the slope m. A Boltzmann plot is a graph of $\ln\left(\frac{I_{ul}}{C_{\tilde{\nu}}\,\tilde{\nu}^4\,S_{ul}}\right)$ versus the upper term value F_u. The slope is proportional to $-1/T$, of course provided that thermodynamic equilibrium is reached,

$$T = -\frac{h\,c}{k_B\,m} \qquad (C.5)$$

Since the points would deviate from straight line, one labels the graph as a nonlinear Boltzmann plot, which would imply departure from thermal equilibrium. Figure C.1 illustrates an example of a Boltzmann plot.

Figure C.2 displays the spectrum from which the Boltzmann plot is constructed.

A Boltzmann plot can be made using the peak intensity or (better) the intensity integrated under each spectral line, but in either case the spectral lines must be fully resolved. The following shows how to make a Boltzmann plot when the spectral lines are not fully resolved. Table C.1 shows an example of a line list.

An emission spectral line is broadened by physical processes in the radiating gas and the properties of the spectrometer used to record the spectral line. A widely-used measure of spectral line width is the full width at half maximum (FWHM.) A spectrum is effectively broken into a finite number of pixels between the minimum $\lambda_{\min}$ and the maximum $\lambda_{\max}$ wavelengths in the spectrum (or the minimum or maximum frequencies ν or wave numbers $\tilde{\nu}$), and the FWHM can be used as the pixel width.

An emission spectrum is computed by evaluating expressions indicated in equation (C.3). One selects a line shape function (i.e., a Gaussian) and an FWHM, and computes the contributions of each line. A snippet of a program code utilizes a Gaussian line shape.
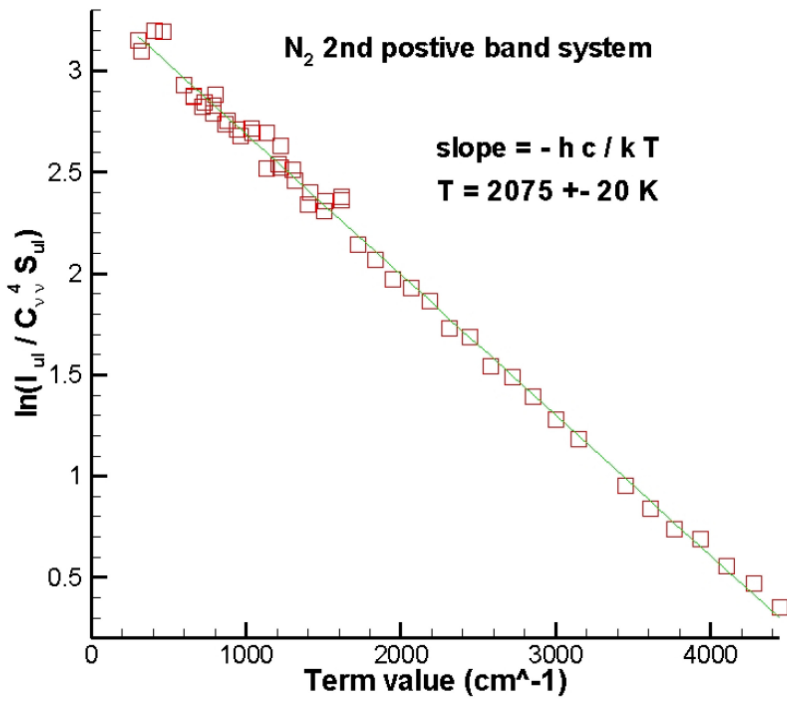
Figure C.1. A Boltzmann plot for a spectrum from the N_2 second positive system.
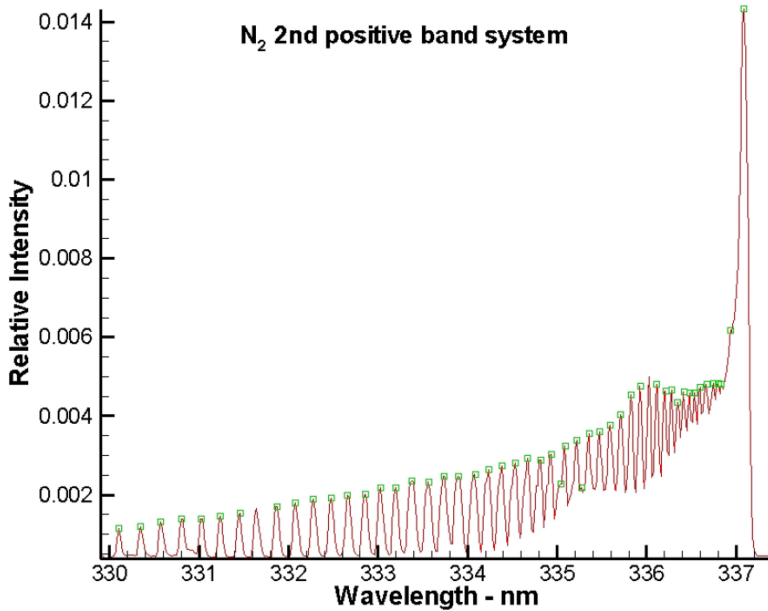
Figure C.2. A Boltzmann plot constructed a N_2 second positive system.

Table C.1. Spectral line lists: an example downloaded from NIST.

Wavelength air (Å)	A_{ul} (s^{-1})	E_u (cm^{-1})	E_l (cm^{-1})	g_u
2118.312	1.03×10^7	0	47 192.38	2
2123.362	1.22×10^7	112.061	47 192.38	4
2129.663	1.52×10^7	0	46 940.97	2
2134.733	1.81×10^7	112.061	46 941.55	4
2145.555	2.33×10^7	0	46 593.32	2
2150.699	2.79×10^7	112.061	46 593.95	4
2168.805	3.06×10^7	0	46 093.424	2
2174.028	3.65×10^7	112.061	46 094.312	4
2199.150	1.75×10^6	0	45 457.244	2
2204.590	3.49×10^6	112.061	45 457.244	4
2204.660	4.53×10^7	0	45 344.165	2
2210.046	5.40×10^7	112.061	45 345.594	4
2257.999	3.77×10^6	0	44 273.133	2

```fortran
!        Guassian line shape program segment
         delwn = (wn_lo-wn_hi) / (npts-1)
         con = 2.0 * sqrt(alog(2.0))
         do 70 k=1, kmax
            ndel = nint(2.5*FWHM_wn/delwn)
            if (wn(k).lt.wn_lo.or.wn(k).gt.wn_hi) go to 70
            n0 = nint((wn(k)-wnmin)/delwn) + 1
            nmin = n0 - ndel
            if (nmin.lt.1)   nmin = 1
            nmax = n0 + ndel
            if (nmax.gt.npts)   nmax = npts
            do n=nmin, nmax
               u = con * (wn(k)-x(n)) / FWHM_wn
               if (u.lt.9.21)   then
                  y(n) = y(n) + peak(k) * exp(-u*u)
                  if (y(n).gt.ymax)   ymax = y(n)
               end if
            end do
70       end do
```

C.2 Modified Boltzmann plot

The intensity I_p falling on a pixel (*i.e*, a small wave number range $\Delta\tilde{\nu}$) is the sum of all of the intensities of the spectral lines that contribute to the intensity range $\Delta\tilde{\nu}$,

$$I_p = \sum_{i=1}^{\text{all lines}} \text{const.}\ f(\tilde{\nu}_i, \Delta\tilde{\nu})\ C_i\ \tilde{\nu}_i^4\ S_i\ e^{-h\,c\,F_i/(k\,T)} \tag{C.6}$$

where $f(\tilde{\nu}_i, \Delta\tilde{\nu})$ is the line shape function. Because the term value F_i varies greatly from line to line, the exponential cannot be taken outside the summation. Therefore, an arbitrary exponential $e^{h\,c\,F_j/(k\,T)}$ is inserted,

$$I_p = e^{-h\,c\,F_j/(k\,T)} \sum_{i=1}^{\text{all lines}} \text{const.}\ f(\tilde{\nu}_i, \Delta\tilde{\nu})\ C_i\ \tilde{\nu}_i^4\ S_i\ e^{-h\,c\,(F_j - F_i)/(k\,T)}. \tag{C.7}$$

The exponential $e^{-h\,c\,F_j/(k\,T)}$ can be isolated, meaning that for assumed values of the term value F_j and temperature T, one can create a Boltzmann plot. The value of F_j is chosen to be F_i for the spectral line making the biggest contribution to I_p. The value of

$$ln\left(\frac{I_p}{C_i\ \tilde{\nu}^4\ S_i}\right) \Big/ \sum_{i=1}^{\text{all lines}} \text{const.}\ f(\tilde{\nu}_i, \Delta\tilde{\nu}_i)\ e^{-h\,c\,(F_j - F_i)/(k\,T)} \tag{C.8}$$

is plotted versus F_j for a trial T, but there is no reason why the temperature inferred from this plot will equal the trial temperature. However, the new temperature can replace the trial temperature, and the process is repeated, i.e., the procedure must be iterated until the trial temperature and the temperature from the Boltzmann plot agree.

An example output from modified Boltzmann plot routine displays the effectiveness of the iteration to find the excitation temperature.

<div align="center">

Trial temperature = 6000.

1 2078.

2 2073.

3 2073.

4 2073.

5 2073.

Std.Dev. Boltzmann plot $= 5.1378 \times 10^{-2}$

$a0 = 3.364 \quad \pm 1.2980 \times 10^{-2}$

Second radiation constant$=1.438\ 79$

$a1 = -6.9404 \times 10^{-4} \quad \pm 6.314 \times^1 0 - 6$

Boltzmann plot temperature $= 2073.$ Std.dev. $= \pm 18.9K$

</div>

References

[1] Wiese W L 1991 *Spectrochim. Acta* B **46** 831

[2] Hornkohl J O, Parigger C G and Lewis J W L 1991 *J. Quant. Spectrosc. Radiat. Transfer* **46** 405

Quantum Mechanics of the Diatomic Molecule (Second Edition)

Christian G Parigger and James O Hornkohl

Appendix D

Aspects of nitric oxide computations

This appendix communicates a collection of notes on the molecular parameters of nitric oxide (NO). These notes contain considerable discussion of the quantum mechanics of the diatomic molecule. The interesting topic of hyperfine structure is ignored.

In the present state of the applied science, the molecular parameters are found by fitting term value differences computed from an approximate Hamiltonian to the best experimental values for the line positions. The computation begins with trial values of the parameters, which are then iteratively refined until the differences between the computed and experimental line positions are minimized in the least squares sense.

This appendix discusses results found from fitting some of the best available NO data. The literature on NO is too vast for a comprehensive review. It can only be hoped that the following offers a representative sampling.

D.1 Matrix elements of the Hamiltonian

This section gives a review of the methods of applied quantum mechanics in diatomic spectroscopy. As an example of high quality experimental spectra, reference will be made to the NO rotation-vibration data reported by Amiot *et al* [1]. Their measured line positions are not reported in the journal article, but their data are still available from the Canadian Depository of Unpublished Data. The Macki and Wells [2] data for the (1,0) band are more accurate than the data of Amiot *et al*, but Macki and Wells report only smoothed line positions instead of measured values.

For their analysis of their NO spectra, Amiot *et al* reference the important paper by Zare *et al* [3], which describes the computation of term values by diagonalization of the Hamiltonian. The Zare *et al*'s method consists of four steps, which will be further discussed.

In the first step, trial values of the molecular parameters and analytical methods are used to evaluate the matrix elements of the Hamiltonian in the Hund's case (a) basis.

The second step is an analytical approximation, called the Van Vleck transformation, which reduces the dimension of the square Hamiltonian matrix to $2(2S + 1) \times 2(2S + 1)$, where S is the total electronic spin quantum number for the dominant state in the basis—if the latter is a Σ state, then the result of the Van Vleck transformation has the dimensions $(2S + 1) \times (2S + 1)$. In addition to reducing the dimensions of the Hamiltonian, the Van Vleck transformation also splits the Hamiltonian into two independent submatrices of opposite parity.

The ground state of NO is usually modeled as a dominant $^2\Pi$ state, which contributes a 4×4 submatrix to the Hamiltonian, weakly mixed with a $^2\Sigma^+$ state, which contributes a 2×2 submatrix. Thus, in this model the Hund's case (a) representation of the Hamiltonian is a 6×6 matrix. Van Vleck's approximate transformation reduces the Hamiltonian to a 4×4 matrix composed of two independent 2×2 matrices of opposite parity. The third step in Zare *et al*'s method is numerical diagonalization of the two submatrices. The fourth step is a matrix computation which gives corrections to the trial values of the molecular parameters. If the computed corrections are not negligibly small, steps 1–4 are iteratively repeated until the corrections become negligibly small.

The following determinations of NO parameters differ from Zare *et al*'s method in one way. The Van Vleck transformation is skipped. Thus, for the ground state of NO the present computations involve numerical diagonalization of a single 6×6 matrix instead of numerical diagonalization of two 2×2 submatrices.

Various different Hamiltonian models for NO ($X\,^2\Pi$) will be investigated below but the conclusion is that the accepted model of a dominant $^2\Pi$ state with a small component of a $^2\Sigma^+$ state adequately describes the available experimental observations. Table D.1 shows the fit of this model to the NO (1,0) band data of Amiot *et al* [1].

Most of the symbols in the following tables have their standard meanings. $T_v = T_e + G_v$ where T_e is the electronic term value and G_v is the vibrational term value. $\Delta\tilde{\nu}$ is the search tolerance used by the fitting program when it searches for an experimental spectral line to match a predicted line.

An experimental line for which there is no predicted line having the same J' and J'' whose vacuum wave number is within the search tolerance $\Delta\tilde{\nu}$ is eliminated from the fit. The table caption entry '405 lines of 419' indicates that 14 experimental lines were rejected from the fit, and σ is the standard deviation of the predicted line positions (vacuum wave number) with respect to the 405 accepted experimental line positions. Values in parenthesis represent 1 standard deviation expressed in the last digits. Values in square brackets were held fixed during the fitting process. Other symbols in the table will be defined below. The ratio of the standard deviation of the fit to the band origin, $\sigma/\tilde{\nu}_{10} \approx 2 \times 10^{-7}$.

Most of the richness of the typical diatomic spectrum is produced by the rotational Hamiltonian, the term in the diatomic Hamiltonian representing the kinetic energy of rotation of the nuclei, given by

$$H_{\text{rot}} = B(r)\,\mathbf{R}^2 \qquad \text{(D.1)}$$

Table D.1. The molecular parameters for the $v = 0$ and $v = 1$ states of the ground electronic state of NO obtained by fitting the model of a dominant $^2\Pi$ state weakly mixed with a $^2\Sigma^+$ state to the (1,0) band data of Amiot *et al.* [1]

$X\ ^2\Pi(v = 1)$	$T_v = 2824.6331(5)$
$B_v = 1.678\ 5715(27)$	$D_v = 5.4893(26) \times 10^{-6}$
$A_v = 122.7026(21)$	$A_{vJ} = 3.475(38) \times 10^{-4}$
$<AL> = -177.8(1.0)$	$<AL>_J = 4.2(1.8) \times 10^{-3}$
$<BL> = -1.3922(76)$	$<BL>_J = -4.2(1.3) \times 10^{-5}$
$X\ ^2\Pi(v = 0)$	$[T_v = 948.66]$
$B_v = 1.696\ 1445(30)$	$D_v = 5.4735(29) \times 10^{-6}$
$A_v = 122.9495(23)$	$A_{vJ} = 3.565(42) \times 10^{-4}$
$<AL> = -180.4(1.1)$	$<AL>_J = 3.4(2.0) \times 10^{-3}$
$<BL> = -1.433(84)$	$<BL>_J = -3.1(1.5) \times 10^{-5}$
$A\ ^2\Sigma^+(v = 0)$	$[T_v = 45087.65]$
$[B_v = 1.986\ 312]$	$[D_v = 5.575 \times 10^{-6}]$
$[\gamma_v = -1.34 \times 10^{-4}]$	

The parameters for the $^2\Sigma^+$ state were held fixed to those values found from a fit to the $A\ ^2\Sigma^+(v = 0) \leftrightarrow X\ ^2\Pi(v = 0)$ γ-system data of Engleman *et al* [4]. The upper state extends to $0.5 \leqslant J' \leqslant 40.5$, includes 405 of 429 lines, with an accuracy of $\Delta\tilde{\nu} = 0.001$ cm^{-1} and $\sigma = 0.000\ 38$ cm^{-1}. The term value difference equals $\tilde{\nu}_{10} = 1875.9731$.

in which **R** is the orbital angular momentum operator for the nuclei whose motion has been reduced to that of a single, fictitious particle of reduced mass μ,

$$\mu = \frac{m_a m_b}{m_a + m_b} \tag{D.2}$$

of the nuclei whose masses are m_a and m_b, and

$$B(r) = \frac{\hbar}{4\pi c \mu r^2} \tag{D.3}$$

where r is the internuclear distance. The rotational parameter $B(r)$ has the units of energy, but the right-hand side of the above equation has been divided by hc (Planck's constant times the speed of light) to give $B(r)$ the spectroscopist's unit of energy which has the units of reciprocal length.

When, as has been assumed here, the normally very small influence of nuclear spin on the term values can safely be ignored, the total angular momentum,

$$\mathbf{J} = \mathbf{L} + \mathbf{R} + \mathbf{S} \tag{D.4}$$

is the sum of the total electronic orbital angular momentum **L**, the total nuclear orbital angular momentum **R**, and the total electronic spin **S**. The rotational Hamiltonian becomes [5]

$$\begin{aligned} H_{\text{rot}} &= B(r)(\mathbf{J} - \mathbf{L} - \mathbf{S})^2 \\ &= B(r)\Bigg[\mathbf{J}^2 + \frac{L_+L_- + L_-L_+}{2} + L_z^2 + \mathbf{S}^2 - (J_+L_- + J_-L_+ + 2J_zL_z) \\ &\qquad - (J_+S_- + J_-S_+ + 2J_zS_z) + (L_+S_- + L_-S_+ + 2L_zS_z) \Bigg] \end{aligned}$$

(D.5)

$$\begin{aligned} = B(r)\Bigg[\mathbf{J}'^2 &+ \frac{L'_+L'_- + L'_-L'_+}{2} + L_{z'}^2 + \mathbf{S}'^2 - (J'_+L'_- + J'_-L'_+ + 2J_{z'}L_{z'}) \\ &- (J'_+S'_- + J'_-S'_+ + 2J_{z'}S_{z'}) + (L'_+S'_- + L'_-S'_+ + 2L_{z'}S_{z'}) \Bigg]. \end{aligned}$$

(D.6)

where unprimed components are in the laboratory coordinate system, primed components are in a coordinate system attached to the molecule, and the raising and lowering operators are defined by, for example,

$$J_\pm = J_x \pm J_y,$$

(D.7)

with similar equations for $S_\pm$ and $L_\pm$. The analytical form of each term in the Hamiltonian is preserved under a coordinate transformation, compare equations (D.5) and (D.6). Matrix elements of Hamiltonian terms are much easier to analytically evaluate in molecular coordinates than in the laboratory coordinates.

As explained in many quantum mechanics texts, specification of the states of a quantum system is normally done with the standard $|nJM\rangle$ states of the system, where J is the quantum number for the total angular (the quantity which obeys the conservation law for angular momentum), M is the quantum number for the laboratory z component of $\mathbf{J}$, and n denotes all other required quantum numbers. The exact equation for the standard $|nJM\rangle$ states of the diatomic molecule is [5]

$$\langle \mathbf{r}_1, \mathbf{r}_2, \ldots, \mathbf{r}_\mathcal{N}, \mathbf{r}|nJM\rangle = \sum_{\Omega=-J}^{J} \langle \mathbf{R}'_e r|n\rangle \, D^{J*}_{M\Omega}(\alpha\beta\gamma)$$

(D.8)

where $\mathbf{r}_1, \mathbf{r}_2, \ldots, \mathbf{r}_\mathcal{N}$ are the laboratory coordinates of the $\mathcal{N}$ electrons; $\mathbf{r}$ is the internuclear vector; α, β, and γ are the Euler angles; R'_e represents $3\mathcal{N} - 1$ rotated electronic coordinates (γ is the missing electronic coordinate); and $D^{J}_{M\Omega}(\alpha\beta\gamma)$ is the matrix element of the rotation operator (note that its complex conjugate appears in the above equation). The Hund's case (a) basis is defined by [5]

$$\langle \mathbf{r}_1, \mathbf{r}_2, \ldots, \mathbf{r}_\mathcal{N}, \mathbf{r}|nJM\Omega\Lambda S\Sigma\rangle = \sqrt{\frac{2J+1}{8\pi^2}} \langle \mathbf{R}'_e r|n\rangle \, |S\Sigma\rangle \, D^{J*}_{M\Omega}(\alpha\beta\gamma).$$

(D.9)

in which Ω is the quantum number for the z' component of J and Σ is the quantum number for the z' component of S. The relationship

$$J_{z'} = L_{z'} + S_{z'}$$

(D.10)

holds because the z'-axis lies on the internuclear axis and the nuclei have no internuclear component of orbital angular momentum (i.e., $R_{z'} = 0$). Thus,

$$\Omega = \Lambda + \Sigma$$

(D.11)

and Λ, the quantum number for $L_{z'}$ is also a case (a) quantum number, although it does not explicitly appear on the right-hand side of equation (D.9).

The Born–Oppenheimer approximation has not been applied in either the exact equation for the $|nJM\rangle$ diatomic states, equation (D.8), or the case (a) basis, equation (D.9). The smallness of the electronic mass in comparison to the nuclear mass produces an approximate separation of the electronic and nuclear motions. In the usual exposition of the Born–Oppenheimer approximation, the approximate separation of the electronic and nuclear motions involves all of the electronic and nuclear internal coordinates. However, in the present formulation the Euler angles play no part in the Born–Oppenheimer separation, which is concerned exclusively with the eigenfunction $\langle \mathbf{R}'_e r | n \rangle$. The quantum number v, the quantum number associated with the internuclear distance r, is extracted from the collection of quantum numbers represented by the symbol n, and the Born–Oppenheimer approximate separation of $\langle \mathbf{R}'_e r | nv \rangle$ is then made,

$$
\begin{aligned}
\langle \mathbf{R}'_e r | nv \rangle &\approx \langle \mathbf{R}'_e; r | n \rangle \, \langle r | v \rangle \\
&= \psi_n(\mathbf{R}'_e; r) \, \psi_v(r)
\end{aligned}
\tag{D.12}
$$

in which the semicolon is a notational device indicating that the electronic eigenfunction $\psi_e(\mathbf{R}'_e; r)$ is a parametric function of the internuclear distance r. This means that the electronic Schrödinger equation has a different solution for each value of the internuclear distance. Because the electronic eigenfunction is a parametric function of r, all electronic matrix elements are functions of r.

Application of the Born–Oppenheimer approximation to the case (a) basis gives

$$
\langle \mathbf{r}_1, \mathbf{r}_2, \ldots, \mathbf{r}_{\mathcal{N}}, \mathbf{r} | nvJM\Omega\Lambda S\Sigma \rangle = \sqrt{\frac{2J+1}{8\pi^2}} \langle \mathbf{R}'_e; r | n \rangle \, \langle r | v \rangle | S\Sigma \rangle \, D^{J*}_{M\Omega}(\alpha\beta\gamma). \tag{D.13}
$$

Matrix elements of the rotational Hamiltonian can be calculated using equations (D.6) and (D.13). Zare *et al* [3] give tables of case (a) matrix elements. They are also given by Lefebvre-Brion and Field [6]. Sign ambiguities between Zare *et al* and Lefebvre-Brion and Field can be resolved through application of equations (D.6) and (D.9) [5]. Table D.5 gives example matrix elements of H_{rot} in a state consisting of a mixture of $^2\Pi$ and $^2\Sigma$ case (a) basis states. The diagonal matrix elements of the rotational Hamiltonian, $\langle nJM\Omega\Lambda S\Sigma | H_{\text{rot}} | nJM\Omega\Lambda S\Sigma \rangle$, are given by

$$
\begin{aligned}
&B_v \, \langle nJM\Omega\Lambda S\Sigma | \mathbf{J}^2 + L_{z'}^2 - 2J_{z'}L_{z'} - 2J_{z'}S_{z'} + 2L_{z'}S_{z'} | JM\Omega\Lambda S\Sigma \rangle \\
&= B_v \, [J(J+1) - \Omega^2 + S(S+1) - \Sigma^2],
\end{aligned}
\tag{D.14}
$$

where the rotational constant B_v is defined by

$$
B_v = \frac{\hbar}{4\pi c \mu} \langle nv | r^{-2} | nv \rangle = \frac{\hbar}{4\pi c \mu} \langle v | r^{-2} | v \rangle. \tag{D.15}
$$

Because the internuclear distance is held constant for evaluation of an electronic matrix element, the rotational constant is diagonal with respect to the electronic quantum numbers n.

The operations involving $\mathbf{J}$ and $\mathbf{S}$ are straightforward. Operation of $\mathbf{J}^2$, J_z, and $J_{z'}$ on the standard $|nJM\rangle$ and $|nJ\Omega\rangle$ states obey,

$$\mathbf{J}^2 \, |nJM\rangle = J(J+1) \, |nJM\rangle \tag{D.16}$$

$$J_z \, |nJM\rangle = M \, |nJM\rangle \tag{D.17}$$

$$J_{z'} \, |nJ\Omega\rangle = \Omega \, |nJ\Omega\rangle \tag{D.18}$$

The only possible point of confusion here is the standard state $|nJ\Omega\rangle$, which is referenced to the rotated, molecule fixed, z-axis (i.e., the z'-axis) instead of the laboratory z-axis. For any system, the standard $|nJM\rangle$ and $|nJ\Omega\rangle$ states are related by

$$\langle \mathbf{r}_1, \mathbf{r}_2, \dots, \mathbf{r}_\mathcal{N} |nJM\rangle = \sum_{\Omega=-J}^{J} \langle \mathbf{r}_1', \mathbf{r}_2', \dots, \mathbf{r}_\mathcal{N}' |nJ\Omega\rangle \, D_{M\Omega}^{J*}(\alpha\beta\gamma) \tag{D.19}$$

where, for the moment, $\mathcal{N}$ is the number of particles having spatial coordinates in the system. This is a general result holding for any quantum system, see, e.g., Thompson's [7] equation (6.19) or equation (xx) of [5].

The operations involving $\mathbf{L}$ are more complicated. The operators $\mathbf{J}^2$ and $J_\pm$ act on the rotation matrix element but not $\langle \mathbf{R}_e' r |nv\rangle$ or the electronic spin states $|S\Sigma\rangle$. The operator $\mathbf{S}^2$ affects nothing but the spin ket $|S\Sigma\rangle$. The total electronic orbital angular momentum,

$$\mathbf{L} = \sum_{i=1}^{\mathcal{N}} \mathbf{l}_i \tag{D.20}$$

in which l_i is the orbital angular momentum of the ith electron is a function of $3\mathcal{N}$ coordinates where $\mathcal{N}$ is the number of electrons. The symbol $\mathbf{R}_e'$ represents only $3\mathcal{N} - 1$ electronic coordinates, and the third Euler angle γ is the remaining electronic coordinate. Thus, $3\mathcal{N} - 1$ components of L operate on $\langle \mathbf{R}_e' |nv\rangle$ and the remaining component l_γ acts on $D_{M,\Omega}^{J*}(\alpha\beta\gamma)$. A Clebsch–Gordon expansion of the rotation matrix element gives

$$\langle \mathbf{r}_1, \mathbf{r}_2, \dots, \mathbf{r}_\mathcal{N}, \mathbf{r} |nJM\Omega\Lambda S\Sigma\rangle = \sqrt{\frac{2J+1}{8\pi^2}} \, \langle \mathbf{R}_e' r |nv\rangle \, |S\Sigma\rangle$$
$$\times \sum_{M_N=-N}^{N} \sum_{M_S=-S}^{S} \langle N M_N \, S M_S |JM\rangle \, \langle N\Lambda S\Sigma |J\Omega\rangle \, D_{M_N\Lambda}^{N*}(\alpha\beta\gamma) \, D_{M_S\Sigma}^{S*}(\alpha\beta\gamma). \tag{D.21}$$

in which N, the laboratory referenced M_N, and the molecule referenced Λ are the quantum numbers associated with the total orbital angular momentum $\mathbf{N}$,

$$\mathbf{N} = \mathbf{L} + \mathbf{R} \tag{D.22}$$

For the one electron for which γ is the angular coordinate of rotation about the internuclear axis,

$$l_{z'} D_{M_N\Lambda}^{N*}(\alpha\beta\gamma) = -i\frac{\partial}{\partial\gamma}D_{M_N\Lambda}^{N*}(\alpha\beta\gamma)$$
$$= -i\frac{\partial}{\partial\gamma}e^{iM_N\alpha}\, d_{M_N\Lambda}^{N}(\beta)\, e^{i\Lambda\gamma} \qquad \text{(D.23)}$$
$$= \Lambda\, D_{M_N\Lambda}^{N*}(\alpha\beta\gamma).$$

Thus, operation of l_γ in the case (a) basis is given by

$$l_\gamma\, |nJM\Omega\Lambda S\Sigma\rangle = \Lambda\, |nJM\Omega\Lambda S\Sigma\rangle. \qquad \text{(D.24)}$$

Calculation of off-diagonal matrix elements of the rotational Hamiltonian is complicated by the nonstandard behavior of the case (a) states under operation of the raising and lowering operators. The rotation matrix element carries two magnetic quantum numbers, one more than mathematically admitted by the definition of angular momentum. The familiar behavior of standard $|nJM\rangle$ under raising and lowering operators,

$$J_\pm\, |nJM\rangle = \sqrt{J(J+1) - M(M\pm1)}\, |nJ,\, M\pm1\rangle$$
$$= C_\pm(JM)\, |nJ,\, M\pm1\rangle \qquad \text{(D.25)}$$

does not hold for the rotation matrix element, even though it looks like an angular momentum eigenfunction because it is specified in terms of angular coordinates and quantum numbers. The rotation matrix elements obey [5]

$$J_\pm D_{M\Omega}^{J}(\alpha\beta\gamma) = -C_\mp(JM)\, D_{M\mp1,\,\Omega}^{J}(\alpha\beta\gamma), \qquad \text{(D.26)}$$

$$J'_\pm D_{M\Omega}^{J}(\alpha\beta\gamma) = C_\pm(J\Omega)\, D_{M,\,\Omega\pm1}^{J}(\alpha\beta\gamma), \qquad \text{(D.27)}$$

$$J_\pm D_{M\Omega}^{J*}(\alpha\beta\gamma) = C_\pm(JM)\, D_{M\pm1,\,\Omega}^{J*}(\alpha\beta\gamma), \qquad \text{(D.28)}$$

$$J'_\pm D_{M\Omega}^{J*}(\alpha\beta\gamma) = -C_\pm(J\Omega)\, D_{M,\,\Omega\mp1}^{J*}(\alpha\beta\gamma). \qquad \text{(D.29)}$$

These equations show that the rotation matrix element does not have the mathematical properties of an angular momentum eigenfunction. One can conclude, with the support of mathematical certainty, that $D_{M\Omega}^{J}(\alpha\beta\gamma)$ is not an angular momentum eigenfunction. Armed with the ability to count to two, one can draw the same conclusion from the symbol $D_{M\Omega}^{J}(\alpha\beta\gamma)$. Nevertheless, essentially without exception in diatomic literature, the rotation matrix element is treated as if it were an angular momentum eigenfunction, and this is the source of considerable confusion.

Using equation (D.29) for the nonstandard case (a) basis states but using the standard result

$$S_\pm\, |S\Sigma\rangle = C_\pm(S\Sigma)\, |S,\, \Sigma\pm1\rangle \qquad \text{(D.30)}$$

for the electronic spin states because $|S\Sigma\rangle$ is standard angular momentum state of the type given in equation (D.25), one finds (table D.2)

Table D.2. Matrix elements of the rotational Hamiltonian (equation (D.6)).

$\langle nvJM\Omega\Lambda S\Sigma|H_{\rm rot}|nvJM\Omega\Lambda S\Sigma\rangle$

$= \langle nvJM\Omega\Lambda S\Sigma|B(r)(\mathbf{J}^2 + L_z^2 + \mathbf{S}^2 - 2J_z L_z - 2J_z S_z + 2L_z S_z)|nvJM\Omega\Lambda S\Sigma\rangle$

$= \langle nv|B(r)|nv\rangle[J(J+1) - \Omega^2 + S(S+1) - \Sigma^2]$

$= B_v[J(J+1) - \Omega^2 + S(S+1) - \Sigma^2]$

$\langle nvJM\Omega\Lambda S\Sigma|H_{\rm rot}|nvJM, \Omega\pm 1, \Lambda S, \Sigma\pm 1\rangle$

$= \langle nvJM\Omega\Lambda S\Sigma|-B(r)(J'_+ S'_- + J'_- S'_+)|nvJM, \Omega\pm 1, \Lambda S, \Sigma\pm 1\rangle$

$= \langle nv|B(r)|nv\rangle\, C_\pm(J\Omega)\, C_\pm(S\Sigma)$

$= B_v\sqrt{J(J+1) - \Omega(\Omega\pm 1)}\,\sqrt{S(S+1) - \Sigma(\Sigma\pm 1)}$

$\langle nvJM\Omega\Lambda S\Sigma|H_{\rm rot}|n'v'JM, \Omega\pm 1, \Lambda\pm 1, S\Sigma\rangle$

$= \langle nvJM\Omega\Lambda S\Sigma|-B(r)(J'_- L'_- + J'_+ L'_+)|n'v'JM, \Omega\pm 1, \Lambda\pm 1, S\Sigma\rangle$

$= \langle nv|B(r)(L'_+ + L'_-)|n'v'\rangle\, C_\pm(J\Omega)$

$= <BL>\sqrt{J(J+1) - \Omega(\Omega\pm 1)}$

$\langle nvJM\Omega\Lambda S\Sigma|H_{\rm rot}|n'v'JM\Omega, \Lambda\pm 1, S, \Sigma\mp 1\rangle$

$= \langle nvJM\Omega\Lambda S\Sigma|B(r)(L'_+ S'_- + L'_- S'_+)|n'v'JM\Omega, \Lambda\pm 1, S, \Sigma\mp 1\rangle$

$= \langle nv|B(r)(L'_+ + L'_-)|n'v'\rangle\, C_\mp(S\Sigma)$

$= <BL>\sqrt{S(S+1) - \Sigma(\Sigma\mp 1)}$

$$\langle nvJM\Omega\Lambda S\Sigma|H_{\mathrm{rot}}|nvJM, \Omega \mp 1, \Lambda S, \Sigma \pm 1\rangle$$

$$= -\langle nJM\Omega\Lambda S\Sigma|J'_+S'_- + J'_-S'_+|nJM, \Omega \mp 1, \Lambda S, \Sigma \pm 1\rangle \qquad \text{(D.31)}$$

$$= B_v\sqrt{J(J + 1) - \Omega(\Omega \pm 1)}\sqrt{S(S + 1) - \Sigma(\Sigma \pm 1)}.$$

$$\langle nvJM\Omega\Lambda S\Sigma|H_{\mathrm{rot}}|n'v'JM\Omega, \Lambda \mp + 1, S, \Sigma \pm 1\rangle$$

$$= -\langle nvJM\Omega\Lambda S\Sigma|L'_+S'_- + L'_-S'_+|nJM, \Omega \mp 1, \Lambda S, \Sigma \pm 1\rangle \qquad \text{(D.32)}$$

$$= \langle nv|B(r)(L'_+ + L'_-)|n'v'\rangle\sqrt{S(S + 1) - \Sigma(\Sigma - 1)}$$

$$+ \langle nv|B(r)(L'_+ + L'_-)|n'v'\rangle\sqrt{S(S + 1) - \Sigma(\Sigma + 1)}$$

$$= \langle BL\rangle[\sqrt{S(S + 1) - \Sigma(\Sigma - 1)} + \sqrt{S(S + 1) - \Sigma(\Sigma + 1)}] \qquad \text{(D.33)}$$

where

$$\langle BL\rangle = \langle nv|B(r)(L'_+ + L'_-)|n'v'\rangle \qquad \text{(D.34)}$$

Equation (D.31) and the example given in table D.3 show that the Hund's case (a) matrix representation of $\mathbf{R}^2$ is nondiagonal. Therefore, the matrix of the rotational Hamiltonian, equation (D.1), is also nondiagonal. Strictly speaking, the Hund's case (a) basis is not a valid eigenfunction. At best, it is a poor physical approximation. This is no way detracts from its use as a basis. Before the widespread availability of digital hardware and numerical algorithms, diagonalization of the 6×6 matrix of table D.3 presented an essentially impossible task, but today numerical diagonalization of this matrix is trivial with even a very modest computer. In current practice, in table D.4 the fact that the Hund's case (a) basis does not yield a diagonal Hamiltonian matrix adds only the single line of code, CALL JACOBI, to a computer program.

Table D.5 gives the results of fitting the same data of Amiot *et al* used in table D.1 but with a different $^2\Sigma$ state. A comparison between tables D.1 and D.5 shows that

Table D.3. Matrix elements of $\mathbf{R}^2$ in a state which is a mixture of $^2\Pi$ and $^2\Sigma$ case (a) basis states.

Λ'			-1	-1	1	1	0	0
	Σ'		$-1/2$	$1/2$	$-1/2$	$1/2$	$-1/2$	$1/2$
		Ω'	$-3/2$	$-1/2$	$1/2$	$3/2$	$-1/2$	$1/2$
Λ	Σ	Ω						
-1	$-1/2$	$-3/2$	119.000	10.954	0	0	0	0
-1	$1/2$	$-1/2$	10.954	121.000	0	0	0	0
1	$-1/2$	$1/2$	0	0	121.000	10.954	0	0
1	$1/2$	$3/2$	0	0	10.954	121.000	0	0
0	$-1/2$	$-1/2$	0	0	0	0	121.000	11.000
0	$1/2$	$1/2$	0	0	0	0	11.000	121.000

Table D.4. Matrix elements of $\mathbf{R}^2$ in a state which is a mixture of $^3\Pi$ and $^3\Sigma$ case (a) basis states.

Λ'			-1	-1	-1	1	1	1	0	0	0
	Σ'		-1	0	1	-1	0	1	-1	0	1
		Ω'	-2	-1	0	0	1	2	-1	0	1
Λ	Σ	Ω									
-1	-1	-2	107.000	14.697	0	0	0	0	0	0	0
-1	0	-1	14.697	111.000	14.832	0	0	0	0	0	0
-1	1	0	0	14.832	111.000	0	0	0	0	0	0
1	-1	0	0	0	0	111.000	14.832	0	0	0	0
1	0	1	0	0	0	14.832	111.000	14.697	0	0	0
1	1	2	0	0	0	0	14.697	107.000	0	0	0
0	-1	-1	0	0	0	0	0	0	110.000	14.832	0
0	0	0	0	0	0	0	0	0	14.832	112.000	14.832
0	1	1	0	0	0	0	0	0	0	14.832	110.000

Table D.5. Another fit to the data of Amiot, Bacis, and Guelachvili [1] with a different model Hamiltonian.

$X\,^2\Pi(v=1)$	$T_v = 2824.6331(5)$
$B_v = 1.678\,5715(27)$	$D_v = 5.4893(26) \times 10^{-6}$
$A_v = 122.7029(21)$	$A_{vJ} = 3.471(38) \times 10^{-4}$
$AL_+ = -223.8(1.3)$	$AL_{+J} = 6.9(2.3) \times 10^{-3}$
$BL_+ = -1.7549(95)$	$BL_{+J} = -4.0(1.6) \times 10^{-5}$
$X\,^2\Pi(v=0)$	$[T_v = 948.66]$
$B_v = 1.696\,1444(29)$	$D_v = 5.4735(29) \times 10^{-6}$
$A_v = 122.9498(23)$	$A_{vJ} = 3.561(42) \times 10^{-4}$
$AL_+ = -225.4(1.4)$	$AL_{+J} = 5.8(2.6) \times 10^{-3}$
$BL_+ = -1.79(10)$	$BL_{+J} = -3.9(1.8) \times 10^{-5}$
$A\,^2\Sigma^+(v=0)$	$[T_v = 70000.0]$
$[B_v = 1.2]$	$[D_v = 5.0 \times 10^{-6}]$

Notes. In this example the weak $^2\Sigma^+$ contribution comes from a fictitious $^2\Sigma^+$ state. Angular momentum range $0.5 \leqslant J' \leqslant 40.5$, includes 405 of 419 lines, accuracy $\Delta\bar{\nu} = 0.001$ cm^{-1} and $\sigma = 0.000\,38$ cm^{-1}.

only the mixing parameters AL_+ and BL_+ and the associated corrections for centrifugal stretching AL_{+J} and BL_{+J} are significantly influenced by the change in the parameters of the $^2\Sigma$ state.

Zare *et al* give the equations

$$o_v^\Sigma = \sum_{n'v'} \frac{\langle n'\ ^{2S+1}\Pi\ v'\ J'|\frac{1}{2}AL_+|n\ ^{2S+1}\Sigma\ v\ J\rangle^2}{E_{nvJ} - E_{n'v'J'}} \tag{D.35}$$

$$p_v^\Sigma = 4\sum_{n'v'} \frac{\langle n'\ ^{2S+1}\Pi\ v'\ J'|\frac{1}{2}AL_+|n^{2S+1}\Sigma v J\rangle\langle n'\ ^{2S+1}\Pi\ v'\ J'|BL_+|n\ ^{2S+1}\Sigma\ v\ J\rangle}{E_{nvJ} - E_{n'v'J'}} \tag{D.36}$$

$$q_v^\Sigma = 2\sum_{n'v'} \frac{\langle n'\ ^{2S+1}\Pi\ v'\ J'|AL_+|n\ ^{2S+1}\Sigma\ v\ J\rangle^2}{E_{nvJ} - E_{n'v'J'}} \tag{D.37}$$

for the Van Vleck transformation.

References

[1] Guelachvili G, Amiot C and Bacis R 1978 *Can. J. Phys.* **56** 251
[2] Macki A G and Wells J S 1991 *Wavenumber Calibration tables from Heterodyne Frequency Measurements* NIST Special Publication 821 (Washington DC: NIST)
[3] Zare R N, Schmeltekopf A L, Harrop W J and Albritton D L 1973 *J. Mol. Spectrosc.* **46** 37

[4] Engleman R Jr+, Rouse P E, Peek H M and Baiamonte V D 1970 *Eta and Gamma Band Systems of Nitric Oxide* Los Alamos Sci. Lab. Report LA-4364, Los Alamos, NM

[5] Hornkohl J O and Parigger C G 1996 *Am. J. Phys.* **64** 623

[6] Lefebvre-Brion H and Field R W 2004 *The Spectra and Dynamics of Diatomic Molecules* (New York: Elsevier/Academic)

[7] Thompson W J 1994 *Angular Momentum* (New York: Wiley)

Quantum Mechanics of the Diatomic Molecule (Second Edition)

Christian G Parigger and James O Hornkohl

Appendix E

Parity in diatomic molecules

This appendix communicates the application of the parity operator to the general diatomic eigenfunction [1]. The parity eigenvalue is a product of two factors, one that depends on the total angular momentum quantum number and a second constant factor that can be interpreted as the intrinsic parity of the molecule. These new results allow one to rigorously design an algorithm for the computation of diatomic spectra by utilizing that allowed transitions have nonvanishing rotational line strengths.

E.1 Introduction

The diatomic Hamiltonian matrix is historically parity-partitioned, thereby giving parity a more important role in diatomic spectroscopy than in atomic spectroscopy, e.g., see Zare *et al* [2]. Typically, a diatomic line list will include rotational parity designations for the lower levels [3]. Several authors, e.g., Hougen [4], Røeggen [5], Judd [6], and Larsson [7], have presented treatments of diatomic parity using the approximate Born–Oppenheimer separation of the diatomic eigenfunction into rotational, vibrational, and electronic factors.

In this work, operation of the parity operator on the general Wigner–Witmer [8] diatomic eigenfunction is used to yield the parity eigenvalues that are composed of a constant and an angular momentum dependent part. The computation of diatomic molecular spectra is accomplished without the need to explicitly include parity selection rules. The fundamental Wigner–Witmer diatomic eigenfunction simplifies the determination of rotational line strengths, i.e., Hönl–London factors. Allowed transitions are governed by nonzero rotational line strengths.

E.2 Parity operator

The discrete parity operation can be accomplished with a rotation and a reflection. The parity operator, $\mathcal{P}$, can be written as a product,

$$\mathcal{P} = \mathrm{C}_2 \, \sigma_v. \tag{E.1}$$

E-1

The determinant of the matrix representations $\sigma_v(y, z)$ and $C_2(x)$ in laboratory xyz-coordinates are -1 and $+1$, respectively. The C_2 operator is a proper rotation that can be expressed as a discrete transformation of Euler angles. The Euler angles are the arguments of the Wigner D-function used to formulate rotational symmetry; consequently, the eigenvalues of C_2 are controlled by the angular momentum, J. The $\sigma_v(y, z)$ operation results in a constant factor, and the C_2 operation yields the angular momentum dependent part of the parity eigenvalue.

E.3 Rotation operator and Wigner D-function

Molecular eigenfunctions are normally expressed in rotated coordinates. The representations of the eigenfunction in original and rotated coordinate systems are connected with the rotation operator, $\mathcal{R}(\alpha, \beta, \gamma)$; Euler angles α, β and γ; and the Wigner D-functions,

$$
\begin{aligned}
\langle \mathbf{r}_1, \mathbf{r}_2, \ldots, \mathbf{r}_\mathcal{N} \,|JM\rangle &= \sum_{\Omega=-J}^{J} \langle \mathbf{r}_1, \mathbf{r}_2, \ldots, \mathbf{r}_\mathcal{N} \,|\mathcal{R}(\alpha, \beta, \gamma)|J\Omega\rangle\langle J\Omega \,|\mathcal{R}^\dagger(\alpha, \beta, \gamma)|JM\rangle \\
&= \sum_{\Omega=-J}^{J} \langle \mathbf{r}_1', \mathbf{r}_2', \ldots, \mathbf{r}_\mathcal{N}' \,|J\Omega\rangle \, D_{M\Omega}^{J*}(\alpha, \beta, \gamma).
\end{aligned}
\tag{E.2}
$$

Angular momentum is the generator of rotations; therefore, one can expect that application of the discrete operator C_2 to the arguments of the D-function would yield a relationship between angular momentum and parity.

In terms of spatial and angular coordinates appropriate to the diatomic molecule, equation (E.2) can be written as

$$
\begin{aligned}
&\langle \rho, \zeta, \chi, \mathbf{r}_2, \ldots, \mathbf{r}_n, \mathrm{r}, \theta, \phi \,|nvJM\rangle \\
&= \sum_{\Omega=-J}^{J} \langle \rho, \zeta, \chi', \mathbf{r}_2', \ldots, \mathbf{r}_N', \mathrm{r}, \theta', \phi' \,|nvJ\Omega\rangle \, D_{M\Omega}^{J*}(\alpha, \beta, \gamma).
\end{aligned}
\tag{E.3}
$$

Here, ρ is the distance of one electron (the electron arbitrarily labeled 1 but it could be any one of the electrons), ζ is the distance of that electron above or below the plane that passes through the center of mass of the two nuclei (the coordinate origin), and χ is the angle of rotation of that electron about the internuclear vector $\mathbf{r}(\mathrm{r}, \theta, \phi)$. The vibrational quantum number, v, has been extracted from the quantum numbers collection, n, which represents all required quantum numbers except J, M, Ω, and v.

The variables ρ, ζ, and r are scalars, which are unaffected by rotations. The physical rotation ϕ and the angle of coordinate rotation α are about the same axis, namely the z-axis. The physical rotation θ and the angle of coordinate rotation β are also about the same axis, namely the first intermediate y-axis of the full coordinate rotation. The angles χ and γ are both rotations about the z'-axis. Thus,

$$
\phi' = \phi - \alpha, \quad \theta' = \theta - \beta, \quad \chi' = \chi - \gamma.
\tag{E.4}
$$

In coordinate rotations, one is at liberty to choose α, β, and γ. If one chooses for the angles $\alpha = \phi$, $\beta = \theta$, and $\gamma = \chi$, then all angular dependence of $\langle \rho, \zeta, \chi', \mathbf{r}'_2, \ldots, \mathbf{r}'_N, \mathrm{r}, \theta', \phi' | nvJ\Omega \rangle$ is removed. This yields the Wigner and Witmer [8] diatomic eigenfunction,

$$\langle \rho, \zeta, \chi, \mathbf{r}_2, \ldots, \mathbf{r}_n, \mathrm{r}, \theta, \phi | nJM \rangle$$
$$= \sum_{\Omega=-J}^{J} \langle \rho, \zeta, \mathbf{r}'_2, \ldots, \mathbf{r}'_N, \mathrm{r} | nv \rangle \, D^{J*}_{M\Omega}(\phi, \theta, \chi). \tag{E.5}$$

The values of the quantum numbers, J and Ω, influence the electronic–vibrational eigenfunction $\langle \rho, \zeta, \mathbf{r}'_2, \ldots, \mathbf{r}'_N, r | nv \rangle$, but the electronic–vibrational eigenfunction is not an angular momentum state vector.

E.4 Parity of diatomic states

Parity is rotationally invariant. Inversion of the signs of all rotated coordinates inverts the signs of all unrotated coordinates, and vice versa. Therefore, the parity operator can be represented by $C_2(x') \, \sigma_v(y', z')$. The application to the right-hand side of the Wigner–Witmer diatomic eigenfunction (E.5) yields the parity eigenvalues,

$$p = -p_{\Sigma} \, (-1)^J \qquad J \text{ half–integer}, \tag{E.6}$$

$$p = p_{\Sigma} \, (-1)^J \qquad J \text{ integer}. \tag{E.7}$$

The constant part of the parity eigenvalue, p_{Σ}, is labeled in accord with standard spectroscopic notation. The imaginary values of $(-1)^J$ occurring when J is half-integer can be avoided if one adopts the convention [3] to always subtract 1/2 from J when J is half-integer. With this convention, equation (E.6) is replaced by

$$p = -p_{\Sigma} \, (-1)^{J-1/2} \qquad J \text{ half–integer}. \tag{E.8}$$

The value of p_{Σ} does not depend upon quantum numbers. It is a global value applying to all states of a given molecule. If the diatomic molecule can be said to have an intrinsic parity, then it is clearly p_{Σ}. One would expect the product of the intrinsic parities of the fundamental particles composing the molecule to equal p_{Σ}.

E.5 Parity in an algorithm for computing diatomic spectra

The following describes an algorithm in which equations (E.7) and (E.8) become practical equations for computing diatomic parity.

Consider the algorithm for computation of the wavelengths and intensities in the spectrum of a molecule from the first principles of quantum mechanics. The upper H' and lower H Hamiltonian matrices are computed and numerically diagonalized by unitary matrices, U' and U. The upper $F'_{n'v'J'}$ and lower F_{nvJ} terms are the eigenvalues of the Hamiltonians,

$$F'_{n'v'J'} = U'^{\dagger} H' \, U' \tag{E.9a}$$

$$F_{nvJ} = U^\dagger H\, U,$$ (E.9b)

and the vacuum wave numbers, $\tilde{\nu}$, of the predicted spectral lines,

$$\tilde{\nu} = F'_{n'v'J'} - F_{nvJ},$$ (E.10)

are term differences. Of the very large number of computed term differences, only those for which the Condon and Shortley [9] line strength does not vanish are spectral lines. The line strength, $S(nvJ, n'v'J')$, is the sum over all M and M' of the irreducible tensor $T_k^{(q)}$ expectation values, $\langle nvJM\,|T_k^{(q)}|n'v'J'M'\rangle$. The exact separation of the total angular momentum in the Wigner–Witmer diatomic eigenfunction results in a diatomic line strength composed of two parts,

$$S(nvJ, n'v'J') = S(nv, n'v')\, S(J, J'),$$ (E.11)

the electronic–vibrational strength, $S(nv, n'v')$, and the unitless rotational line strength or Hönl–London factor, $S(J, J')$. The Born–Oppenheimer approximation separates the electronic–vibrational strength into electronic and vibrational parts. In the Hund's case (a) basis built from the Wigner–Witmer eigenfunction, the third Euler angle, $\chi = \gamma$, appears in the Wigner D-function,

$$
\begin{aligned}
|a\rangle &= |nvJM\Omega S\Sigma\rangle \\
&= \sqrt{\frac{2J+1}{8\pi^2}}\, \langle \rho,\, \zeta,\, \mathbf{r}'_2,\, \dots,\, \mathbf{r}'_N,\, \mathbf{r}\,|nv\rangle\, |S\Sigma\rangle\, D_{M\Omega}^{J*}(\phi,\, \theta,\, \chi).
\end{aligned}
$$ (E.12)

The algorithm for computation of the vacuum wave numbers, $\tilde{\nu}$, and diatomic spectral line strengths, $S(nvJ, n'v'J')$, is a straightforward application of quantum mechanics, but except for the very simplest molecules is also very far removed from the realm of the possible. However, with two very stringent caveats, the algorithm can be implemented for the diatomic molecule. The first caveat is that the vacuum wave numbers, $\tilde{\nu}$, for many spectral lines in many bands of a band system must have been experimentally measured with high accuracy, such as that provided by Fourier transform spectroscopy. The second caveat is that using semiempirical molecular constants one must be able to build upper and lower Hamiltonian matrices whose eigenvalue differences accurately predict the measured vacuum wave numbers. A fitting process is required [2]. One assumes trial values for the molecular constants, computes the spectral lines positions, $\tilde{\nu}$, and from the differences between $\tilde{\nu} - \tilde{\nu}_{\text{exp}}$ finds the corrections to the molecular parameters. The difference between computed and measured line positions will typically equal the measurement error margins.

As a specific example, the line position data of Faris and Cosby [10] are used for the NO beta (3,0) band for the purpose of then creating a complete line list for the band with line strengths. Figure E.1 illustrates a spectrum generated from the NO line list.

A multiphoton 1+1 excitation was used to observe 10 of the 12 possible branches [10], with particular attention given to the parity designations of the numerous Λ doublets. These data are particularly suited for testing applications of the algorithm for the calculation of diatomic spectra. A total of 428 lines were fitted with a
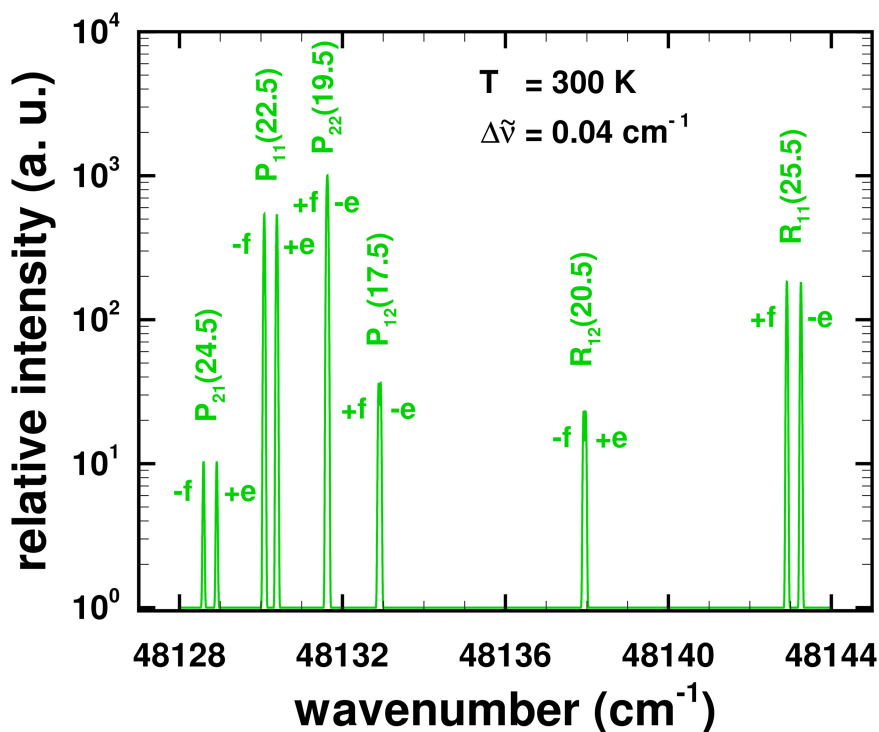
Figure E.1. Section of computed spectrum of the NO $B\,^2\Pi - X\,^2\Pi$ (3,0) band. The lines are further described in table E.1 [1].

standard deviation of 0.030 cm^{-1}, and a line list having no missing lines for the range of upper and lower J values was computed. Table E.1 provides details of the lines displayed in figure E.1. The computed parity eigenvalues agree with those assigned by Faris and Cosby [10].

The Hund's case (a) basis is mathematically complete. A sum of basis functions, $|a\rangle$, can be quantitatively very accurate. The parity operator, $\mathcal{P}$, commutes with the Hamiltonian. Thus, the orthogonal matrix that diagonalizes the case (a) representation of the Hamiltonian will also diagonalize the case (a) representation of $\mathcal{P}$.

The exact separation of the coordinates of the total angular momentum in the Wigner D-function greatly simplifies implementation of the algorithm, which uses nonvanishing line strengths to determine if a computed term difference represents an allowed spectral line. The Hönl–London factors are computed from the Hund's case (a) transition moment and the matrices, U and U', which diagonalize the upper and lower Hamiltonians.

A single selection rule handles all types of diatomic spectra. If the Hönl–London factor, $S(J, J')$, is nonvanishing, then the transition is allowed. Parity plays no part in the fitting process that determines the molecular parameters, but the parity eigenvalues are computed from the finalized values of the molecular parameters. The presented algorithm can be used to predict molecular spectra for the purpose of fitting measured data [11].

Table E.1. Lines of the NO B $^2\Pi - X$ $^2\Pi$ (3,0) band (see figure E.1).

J		p	$F_{J'}$ (cm^{-1})	F_J (cm^{-1})	$\tilde{\nu}$ (cm^{-1})	$S(J, J')$	$\tilde{\nu}$-$\tilde{\nu}_{\text{exp}}$ (cm^{-1})
24.5	P_{21}	$-f$	49 111.456	982.866	48 128.590	0.813	0.021
24.5	P_{21}	$+e$	49 111.501	982.588	48 128.914	0.812	0.078
22.5	P_{11}	$-f$	48 952.618	822.538	48 130.080	21.749	0.014
22.5	P_{11}	$+e$	48 952.673	822.282	48 130.390	21.805	-0.020
19.5	P_{22}	$+f$	48 876.118	744.504	48 131.615	18.832	-0.007
19.5	P_{22}	$-e$	48 876.146	744.505	48 131.641	18.786	
17.5	P_{12}	$+f$	48 747.194	614.306	48 132.888	0.515	-0.013
17.5	P_{12}	$-e$	48 747.244	614.307	48 132.936	0.527	-0.012
20.5	R_{12}	$-f$	48 952.618	814.699	48 137.919	0.881	0.034
20.5	R_{12}	$+e$	48 952.673	814.701	48 137.971	0.880	-0.077
25.5	R_{11}	$+f$	49 210.930	1068.021	48 142.908	25.424	0.034
25.5	R_{11}	$-e$	49 210.985	1067.731	48 143.254	25.317	-0.018

Notes. The Hönl–London factors, $S(J, J')$, and parity eigenvalues, p, are derived from numerical diagonalization of Hamiltonians in Hund's case (a) basis. The $P_{22(19.5)}$ Λ doublet is not resolved in the experiments [10].

References

[1] Hornkohl J O and Parigger C G 2017 *Int. J. Mol. Theor. Phys.* **1** 00103

[2] Zare R N, Schmeltekopf A L, Harrop W J and Albritton D L 1973 *J. Mol. Spectrosc.* **46** 37

[3] Brown J M, Hougen J T, Huber K P, Johns J W C, Kopp I, Lefebvre-Brion H, Merer A J, Ramsay D A, Rostas J and Zare R N 1975 *J. Mol. Spectrosc.* **55** 500

[4] Hougen J T 2021 *The Calculation of Rotational Energy Levels and Rotational Line Intensities in Diatomic Molecules* (Gaithersburg, MD: National Institute of Standards and Technology) http://physics.nist.gov/DiatomicCalculations, 2001. Originally published as *The Calculation of Rotational Energy Levels and Rotational Line Intensities in Diatomic Molecules*, J. T. Hougen, NBS Monograph 115 (1970)

[5] Røeggen I 1971 *Theor. Chim. Acta* **21** 398

[6] Judd B 1975 *Angular Momentum Theory for Diatomic Molecules* (New York: Academic)

[7] Larsson M 1981 *Phys. Scr.* **23** 835

[8] Wigner E and Witmer E E 1928 *Z. Phys.* **51** 859 H. Hettema, *Quantum Chemistry: Classic Scientific Papers*, p. 287, (Singapore: World Scientific) 2000

[9] Condon E U and Shortley G 1953 *The Theory of Atomic Spectra* (Cambridge: Cambridge University Press)

[10] Faris G W and Cosby P C 1992 *J. Chem. Phys.* **97** 7073

[11] Parigger C G, Woods A C, Surmick D M, Gautam G, Witte M J and Hornkohl J O 2015 *Spectrochim. Acta* B **107** 132

Quantum Mechanics of the Diatomic Molecule (Second Edition)

Christian G Parigger and James O Hornkohl

Appendix F

Rotational line strengths for the CN BX (5,4) band

This appendix communicates rotational line strengths for the cyanide (CN) $B\,^2\Sigma^+ - X\,^2\Sigma^+$ (5,4) band [1]. Rotational line strengths, computed from eigenvectors of Hund's case (a) matrix representations of the upper and lower Hamiltonians using Wigner–Witmer basis functions, show a larger than expected influence from the well-known perturbation in the (5,4) band. Comparisons with National Solar Observatory (NSO) experimental Fourier transform spectroscopy data reveal nice agreement of measured and predicted spectra.

F.1 Introduction

The CN violet $B\,^2\Sigma^+ - X\,^2\Sigma^+$ band system is one of the most studied band systems. Ram *et al* [2] and Brooke *et al* [3] have summarized the available experimental and theoretical information. Of the many known bands in the violet system, only the (5,4) band is considered here. This band exhibits a weak, quantitatively understood perturbation [4] caused by mixing of the $v = 17$ level of $A^2\Pi$ with the $v = 5$ level of $B\,^2\Sigma^+$. The particular perturbation of the CN (5,4) band is not considered in the study by Brooke *et al* [3] but is evaluated in this work by isolating the spectral features of this band that is part of the CN violet system. Numerical diagonalizations of upper and lower Hamiltonians with and without the perturbation are investigated and compared with available experimental spectra. The simulations rely on determining rotational strengths without parity-partitioned Hamiltonians. It is anticipated that the investigated (5,4) band modifications can be possibly confirmed with the new PGOPHER program that was recently released by Western [5].

F.2 CN (5,4) band spectra

For the computation of rotational spectra, the square of transition moments are numerically computed using the eigenvectors of upper and lower Hamiltonians. This approach can also be selected in the new PGOPHER program [5]. For the diatomic molecule, the results effectively yield the Hönl–London factors, yet we do not utilize

tabulated Hönl–London factors that are available in standard textbooks. Table F.1, and figures F.1 and F.2 compare results obtained with and without taking into account the mixing. Results of modeling the angular momentum states of the upper $v = 5$ vibrational level as a mixture of $^2\Sigma$ and $^2\Pi$ Hund's case (a) basis functions, a so-called 'de-perturbation" or perturbation analysis, agree well that of Ito *et al* [4] whose used the line position measurements of Engleman [6]. The 100 lines of the more recent data of Ram *et al* [2] were fitted with a standard deviation of 0.025 cm^{-1}. Failure to include spin-orbit mixing of the $B^2\Sigma^+$ and $A^2\Pi$ basis states increased the standard deviation to 0.25 cm^{-1}.

The table and synthetic spectra reveal that the changes caused by spin-orbit mixing are relatively very much larger for the rotational line strengths, $S(J', J)$, than for the line positions, $\tilde\nu$. The simulation results compare nicely with measured spectra [2] available from the NSO at Kitt Peak [7]. Figure F.3 displays the recorded and simulated spectra for a resolution of 0.03 cm^{-1}.

The influence of $^2\Sigma^+ + {}^2\Pi$ mixing on the rotational line strengths, $S(J', J)$, was recognized because computation of $S(J', J)$ is an integral part of the unique line position fitting algorithm. Upper and lower Hamiltonian matrices in the Hund's case (a) basis are numerically diagonalized, and the spectral line vacuum wave number $\tilde\nu$ is the difference between upper and lower Hamiltonian eigenvalues.

Table F.1. Lines in the CN $B^2\Sigma^+ X^2\Sigma^+$ (5,4) band near the perturbation.

J'	J		p'	$\tilde\nu$	$S_{J'J}$	$\Delta\tilde\nu$	$S_{J'J}^{(0)}$	$\Delta\tilde\nu^{(0)}$
9.5	8.5	R_{11}	$-e$	28 013.117	9.474	-0.010	9.474	0.337
9.5	8.5	R_{22}	$+f$	28 017.421	9.474	0.001	9.474	-0.059
10.5	9.5	R_{11}	$+e$	28 016.992	9.1988	-0.004	10.476	0.600
10.5	9.5	R_{22}	$-f$	28 021.651	11.171	-0.000	10.476	-0.067
11.5	10.5	R_{11}	$-e$	28 020.540	7.868	-0.041	11.478	1.193
11.5	10.5	R_{22}	$+f$	28 025.866	12.240	0.006	11.478	-0.067
12.5	11.5	R_{22}	$-f$	28 030.125	13.288	0.007	12.480	-0.072
12.5	11.5	R_{11}	$+e$	28 030.431	13.812		12.480	
13.5	12.5	R_{11}	$-e$	28 032.081	17.455	-0.053	13.481	-1.870
13.5	12.5	R_{22}	$+f$	28 034.428	14.325	0.011	13.481	-0.073
14.5	13.5	R_{11}	$+e$	28 035.672	17.919	-0.005	14.483	-1.102
14.5	13.5	R_{22}	$-f$	28 038.773	15.356	0.013	14.483	-0.076
15.5	14.5	R_{11}	$-e$	28 039.742	18.442	0.007	15.484	-0.807
15.5	14.5	R_{22}	$+f$	28 043.161	16.383	0.009	15.484	-0.084
16.5	15.5	R_{11}	$+e$	28 043.989	19.132	0.011	16.485	-0.655
16.5	15.5	R_{22}	$-f$	28 047.590	17.405	0.006	16.485	-0.091

Notes. $\tilde\nu$ are the fitted line positions, $S(J', J)$ are the rotational line strengths computed in the fitting algorithm. $S^{(0)}(J', J)$ and $\Delta\tilde\nu^{(0)}$ are the line strengths and errors in the fitted line positions, respectively, when the off-diagonal spin-orbit coupling constants $\langle AL + \rangle$ and $\langle BL + \rangle$ are set equal to 0. Spin-orbit mixing of $B^2\Sigma^+$ and $A^2\Pi$ shifts the upper e parity levels. An error in the $\nu(J', J)$ associated with these upper e parity levels is produced if the mixing is ignored. A relatively large fractional error, e.g., -3.974/17.455 versus -1.870/28032 for $R_{11}(12.5)$, can occur in the rotational line strengths, $S(J', J)$.
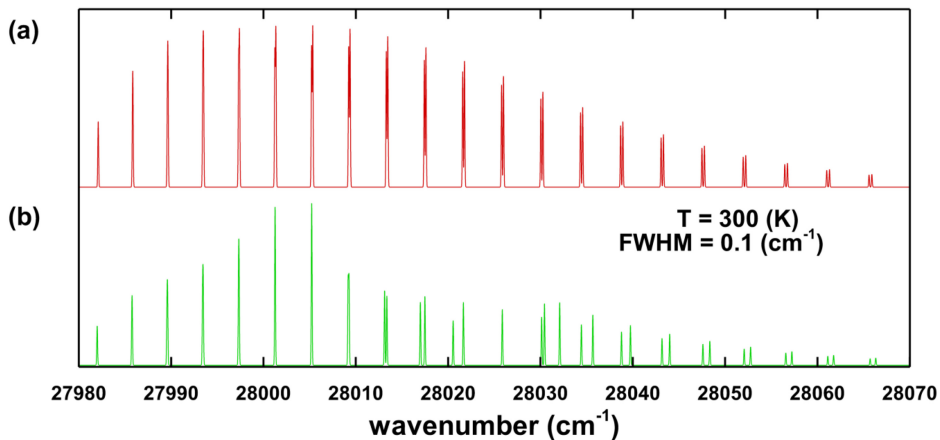
Figure F.1. Synthetic emission spectra showing the influence of inclusion of the $v = 17$, $A^2\Pi$ basis in the upper $v = 5$ state of the CN violet (5,4) band. In the upper spectrum, (a), the upper states are pure $^2\Sigma^+$. The $v = 17$, $A^2\Pi$ energy eigenvalues lie very near the $v = 5$, $B^2\Sigma^+$ eigenvalues, and this explains the large influence of the $A^2\Pi$ basis. In the lower spectrum, (b), the upper states are treated as the sum $c_\Sigma\,{}^2\Sigma^+ + c_\Pi\,{}^2\Pi$ with $c_\Sigma \gg c_\Pi$. Only R-branch lines are shown here, including those given in table F.1 [1].
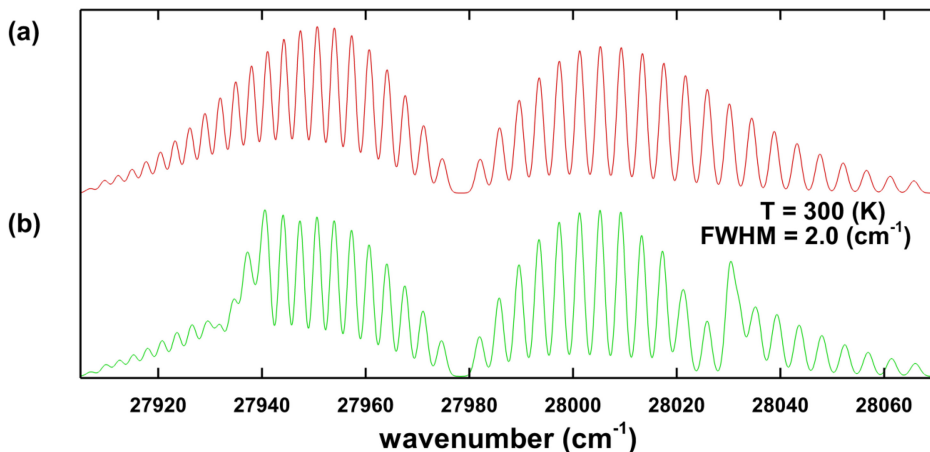
Figure F.2. The lower resolution spectra include both the P and R branches. (a) pure, (b) addition of a small amount of $^2\Pi$ to the upper basis affects the lower spectrum of the violet (5,4) band, even at low resolution [1].

To determine which of the many eigenvalue differences represent allowed spectral lines, the factor $S(J', J)$ is computed from the upper and lower eigenvectors for each eigenvalue difference. A nonvanishing $S(J', J)$ denotes an allowed diatomic spectral line. Parity-partitioned effective Hamiltonians are not used. Parity and branch designation are not required in the fitting algorithm. Input data to the fitting program is a table of vacuum wave number $\tilde{\nu}$ versus J' and J. The nonvanishing of the rotational strength is the only selection rule used. Applications of this rule lead to the establishment of spectral databases for diatomic molecular spectroscopy of
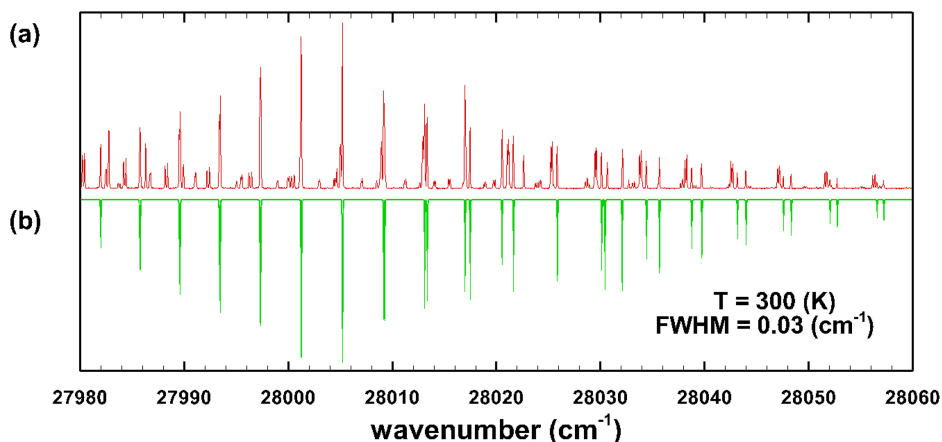
Figure F.3. Comparison of measured and simulated spectra. (a) Segment of the recorded [2] Fourier transform spectrum 920 212R0.005 [7], (b) computed spectrum for a temperature of 300 K and a spectral resolution of 0.03 cm^{-1}. The computed (5.4) band is flipped vertically to show how the predicted line positions of the R-branch match the vacuum wave numbers of the experimental spectrum [1].

selected transitions [8]. Over and above the PGOPHER program [5], there are other extensive efforts in predicting diatomic molecular spectra including, such as the so-called DUO program [9] for diatomic spectroscopy.

F.3 Wigner–Witmer diatomic eigenfunction

The Hund's case (a) basis functions were derived from the Wigner and Witmer [10] diatomic eigenfunction,

$$\langle \rho, \zeta, \chi, \mathbf{r}_2, \ldots, \mathbf{r}_N, r, \theta, \phi \,|nvJM\rangle = \sum_{\Omega=-J}^{J} \langle \rho, \zeta, \mathbf{r}'_2, \ldots, \mathbf{r}'_N, r \,|nv\rangle \, D^{J*}_{M\Omega}(\phi, \theta, \chi). \quad \text{(F.1)}$$

The coordinates are ρ the distance of one electron (the electron arbitrarily labeled 1 but it could be any one of the electrons) from the internuclear vector $\mathbf{r}(r, \theta, \phi)$, the distance ζ of that electron above or below the plane perpendicular to $\mathbf{r}$ and passing through the center of mass of the two nuclei (the coordinate origin), the angle χ for rotation of that electron about the internuclear vector $\mathbf{r}$, and the remaining electronic coordinates $\mathbf{r}_2, \ldots, \mathbf{r}_N$ in the fixed and $\mathbf{r}'_2, \ldots, \mathbf{r}'_N$ in the rotating coordinate system. The vibrational quantum number v has been extracted from the quantum numbers collection n which represents all required quantum numbers except J, M, Ω, and v. The Wigner–Witmer diatomic eigenfunction has no application in polyatomic theory, but for the diatomic molecule the exact separation of the Euler angles is a clear advantage over the Born–Oppenheimer approximation for the diatomic molecule in which the angle of electronic rotation, χ, is unnecessarily separated from the angles describing nuclear rotation, θ and ϕ. Equation (F.1) can be derived by writing the general equation for coordinate (passive) rotations α, β, and γ of the eigenfunction, replacing two generic coordinate vectors with the

diatomic vectors $\mathbf{r}(r, \theta, \phi)$ and $\mathbf{r}'(\rho, \zeta, \chi)$, and equating the angles of coordinate rotation to the angles of physical rotation ϕ, θ, and ϕ. The general equation for coordinate rotation holds in isotropic space, and therefore the quantum numbers J, M, and Ω in the Wigner–Witmer eigenfunction include all electronic and nuclear spins. If nuclear spin were to be included, J, M, and Ω would be replaced by F, M_F, and Ω_F, but hyperfine structure is not resolved in the (5, 4) band data reported by [2], and equation (F.1) is written with the appropriate spectroscopic quantum numbers.

It is worth noting that the rotation matrix element $D_{M\Omega}^{J}(\phi, \theta, \chi)$ and its complex conjugate $D_{M\Omega}^{J*}(\phi, \theta, \chi)$ do not fully possess the mathematical properties of quantum mechanical angular momentum. It is well known that a sum of Wigner D-functions is required to build an angular momentum state. The equation

$$J'_\pm \, D_{M\Omega}^{J*}(\phi, \theta, \chi) = \sqrt{J(J+1) - \Omega(\Omega \mp 1)} \, D_{M,\,\Omega \mp 1}^{J*}(\phi, \theta, \chi) \tag{F.2}$$

is not a phase convention [11–13] but a mathematical result readily obtained from equation (F.1) and

$$J'_\pm \, |J\Omega\rangle = \sqrt{J(J+1) - \Omega(\Omega \pm 1)} \, |J, \Omega \pm 1\rangle, \tag{F.3}$$

in which the prime on the operator $J'_\pm$ indicates that it is written in the rotated coordinate system where the appropriate magnetic quantum number Ω.

F.4 Hund's basis functions

The Hund's case (a) basis function based upon the Wigner–Witmer diatomic eigenfunction is

$$\begin{aligned}
|a\rangle &= \langle \rho, \zeta, \chi, \mathbf{r}'_2, \ldots, \mathbf{r}'_\mathcal{N}, r, \theta, \phi \,| nvJMS\Lambda\Sigma\Omega \rangle \\
&= \sqrt{\frac{2J+1}{8\pi^2}} \, \langle \rho, \zeta, \mathbf{r}'_2, \ldots, \mathbf{r}'_\mathcal{N}, r \,| nv \rangle \, |S\Sigma\rangle \, D_{M\Omega}^{J*}(\phi, \theta, \chi).
\end{aligned} \tag{F.4}$$

As noted above, a sum of $|a\rangle$ basis functions is required to build an eigenstate of angular momentum. The basis function would also not be an eigenstate of the parity operator. The case (a) matrix elements, $p_{ij}^{(a)}$, of the parity operator $\mathcal{P}$,

$$p_{ij}^{(a)} = p_\Sigma (-)^J \delta(J_i J_j) \, \delta(\Omega_i, -\Omega_j) \, \delta(\Lambda_i, -\Lambda_i) \, \delta(n_i n_j), \tag{F.5}$$

show that a single $|a\rangle$ basis function is not an eigenstate of parity. The procedure called parity symmetrization adds $|JM\Omega\rangle$ and $|JM, -\Omega\rangle$ basis functions, thereby destroying the second magnetic quantum number Ω and yielding a function which at least possesses the minimal mathematical properties of an eigenstate of angular momentum, parity, and the other members of the complete set of commuting operators. The general procedure would be to continue adding basis functions to the upper and lower bases until eigenvalue differences between the upper and lower Hamiltonians accurately predict measured line positions.

F.5 The upper Hamiltonian matrix for the (5,4) band

Electronic spin **S** interactions with electronic orbital momentum **L** and nuclear orbital momentum **R** produce both diagonal and off-diagonal matrix elements in the Hund's case (a) representation of the Hamiltonian. The off-diagonal elements connect different basis states. For example, both of the mentioned spin-orbit interactions connect $^2\Sigma^+$ and $^2\Pi$. Because Van Vleck transformed Hamiltonians are not used, the appropriate parameters for the strength of these interactions are $\langle AL + \rangle$ and $\langle BL + \rangle$. Table F.2 lists the molecular parameters used in the Hamiltonian matrices. Tables F.3 and F.4 show the Hamiltonian matrices without and with spin-orbit interactions, respectively.

F.6 A diatomic line position fitting algorithm

A basic tool for the diatomic spectroscopist is a computer program that accepts a table of experimentally measured vacuum wave numbers $\tilde{\nu}_{\mathrm{exp}}$ versus J' and J, and outputs a set of molecular parameters with which one can reproduce the $\tilde{\nu}_{\mathrm{exp}}$ with a standard deviation comparable to the estimated experimental error. In practice, an experimental line list frequently shows gaps, vis. spectral lines are missing. Following a successful fitting process, one can use the molecular parameters to predict all lines. A computed line list is especially useful when it includes the Condon and Shortley [15] line strength from which the Einstein coefficients and oscillator strength [16, 17] and the HITRAN line strength [18] can be calculated. A feature of the line fitting program described below is its use of nonzero rotational strengths (see equation (F.8)) to mark which of the many computed differences between upper and lower term values represents the vacuum wave number of an allowed spectral line.

Table F.2. Molecular parameters used in this work, which relies on Hamiltonians that are not parity-partitioned.

	$X\,^2\Sigma^+$	$B\,^2\Sigma^+$	$A\,^2\Pi$
	$v = 4$	$v = 5$	$v = 17$
B_v	1.820 866(13)	1.845 727(13)	1.404 833
D_v	$6.172(36) \times 10^{-6}$	$8.003(38) \times 10^{-6}$	5.66×10^{-6}
A_v			-50.5253
γ_v	$-1.98(43) \times 10^{-4}$	$-1.921(44) \times 10^{-2}$	
γ_{D_v}	$-1.98(43) \times 10^{-4}$		
T_v	8011.7871	35 990.1780(25)	36 010.5732
$<AL + >$		4.25(0.03)	
$<BL + >$		0.0205(0.001)	

Notes. Values not followed by a number in parenthesis were held fixed or an error estimate was not computed. A value in parenthesis is the standard deviation in the fitted value. Parameters for the $A\,^2\Pi$ state were fitted by the Nelder–Mead minimization algorithm using values given by Brooke et al [3] as trial values. Error estimates were not computed, and the values of Brooke et al [3] were only very slightly changed.

Table F.3. Hamiltonian matrix for states modeled as the mixture of $^2\Sigma^+$ and $^2\Pi$ basis states.

				v	5	5	17	17	17	17
				Λ	0	0	-1	-1	1	1
				Σ	-0.5	0.5	-0.5	0.5	-0.5	0.5
v	Λ	Σ	Ω		-0.5	0.5	-1.5	-0.5	0.5	1.5
5	0	-0.5	-0.5		36 351.6409	-25.6707	0	0	0	0
5	0	0.5	0.5		-25.6707	36 351.6409	0	0	0	0
17	-1	-0.5	-1.5		0	0	36 257.6340	-19.5866	0	0
17	-1	0.5	-0.5		0	0	-19.5866	36 310.9646	0	0
17	1	-0.5	0.5		0	0	0	0	36 310.9646	-19.5866
17	1	0.5	1.5		0	0	0	0	-19.5866	36 257.6340
			E_{vJ}		36 377.3116	36 325.9702	36 251.2135	36 317.3851	36 317.3851	36 251.2135

Off-diagonal spin-orbit coupling has been removed. Consequently, the 2×2 matrices along the main diagonal are independent, and could be individually diagonalized. The bottom row contains the energy eigenvalues. Using matrices like these to model upper states of the CN violet (5,4) band, the 100 experimental spectral lines reported by Ram *et al* [2] were fitted with a standard deviation of 0.25 cm^{-1}. This Hamiltonian was computed for $\langle AL+\rangle = \langle BL+\rangle = 0$ but is otherwise identical to the Hamiltonian in table F.4. Standard Hund's case (a) matrix elements [11, 13] were used.

Table F.4. Off-diagonal spin-orbit coupling 6×6 matrix.

v	Λ	Σ	Ω	5	5	17	17	17	17
				0	0	−1	−1	1	1
				−0.5	0.5	−0.5	0.5	−0.5	0.5
				−0.5	0.5	−1.5	−0.5	0.5	1.5
5	0	−0.5	−0.5	36 351.6409	−25.6707	2.8566	2.3274	2.8639	0
5	0	0.5	0.5	−25.6707	36 351.6409	0	2.8639	2.3274	2.8566
17	−1	−0.5	−1.5	2.8566	0	36 257.6340	−19.5866	0	0
17	−1	0.5	−0.5	2.3274	2.8639	−19.5866	36 310.9646	0	0
17	1	−0.5	0.5	2.8639	2.3274	0	0	36 310.9646	−19.5866
17	1	0.5	1.5	0	2.8566	0	0	−19.5866	36 257.6340
E_{mJ}				36 377.3957	36 327.7869	36 250.9625	36 317.3525	36 315.8194	36 251.1620

F-8

Consequently, the fitting process creates a complete line list including rotational factors. Parity plays no part in the fitting process, but the same orthogonal matrix that diagonalizes the case (a) from the three independent 2×2 matrices of table F.3, the off-diagonal matrix elements mix the Hund's case (a) basis states, and the standard deviation of the spectral line fit mentioned in table F.3 is reduced by a factor of 10 to 0.025 cm^{-1}. The spin-orbit coupling constants $\langle AL + \rangle = 4.25(0.03)$ and $\langle BL + \rangle = 0.205(0.001)$ were used in computation of this Hamiltonian. This single 6×6 matrix describing $^2\Pi -^2\Sigma^+$ mixing can be compared with the two 3×3 parity-partitioned matrices of Brown and Carrington [14].

The Hamiltonian matrix will also diagonalize the case (a) parity matrix whose elements are given in equation (F.5). The $p = \pm 1$ parity eigenvalue becomes a computed quantity, and the *e/f* parity designation is established from the parity eigenvalue using the accepted convention Brown *et al* [19].

Trial values of upper and lower state molecular parameters, typically taken from previous works by other for the band system in question, are used to compute upper H' and lower H Hamiltonian matrices in the case (a) basis given by equation (F.4) for specific values of J' and J. The upper and lower Hamiltonians are numerically diagonalized,

$$T' = \tilde{U}' \, H' \, U' \tag{F.6a}$$

$$T = \tilde{U} \, H \, U \tag{F.6b}$$

giving the upper T' and lower T term values. The vacuum wave number $\tilde{\nu}$ is determined,

$$\tilde{\nu}_{ij} = T'_i - T_j, \tag{F.7}$$

and the rotational strength is evaluated,

$$S_{ij}(J', J) = (2J + 1) \left| \sum_n \sum_m \tilde{U}'_{in} \langle J\Omega; q, \Omega' - \Omega \,|J'\Omega'\rangle \, U_{mj} \, \delta(\Sigma'_n \Sigma_m) \right|^2. \tag{F.8}$$

The degree of the tensor operator, q, responsible for the transitions amounts to $q = 1$ for electric dipole transitions. For a nonzero rotational factors, $S(J', J)$, the vacuum wave number $\tilde{\nu}_{ij}$ is added to a table of computed line positions to be compared with the experimental list $\tilde{\nu}_{\exp}$ versus J' and J. The Clebsch–Gordan coefficient, $\langle J\Omega; q, \Omega' - \Omega \,|J'\Omega'\rangle$, is the same one appearing in the pure case (a)—case (a) formulae for $S(J', J)$. For a specific values of J' and J, one constructs tables for $\tilde{\nu}_{\exp}$ and computed $\tilde{\nu}_{ij}$. The errors $\Delta\tilde{\nu}_{ij}$,

$$\Delta\tilde{\nu}_{ij} = \tilde{\nu}_{ij} - \tilde{\nu}_{\exp}, \tag{F.9}$$

are computed where each $\tilde{\nu}_{ij}$ is the one that most closely equals one of the $\tilde{\nu}_{\exp}$. Once values of $\tilde{\nu}_{ij}$ and $\tilde{\nu}_{\exp}$ are matched, each is marked unavailable until a new list of $\tilde{\nu}_{ij}$ is computed. The indicated computations are performed for all values of J' and J in the experimental line list, and corrections to the trial values of the molecular

parameters are subsequently determined from the resulting $\Delta\tilde{\nu}_{ij}$. The entire process is iterated until the parameter corrections become negligibly small. As this fitting process successfully concludes, one obtains a set of molecular parameters that predict the measured line positions $\tilde{\nu}_{\text{exp}}$ with a standard deviation that essentially equals the experimental estimates for the accuracy of the $\tilde{\nu}_{\text{exp}}$.

F.7 Discussion

The influence on intensities in the (5,4) band of the CN violet system caused by the weak spin-orbit mixing, figures F.1 and F.2, is significantly larger than initially anticipated. This was noticed because computation of the rotational strengths is an integral part of our line position fitting program. The eigenvectors that diagonalize the Hamiltonian to yield fitted line position $\tilde{\nu}$ also yield $S(J', J)$. The eigenvectors of Van Vleck transformed effective Hamiltonians are rarely discussed in the literature; equally, the calculations of Hönl–London factors appear problematic. In established diatomic molecular practice, Hönl–London factors are determined independently of line positions. Analytical approximations utilize the parameter $Y = A/B$ to account for the influence of spin-orbit interaction on $S(J', J)$. Kovács [20] gives many examples, Li *et al* [21] give a more recent application. These analytical approximations can accurately account for intermediate spin-orbit coupling which smooth transitions between case (a) and case (b) with increasing J' and J, but show limited sensitivity to abrupt changes in $S(J', J)$ near perturbations such as those seen the (5, 4) band in the CN violet system.

It is noted in passing that the $S^{(0)}(J', J)$ in table F.1 that describe rotational strengths without off-diagonal spin-orbit constants, are exactly equal to pure case (b) Hönl–London factors for $^2\Sigma^+ - \,^2\Sigma^+$ transitions, even though all computations were carried out in the Hund's case (a) basis. This observation merely makes the point that the Hund's case (b) is defined due to the physical absence of spin-orbit coupling.

F.8 Conclusion

The Wigner–Witmer diatomic eigenfunction makes it possible to form an exact, mathematical connection between computation of $\tilde{\nu}$ and $S(J', J)$ in a single algorithm. The concept of the nonvanishing rotational strengths as the omnipotent selection rule initially conceived as a simplifying convenience in a computer algorithm is now seen to be more valuable, as evidenced in this work's analysis of the CN (5,4) band perturbations by isolating a specific branch. Future work is planned for comparisons of the CN (10,10) band spectra that include perturbation and that show promising agreements with experiments and PGOPHER predictions.

References

[1] Hornkohl J O and Parigger C G 2017 *Int. J. Mol. Theor. Phys.* **1** 00102

[2] Ram R S, Davis S P, Wallace L, Englman R, Appadoo D R T and Bernath P F 2006 *J. Mol. Spectrosc.* **237** 225

[3] Brooke J S A, Ram R S, Western C M, Li G, Schwenke D W and Bernath P F 2014 *J. Quant. Spectrosc. Radiat. Transfer* **210** Astrophys. J. Supp. Series

[4] Ito H, Fukuda Y, Ozaki Y, Kondow T and Kuchitsu K 1987 *J. Mol. Spectrosc.* **121** 84

[5] Western C M 2017 *J. Quant. Spectrosc. Radiat. Transfer* **186** 221

[6] Engleman R 1974 *J. Mol. Spectrosc.* **49** 106

[7] Kroto H W 2016 National Solar Observatory (NSO) at Kitt Peak, McMath-Pierce Fourier Transform Spectrometer (FTS) data, (accessed December 20, 2016). ftp://vso.nso.edu/FTS_cdrom/FTS30/920212R0.005.

[8] Parigger C G, Woods A C, Surmick D M, Gautam G, Witte M J and Hornkohl J O 2015 *Spectrochim. Acta* B **107** 132

[9] Yurchenko S N, Lodi L, Tennyson J and Stolyarov A V 2016 *Comput. Phys. Commun.* **202** 262

[10] Wigner E and Witmer E E 1928 *Z. Phys.* **51** 859
Hettema H 2000 *Quantum Chemistry: Classic Scientific Papers* p 287 (Singapore: World Scientific)

[11] Zare R N, Schmeltekopf A L, Harrop W J and Albritton D L 1973 *J. Mol. Spectrosc.* **46** 37

[12] Howard B J and Brown J M 1976 *J. Mol. Phys.* **31** 1517

[13] Lefebvre-Brion H and Field R W 2004 *The Spectra and Dynamics of Diatomic Molecules* (New York: Elsevier/Academic)

[14] Brown J M and Carrington A 2003 *Rotational Spectroscopy of Diatomic Molecules* (Cambridge: Cambridge University Press)

[15] Condon E U and Shortley G 1953 *The Theory of Atomic Spectra* (Cambridge: Cambridge University Press)

[16] Hilborn R C 1982 *Am. J. Phys.* **50** 982 http://arxiv.org/ftp/physics/papers/0202/0202029.pdf

[17] Thorne A P 1988 *Spectrophysics* 2nd edn (London: Chapman and Hall)

[18] Rothman L S *et al* 1998 *J. Quant. Spectrosc. Radiat. Transfer* **60** 665

[19] Brown J M, Hougen J T, Huber K P, Johns J W C, Kopp I, Lefebvre-Brion H, Merer A J, Ramsay D A, Rostas J and Zare R N 1975 *J. Mol. Spectrosc.* **55** 500

[20] Kovács I 1969 Rotational Structure in the Spectra of Diatomic Molecules *Rotational Structure in the Spectra of Diatomic Molecules* (American Elsevier: New York)

[21] Li G, Harrison J J, Ram R S, Western C M and Bernath P F 2012 *J. Quant. Spectrosc. Radiat. Transfer* **113** 67

Appendix G

Intrinsic parity of the diatomic molecule

This appendix discusses appearances of selected homonuclear spectra. In quantum field theory, the parity of a state is broken into two parts: one depending on the angular momentum and the second part, called the *intrinsic parity*, that is independent of angular momentum. Particles currently viewed as fundamental (e.g., the photon and electron) are assigned an intrinsic parity. Since parity is multiplicative, the intrinsic parity of a collection of fundamental particles is the product of the individual intrinsic parities. Thus, nucleons have an intrinsic parity of $+1$, and the intrinsic parity of an atomic or molecular system having N electrons is simply $(-)^N$. Does intrinsic parity have any relevance in atomic and molecular physics? By comparing experimental spectra recorded by others with synthetic spectra computed by us using intrinsic parity $(-)^N$ in the computations, we conclude that intrinsic parity is relevant to the spectra of homonuclear diatomic molecules.

The unresolved hyperfine structure (unresolved nuclear spin states) of a diatomic molecule state effectively give the state a degeneracy factor (statistical weight) $g = (2I_a + 1)(2I_b + 1)$, where I_a is the nuclear spin of one nucleus and I_b the nuclear spin of the second nucleus. When the two nuclei are identical, the total nuclear spin statistical weight remains $(2I + 1)^2$ where $I = I_a = I_b$, but the number of nuclear spin states g_+ for which the parity is $+1$ and the number of states g_- for which the parity is -1 are unequal. This leads to the alternation of intensity in the spectrum of a homonuclear diatomic molecule. The experimental spectra given in the bottom trace in figures (G.1)–(G.3) are examples. In each figure above the experimental spectrum is a computed diatomic spectrum, which agrees agrees reasonably well with the experimental spectrum, and the top trace in each figure is another computed spectrum which is in qualitative disagreement with the experimental spectrum. The only difference between the two computed spectra are the parity values used in their computation.
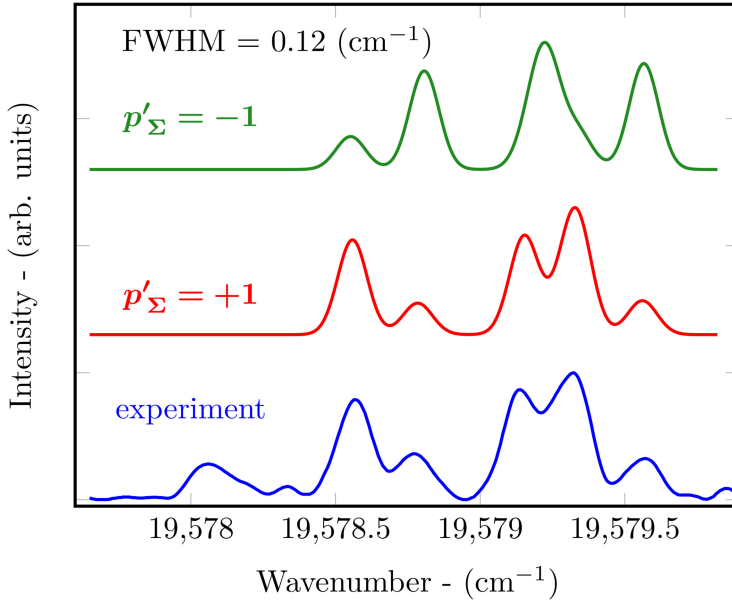
Figure G.1. Two synthetic $^{13}C_2$ $d^3\Pi_g - a^3\Pi_u$ spectra compared with an experimental spectrum [1]. The Λ-doublets are partially resolved. The intrinsic parity of an neutral diatomic molecule is $+1$ (i.e., the number of electrons is even). For the upper $d^3\Pi_g$ state, $p'_{gu} = +1$, while for the lower $a^3\Pi_u$ state, $p_{gu} = -1$. Thus, $p'_{\Sigma} = p_0 \, p'_{gu} = +1$ and $p_{\Sigma} = p_0 \, p_{gu} = -1$. The molecular parameters were found by fitting the line position data of [1]

The synthetic spectra in Figs (G.1)–(G.3) were computed using the following algorithm.

- For given upper total angular momentum quantum J' and lower quantum number J, the upper and lower Hamiltonian matrices H' and H are computed in the Hund's case (a) basis and are numerically diagonalized to obtain the eigenvalues F' and F and eigenvectors U' and U,

$$F' = U'^{\dagger} \, H' \, U' \qquad (G.1)$$

$$F = U^{\dagger} \, H \, U \qquad (G.2)$$

- The Hönl–London factors $S_{J'J}$ are computed,

$$S_{J'J} = (2J + 1) \left| \sum_{a'} \sum_{a} \langle J \,|a\rangle \, \langle a| C_{J\Omega q\kappa}^{J'\Omega'} |a'\rangle \, \langle a' \,|J'\rangle \right|^2 \qquad (G.3)$$

and the term difference (i.e., line position) is computed for each nonvanishing Hönl–London factor,

$$\tilde{\nu} = F' - F, \qquad \text{if } S_{J'J} \neq 0 \qquad (G.4)$$
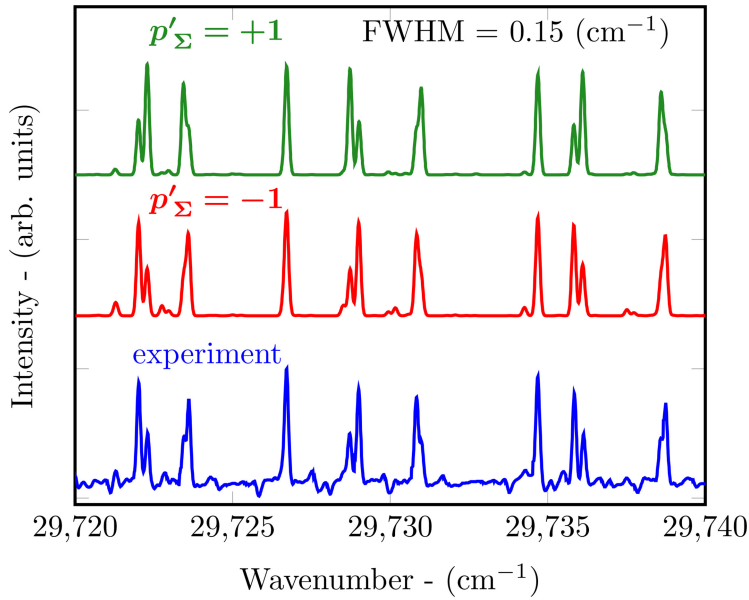
Figure G.2. Two synthetic $C^3\Pi_u - B^3\Pi_g$ N_2 second positive system spectra compared with an experimental spectrum [2]. The Λ-doublets are partially resolved. This spectrum reverses the situation of figure G.1. The intrinsic parity is again $+1$, but here $p'_{gu} = -1$ and $p_{gu} = +1$, and one finds $p'_\Sigma = p_0\, p'_{gu} = -1$ and $p_\Sigma = p_0\, p_{gu} = +1$. The molecular parameters were found by fitting the line position data [2].
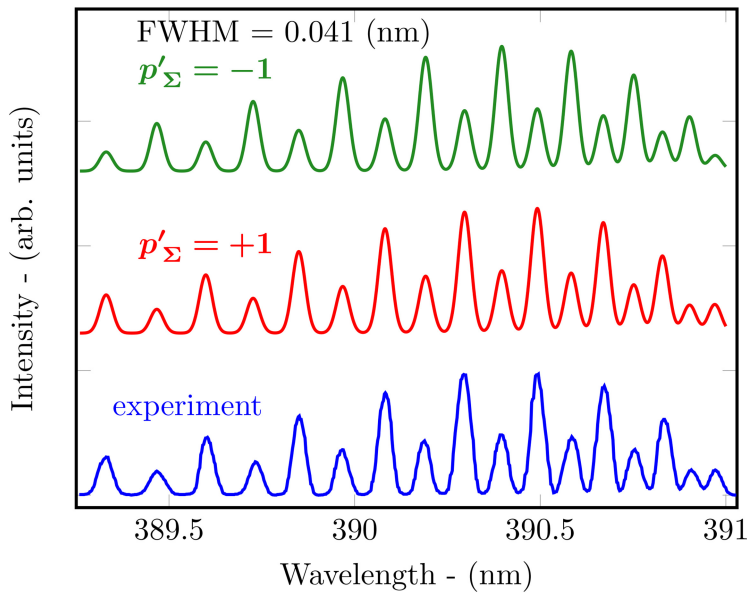
Figure G.3. There are no Λ-doublets in a $^2\Sigma_u^+ - {}^2\Sigma_g^+$ spectrum, but the parity alternates from line to line causing an alternation of intensity. The two synthetic spectra are compared with an experimental spectrum [3]. The intrinsic parity of the singly ionized N_2^+ molecule is -1. Thus, $p'_\Sigma = p_0\, p'_{gu} = 1$ and $p_\Sigma = p_0\, p_{gu} = +1$. The molecular parameters were found by fitting the line position data of [4].

- A line list is created by repeating the above for all required J' and J.

- A thermal distribution of excited states and a Gaussian spectrometer slit function having a specified full width at half maximum are assumed.

- The spectrum was broken into a number of pixels, and the the contribution of each line in the computed line list to each pixel is computed.

The matrix elements of parity in the Hund's case (a) basis are the product of a constant p_Σ and $(-)^J$,

$$p_{ij} = p_\Sigma\, (-)^J\, \delta_{J_i J_j}\, \delta_{\Omega_i, -\Omega_j}\, \delta_{\Lambda_i, -\Lambda_j}\, \delta_{n_i n_j}. \tag{G.5}$$

The quantum number n denotes the electronic basis, and other symbols have the standard meanings given them in diatomic spectroscopy. Parity is a member of the complete set of commuting observables. Therefore, the orthogonal matrices U' and U that diagonalize the upper and lower Hamiltonians computed in the case (a) basis will also diagonalize the upper and lower parity matrices computed in the case (a) basis.

The only difference between the two computed spectra in each of figures (G.1)–(G.3) are the values of the upper p'_Σ and lower p_Σ. When computing the synthetic spectra given in figures (G.1)–(G.3), we imposed the selection rule $p_\Sigma \neq p'_\Sigma$. Trial and error quickly finds one of two possibilities, but having a theoretical reason for choosing the value of p_Σ for a diatomic state is clearly desirable.

Equation (G.5) shows a breaking of parity into two parts, p_Σ and $(-)^J$. In quantum field theory, parity is similarly broken into two parts, one depending upon parity and the other independent of parity and called the *intrinsic parity*. Intrinsic parity is believed to be a characteristic property of a fundamental particle. For example, the electron has been assigned the intrinsic parity -1. Parity is multiplicative, and the intrinsic parity of a composite particle is the product of the intrinsic parities of particles composing it, e.g., nucleons have an intrinsic parity of $+1$. An atom or molecule has an intrinsic parity of $(-)^N$, where N is the number of electrons. Ionization and electron attachment can obviously change the intrinsic parity of a molecule, but standard electromagnetic transitions cannot. The selection rule $p'_\Sigma \neq p_\Sigma$ used in the computation of the spectra shown in figures (G.1)–(G.3) eliminates consideration of p_Σ as intrinsic parity. However, the value of p_Σ appears to be correctly given as the product of the intrinsic parity eigenvalue p_0 and the *gerade/ungerade* parity eigenvalue p_{gu},

$$p_\Sigma = (-)^N p_{\mathrm{gu}} \tag{G.6}$$

$$= p_0\, p_{\mathrm{gu}}. \tag{G.7}$$

Based upon the very limited number of comparisons with experiment given in the attached figures, we tentatively conclude that equation (G.7) describes how intrinsic parity influences the spectrum of a homonuclear diatomic molecule.

As long as the weak force is excluded from consideration, none will doubt that the unitary transformation that diagonalizes the Hamiltonian matrix will also diagonalize the parity matrix, but equation (G.5) is new and its derivation is required. The derivation of the Hund's case (a) matrix representation of parity is based upon the Wigner–Witmer diatomic eigenfunction, not the Born–Oppenheimer approximation, and thus represents a radical departure from current diatomic theory. The considered Hamiltonian matrices are not effective Hamiltonians but are simply composed of case (a) matrix elements. Furthermore, the Hamiltonians are not separated into positive and negative parity submatrices, and Van Vleck reductions of the matrix dimensions are not performed.

References

[1] Amiot C 1983 *Astrophys. J. Suppl. Ser.* **52** 329
[2] Roux F, Michaud F and Vervloet M 1989 *Can. J. Phys.* **67** 143
[3] Lazdinis S S and Carpenter R F 1973 *J. Chem. Phys.* **59** 5203
[4] Michaud F, Roux F, Davis S P, Nguyen A-D and Laux C O 2000 *J. Mol. Spectrosc.* **203** 1

Quantum Mechanics of the Diatomic Molecule (Second Edition)

Christian G Parigger and James O Hornkohl

Appendix H

Review of diatomic laser-induced breakdown spectroscopy

This appendix summarizes diatomic molecular spectroscopy applications in laser-induced breakdown spectroscopy (LIBS) that were recently communicated in a line shape conference [1]. Moreover, this appendix serves as well as a summary on how to apply the diatomic spectroscopy computations in part I for analysis of measured emission spectra.

In principle, an atomic or molecular spectrum would be computed as follows: upper and lower Hamiltonians would be enumerated in a complete basis, and numerically diagonalized to give the upper and lower energy eigenvalues and eigenvectors. The transition moments for the appropriate operator, e.g., the electric dipole transition moments, would be evaluated from the eigenvectors. The vacuum wave numbers $\tilde{\nu}$, i.e., energy eigenvalue differences, would be found for all non-vanishing transition moments. The line strengths for each spectral line of wave number $\tilde{\nu}$ would be determined as sum of the squares of the transition moments over all transitions producing the same $\tilde{\nu}$. A line list that includes line strengths would be generated by repeating the above computations over the required range of upper and lower total angular momentum quantum numbers. The spectrum from $\tilde{\nu}_{\min}$ to $\tilde{\nu}_{\max}$ would be separated into a number of pixels, and subsequently the contribution of each line to each pixel is calculated using the line list. This appendix reviews how this algorithm can be implemented for a diatomic spectrum if the required molecular parameters are available.

H.1 Introduction

This work reports our algorithm used to compute the synthetic spectra of diatomic molecules. Figure H.1 shows a measured spectrum of interest in LIBS [1–14], and it also shows two computed C_2 Swan spectra fitted to the experimental spectrum. With one caveat, the algorithm is the textbook method for computation of a spectrum. The caveat is that a comprehensive set of accurate diatomic parameters is required for its implementation. We describe our algorithm and give an explanation of why it

is based on the Wigner–Witmer diatomic eigenfunction [15] and not the Born–Oppenheimer approximation [16].

H.2 Computation of a diatomic spectrum

Except for the baseline corrections, the synthetic spontaneous emission spectra in figure (H.1) were computed using the following algorithm.

- For given upper total angular momentum quantum number J' and lower quantum number J, the upper and lower Hamiltonian matrices H' and H are computed in the Hund's case (a) basis and numerically diagonalized to obtain the eigenvalues F' and F and eigenvectors U' and U,
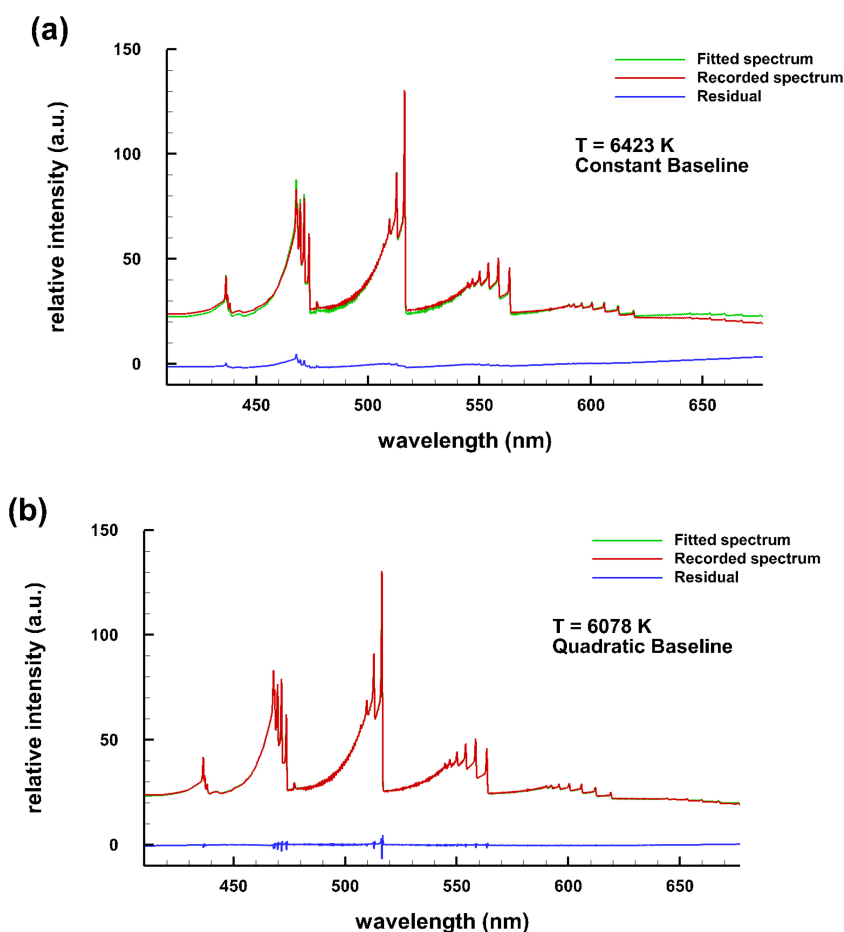
Figure H.1. A recorded C_2 Swan spectrum [17] compared with two computed Swan spectra containing (a) a small constant and (b) a quadratic baseline. The temperature and baseline values were obtained by trial and error implemented with the Nelder–Mead extremum algorithm by varying the temperature for here a thermal distribution of excited states [1].

$$F' = U'^{\dagger}\, H'\, U',\tag{H.1}$$

$$F = U^{\dagger}\, H\, U.\tag{H.2}$$

- The Hönl–London line-strength factors $S_{J'J}$ are computed [18],

$$S_{J'J} = (2J + 1)\left|\sum_{a'}\sum_{a}\langle J\,|a\rangle\,\langle a|C_{J\Omega q\kappa}^{J'\Omega'}|a'\rangle\,\langle a'\,|J'\rangle\right|^2\tag{H.3}$$

and the term difference, i.e., line position, is computed for each nonvanishing Hönl–London line-strength factor,

$$\tilde{\nu} = F' - F \qquad \text{if } S_{J'J} \neq 0.\tag{H.4}$$

- A line list which includes line strengths is created by repeating the above for all required J' and J.
- A thermal distribution of excited states and a Gaussian spectrometer slit function having a specified full width at half maximum are assumed.
- The spectrum is separated into a number of pixels, and the the contribution of each line in the computed line list to each pixel is computed.

Use of the above algorithm requires the Wigner–Witmer diatomic eigenfunction,

$$\langle \mathbf{r}_1, \mathbf{r}_2, \dots, \mathbf{r}_N, \mathbf{r}\,|nvJM\rangle = \sum_{\Omega=-J}^{J} \langle \rho, \zeta, \mathbf{r}_2', \dots, \mathbf{r}_N', r\,|nv\rangle\, D_{M\Omega}^{J*}(\phi, \theta, \chi),\tag{H.5}$$

in which the total angular momentum states are *exactly* separated instead of a Born–Oppenheimer eigenfunction in which segregation of electronic and nuclear coordinates is enforced, thereby preventing separation of the total angular momentum. The quantum numbers in equation (H.5) are the vibrational quantum number v, the total angular momentum quantum number J, the magnetic quantum number M for the z-component of $\mathbf{J}$, the magnetic quantum number Ω for the z' component of $\mathbf{J}$, and n, which is a symbol representing all other required quantum numbers and labels for continuum indices. In equation (H.5), primed and unprimed coordinates are related by coordinate rotation,

$$\begin{bmatrix} x' \\ y' \\ z' \end{bmatrix} = \mathcal{D}(\phi, \theta, \chi)\begin{bmatrix} x \\ y \\ z \end{bmatrix}.\tag{H.6}$$

The Euler angles ϕ, θ, and χ and the coordinate rotation matrix $\mathcal{D}(\phi, \theta, \chi)$ used here,

$$\mathcal{D}(\phi, \theta, \chi) = \begin{bmatrix} \cos\phi\cos\theta\cos\chi - \sin\phi\sin\chi & \sin\phi\cos\theta\cos\chi + \cos\phi\sin\chi & -\sin\theta\cos\chi \\ -\cos\phi\cos\theta\sin\chi - \sin\phi\cos\chi & -\sin\phi\cos\theta\sin\chi + \cos\phi\cos\chi & \sin\theta\sin\chi \\ \cos\phi\sin\theta & \sin\phi\sin\theta & \cos\theta \end{bmatrix}.\tag{H.7}$$

are those used almost universally in the quantum theory of angular momentum [19–25]. Kovács [26] uses a different set of Euler angles. Primes do not appear on ρ (the distance of one of the electrons from the internuclear axis), ζ (the distance of this electron above or below the plane perpendicular to the internuclear axis and passing through the origin at the center of mass of the nuclei), and r (the internuclear distance) because they are scalars whose value is the same in all coordinate systems. The polar coordinates r, θ, and ϕ are those of the fictitious particle of reduced mass of the two nuclei who motion has replaced their motion. There are N electrons and their coordinates are labeled 1, 2, $\cdots$, N. The cylindrical coordinates ρ, χ, and ζ are those of one of the electrons. In accord with standard practice in angular momentum theory, the quantum numbers J, M, and Ω refer to the *total* angular momentum. The spectroscopic quantum numbers F, M_F, and Ω_F replace J, M, and Ω in equation (H.5) when it is written in spectroscopic notation.

In the Wigner–Witmer diatomic eigenfunction, the Euler angles ϕ, θ, and χ are both the parameters of coordinate rotation and the angles of physical rotation. The diatomic molecule is perhaps the most complicated actual system in which a single set of Euler angles can serve both purposes. For example, in polyatomic theory the Euler angles ϕ, θ, and χ are physical rotations describing a frame to which the nuclei are attached, and are not the parameters of coordinate rotation α, β, and γ that one would use to demonstrate rotational invariance and conservation of the total angular momentum in a polyatomic model which included vibrational angular momentum.

The Wigner–Eckart theorem breaks the transition moment into two parts: the so-called reduced matrix element, whose value is controlled by the initial and final total angular quantum numbers and the degree of transition tensor operator, and the Clebsch–Gordan coefficient, whose value is controlled by the magnetic quantum numbers and the indices of the components of the tensor operator. The exact separation of the total angular momentum in the Wigner–Witmer eigenfunction simplifies and improves the accuracy of computation of the Hönl–London strengths. Line positions $\tilde{\nu}$ and Hönl–London factors are normally independently evaluated. In the present algorithm, they are simultaneously computed. Of the myriad upper and lower term differences, only those for which the Hönl–London line-strength factor is nonvanishing become spectral lines.

The Born–Oppenheimer approximation is not totally eliminated from computation of a diatomic spectrum. It is needed to break the electronic–vibrational eigenfunction into the product of electronic and vibrational eigenfunction. The Wigner–Witmer diatomic eigenfunction exactly separates the diatomic line strength into the product of the electronic–vibrational strength $S_{n'v',nv}$ and the Hönl–London line-strength factor $S_{J',J}$,

$$S_{n'v'J',nvJ} = S_{n'v',nv}\, S_{J',J}, \tag{H.8}$$

$$S_{n'v',nv} = \left| a_0 + a_1 \bar{r}_{v'v} + a_2 \bar{r}_{v'v}^2 + \cdots \right|^2 q_{v'v}. \tag{H.9}$$

The Born–Oppenheimer approximation separates the electronic–vibrational strength into the product of the square of the electronic transition moment,

$$R_e(r) = a_0 + a_1 r + a_2 r^2 + \cdots, \tag{H.10}$$

evaluated at the r-centroids $\bar{r}_{v'v}^n$,

$$\bar{r}_{v'v}^n = \frac{\langle v' \,|r^n|v\rangle}{\langle v' \,|v\rangle}, \tag{H.11}$$

and with the Franck–Condon factors $q_{v'v}$,

$$q_{v'v} = \langle v' \,|v\rangle^2. \tag{H.12}$$

Whereas experimental and calculated line positions are often known with an accuracy of $1:10^6$ or better, spectral line intensity is rarely recorded with an accuracy of better than 1%. Thus, use of the Born–Oppenheimer approximation for calculation of the electronic–vibrational strength, but not for calculation of line positions, does not introduce significant error.

H.3 Determination of the molecular parameters

Implementation of the algorithm described above requires a comprehensive set of accurate molecular parameters. This is not a minor proviso, and the situation is further complicated by the fact the use of the Wigner–Witmer eigenfunction modifies the manner in which diatomic parameters are determined from a accurate line position measurements such as those provided by Fourier transform spectroscopy. The basic idea in both current practice [27, 28] and our determination of diatomic parameters is the calculation of matrix elements of the form

$$\langle a_i \,|H_k|a_j\rangle = \langle n_i v_i J_i M_i \Omega_i \Lambda_i S_i \Sigma_i \,|H_k|n_j v_j J_j M_j \Omega_j \Lambda_j S_j \Sigma_j\rangle \tag{H.13}$$

in which $|a\rangle$ is a Hund's case (a) basis function,

$$|a\rangle = |nvJM\Omega\Lambda S\Sigma\rangle = \sqrt{\frac{2J+1}{8\pi^2}} \langle \rho, \zeta, \mathbf{r}_2', \ldots, \mathbf{r}_N', r \,|nv\rangle\, D_{M\Omega}^{J*}(\phi, \theta, \chi)\,|S\Sigma\rangle \tag{H.14}$$

and H_k is a term from the diatomic Hamiltonian

$$H = \sum_k H_k. \tag{H.15}$$

Use of the Wigner–Witmer eigenfunction breaks required matrix elements of the Hamiltonian into two parts: the angular momentum part, which can be calculated exactly, and the electronic–vibrational part, which, except for the very simplest molecules, cannot be calculated with spectroscopic accuracy. Use of a Born–Oppenheimer eigenfunction breaks calculation into three parts: an electronic part, a part consisting of a sum over an infinite number of Born–Oppenheimer vibrational states, and a rotational part. In general, none of the three can be done exactly. Van Vleck transformations, parity partitioning, and the concept of an 'effective

Hamiltonian" reduce the dimensions of the Hamiltonian matrix. We simply compute a Hamiltonian matrix composed of case (a) matrix elements, and let the dimension of the matrix be determined by the range of Ω in equation (H.5) be that required make computed line positions $\tilde{nu}_{\mathrm{cal}}$ equal the experimental positions $\tilde{\nu}_{\mathrm{exp}}$ to within the estimated accuracy of the $\tilde{\nu}_{\mathrm{exp}}$. With the exceptions that (1) our Hamiltonian of unmodified case (a) matrix elements replaces the effective Hamiltonian used by others and (2) instead of using coded selection rules we use nonvanishing of the Hönl–London line-strength factor as the only selection rule, our determination of molecular parameters is identical to that described by [29]. Trial values of upper and lower parameters are assumed, the line positions are computed, corrections to the parameters are computed from the errors in the computed line positions,

$$\Delta\tilde{\nu} = \tilde{\nu}_{\mathrm{cal}} - \tilde{\nu}_{\mathrm{exp}}, \tag{H.16}$$

and the process is repeated until the corrections to the parameters become negligibly small. The algorithm for finding molecular parameters by fitting computed line positions to measured line positions is described in more detail in [30].

H.4 Discussion

The Wigner–Witmer paper [15] appeared about a year after the Born–Oppenheimer paper [16]. The Born and Oppenheimer work treats all molecules, but the Wigner–Witmer paper is strictly limited to the diatomic molecule. Although Born's formulation[16, 31] in terms of

$$\kappa = \left(\frac{m}{M_0}\right)^{1/4} \tag{H.17}$$

in which m is the electronic mass and 'where M_0 can taken as any one of the nuclear masses or their mean' [31] is rarely used, the Born–Oppenheimer approximation became the foundation of molecular theory. Although the Born–Oppenheimer approximation is applicable to all molecules, in their final section Born and Oppenheimer show that the polar angle and azimuthal angle of the polar coordinates r, θ, and ϕ of the internuclear vector in a diatomic molecule are exactly separable in the spherical harmonic $Y_{\ell m}(\theta, \phi)$. The Wigner complex conjugate of the D-symbol, $D_{m\omega}^{j*}(\phi, \theta, \chi)$ is the mathematical extension of the spherical harmonics,

$$Y_{\ell m}(\theta, \phi) = \sqrt{\frac{2\ell + 1}{4\pi}} \, D_{m0}^{\ell*}(\phi, \theta, 0) \tag{H.18}$$

which allows one to deal with the total angular momentum $|jm\rangle$ rather that just the orbital angular momentum $|\ell m\rangle$. The first half of the Wigner–Witmer paper is the logical extension of the Born–Oppenheimer $Y_{\ell m}(\theta, \phi)$ result to include all three Euler angles in diatomic eigenfunction. The two-part Wigner–Witmer paper became famous for its second part, which gives correlation rules relating the electronic states of a diatomic molecule to the $L - S$ coupled states of the separated atoms.

Oddly, the exact diatomic eigenfunction with which Wigner and Witmer determined their correlation rules has been ignored. About 40 years passed between publication the Wigner–Witmer paper and entry of the Wigner D-function into the literature of diatomic theory. By then, the Wigner–Witmer diatomic eigenfunction had apparently been forgotten.

References

[1] Hornkohl J O and Woods A C 2014 *J. Phys.: Conf. Ser.* **548** 012033

[2] Singh J P and Thakur S N (ed) 2020 *Laser-Induced Breakdown Spectroscopy* (New York: Elsevier Science)

[3] Musazzi S and Perini U (ed) 2014 *Laser-Induced Breakdown Spectroscopy* (Heidelberg: Springer)

[4] Cremers D E and Radziemski L J 2006 *Handbook of Laser-Induced Breakdown Spectroscopy* (New York: Wiley)

[5] Noll R 2011 *Laser-Induced Breakdown Spectroscopy.* (Heidelberg: Springer)

[6] Singh J P and Thakur S N (ed) 2007 *Laser-Induced Breakdown Spectroscopy* (Amsterdam: Elsevier Science)

[7] Miziolek A W and Palleschi V (ed) 2006 *Laser-Induced Breakdown Spectroscopy (LIBS)— Fundamentals and Applications* (New York: Cambridge University Press)

[8] Parigger C G 2006 Laser-induced breakdown in gases: Experiments and simulation *Laser-Induced Breakdown Spectroscopy (LIBS)—Fundamentals and Applications* ed A W Miziolek, V Palleschi and I Schechter (New York: Cambridge University Press)

[9] Parigger C G, Surmick D M, Helstern C M, Gautam G, Bol'shakov A A and Russo R 2020 Molecular laser-induced breakdown spectrosocpy *Laser-Induced Breakdown Spectroscopy* ed J P Singh and S N Thakur (New York: Elsevier Science) ch 7

[10] Merten J, Jones M, Hoke S and Allen S A 2014 *J. Phys.: Conf. Ser.* 548 012042

[11] Parigger C G, Helstern C M and Gautam G 2019 *Atoms* **7** 7030074

[12] Tiwari P K, Rai N K, Kumar R, Parigger C G and Rai A K 2019 *Atoms* **7** 7030071

[13] Surmick D M, Dagel D J and Parigger C G 2019 *Atoms* **7** accepted

[14] Parigger C G, Sherbini A M E L and Splinter R 2019 *J. Phys.: Conf. Ser.* accepted

[15] Wigner E and Witmer E E 1928 *Z. Phys.* **51** 859
Hettema H 2000 *Quantum Chemistry: Classic Scientific Papers* p 287 (Singapore: World Scientific)

[16] Born M and Oppenheimer R 1927 *Ann. Phys.* **84** 457
Hettema H 2000 *Quantum Chemistry: Classic Scientific Papers* p 1 (Singapore: World Scientific)

[17] Nemes L, Keszler A M, Hornkohl J O and Parigger C G 2005 *Appl. Opt.* **44** 3661

[18] Nemes L, Hornkohl J O and Parigger C G 2005 *Appl. Opt.* **44** 3686

[19] Rose M E 1995 *Elementary Theory of Angular Momentum* (Mineola, NY: Dover)

[20] Edmonds A R 1974 *Angular Momentum in Quantum Mechanics* 2nd edn (Princeton, NJ: Princeton University Press)

[21] Brink D M and Satchler G R 1993 *Angular Momentum* 3rd edn (Oxford: Oxford University Press)

[22] Biedenharn L C and Louck J D 2009 *Angular Momentum in Quantum Physics* (Cambridge: Cambridge University Press)

[23] Zare R N 1988 *Angular Momentum* (New York: Wiley)

[24] Thompson W J 1994 *Angular Momentum* (New York: Wiley)

[25] Varshalovich D A, Moskalev A N and Khersonskii V K 1988 *Quantum Theory of Angular Momentum* (Singapore: World Scientific)

[26] Kovács I 1969 *Rotational Structure in the Spectra of Diatomic Molecules* (New York: American Elsevier)

[27] Lefebvre-Brion H and Field R W 2004 *The Spectra and Dynamics of Diatomic Molecules* (New York: Elsevier/Academic)

[28] Brown J M and Carrington A 2003 *Rotational Spectroscopy of Diatomic Molecules* (Cambridge: Cambridge University Press)

[29] Zare R N, Schmeltekopf A L, Harrop W J and Albritton D L 1973 *J. Mol. Spectrosc.* **46** 37

[30] Hornkohl J O, Nemes L and Parigger C G 2009 Spectroscopy, dynamics and molecular theory of carbon plasmas and vapors *Advances in the Understanding of the Most Complex High-Temperature Elemental System* ed L Nemes and S Irle (Singapore: World Scientific) ch 4

[31] Huang K and Born M 1954 *Dynamical Theory of Crystal Lattices* (Oxford: Clarendon)

Quantum Mechanics of the Diatomic Molecule (Second Edition)

Christian G Parigger and James O Hornkohl

Appendix I

Program MorseFCF.for

This appendix lists the program 'MorseFCF.for' and the subroutines 'MorseSubs. for.' This program has been utilized in investigations of titanium monoxide (TiO) spectra that were measured following laser-induced breakdown spectroscopy with 1 to 100 TW cm $^{-2}$ irradiance [1]. Franck–Condon factors and r-centroids were computed and listed for selected TiO transitions [1] using Morse potentials chosen to best fit the low lying vibrational levels. The electronic transition moments were taken from the most recently reported *initio* computations for A–X, B–X, and E–X transitions.

I.1 MorseFCF.for

This program computes Franck–Condon factors and first three r-centroids for a Morse potentials and sets of molecular parameters.

```
!      February 12, 2012
!      James O. Hornkohl
!      Program to compute Morse Franck-Condon factors.
       program morfcf
       use DeclaredStuff
       real(8) :: qs, r1s, r2s, r3s
!       real(8) q, r1, r2, r3
!       dimension q(0:100,0:100), r1(0:100,0:100), r2(0:100,0:100), r3(0:100,0:100)
       real(8) :: weu, wexeu, Beu, muu
       real(8) :: wel, wexel, Bel, mul
       real(8) :: au, betau, reu, gammau, xu, alpha
       real(8) :: al, betal, rel, gammal, xl
       real(8) :: rmin, rmax, rsave, tstu, tstl, dr, r, psi, r0
       real(8) :: lgnrmu(0:100), lgnrml(0:100)
       real(8) :: lgnorm
       real(8) :: alphavu(0:100), alphavl(0:100)
       real(8) :: yu, yl, x, y
       integer*4 :: vmaxu, vmaxl, npts, i, j, k, lun
```

```fortran
      integer*4 :: nv, mv
      character*130 :: prnfil, fcffil

      write (*,1000)
 1000 format (15x, 'Franck-Condon Factors from Morse Eigenfunctions')
      write (*,1005)
 1005 format (20x, 'Version for Microsoft 32-bit Compiler', /)
      write (*,1010)
 1010 format ('                        Print file name = ',$)
      read (*,'(a)') prnfil
      write (*,1016)
 1016 format ('                            FCF file name = ',$)
      read (*,'(a)') fcffil
!      write (*,1020)
! 1020 format (5x, 'Enter constants for upper electronic state.')
!   20 write (*,1030)
! 1030 format ('                         we = ',$)
!      read (*,*,err=20) weu
!   30 write (*,1040)
! 1040 format ('                         wexe = ',$)
!      read (*,*,err=30) wexeu
!   40 write (*,1050)
! 1050 format ('                         Be = ',$)
!      read (*,*,err=40) Beu
!   50 write (*,1060)
! 1060 format ('                  reduced mass = ',$)
!      read (*,*,err=50) muu
!   60 write (*,1070)
! 1070 format (' max vibrational quantum number = ',$)
!      read (*,*,err=60) vmaxu
      weu = 373.152d0
      wexeu = 1.5112d0
      Beu =  0.1542393d0
      muu = 18.64966011d0
      vmaxu = 9
      write(*,1075)  weu, wexeu, Beu, muu
1075   Format(4(1pg20.13))
      call const (au, alphavu, lgnrmu, betau, weu, wexeu, Beu, reu, muu, gammau, vmaxu)
!      write (*,1080)
! 1080 format (5x, 'Enter constants for lower electronic state.')
!  100 write (*,1030)
!      read (*,*,err=100) wel
!  110 write (*,1040)
!     read (*,*,err=110) wexel
!  120 write (*,1050)
!      read (*,*,err=120) Bel
!  130 write (*,1060)
!      read (*,*,err=130) mul!
```

```
!   140  write (∗,1070)
!        read (∗,∗,err=140) vmaxl
        wel = 370.201d0
        wexel = 1.3732d0
        Bel = 0.152233d0
        mul = muu
        vmaxl = 9
        call const (al, alphavl, lgnrml, betal, wel, wexel, Bel, rel, mul, gammal, vmaxl)
   150  write (∗,1170)
  1170  format ('␣␣␣␣␣␣␣␣␣␣␣␣r−min␣=␣', $)
        read (∗,∗,err=150) rmin
        if (rmin.eq.0.0) go to 160
        xu = au ∗ dexp(−betau∗(rmin−reu))
        alpha = alphavu(vmaxu)
        lgnorm = lgnrmu(vmaxu)
        tstu = psi (vmaxu, xu, alpha, lgnorm)
        xl = al ∗ dexp(−betal∗(rmin−rel))
        alpha = alphavl(vmaxl)
        lgnorm = lgnrml(vmaxl)
        tstl = psi (vmaxl, xl, alpha, lgnorm)
        write (∗,1180) tstu, tstl
  1180  format ('␣At␣trial␣value␣of␣r␣the␣eigenfunction␣=', 1pg11.4, 3x, 1pg11.4)
        rsave = rmin
        go to 150
   160  rmin = rsave
   170  write (∗,1190)
  1190  format ('␣␣␣␣␣␣␣␣␣␣␣␣r−max␣=␣', $)
        read (∗,∗,err=170) rmax
        if (rmax.eq.0.0) go to 180
        xu = au ∗ dexp(−betau∗(rmax−reu))
        alpha = alphavu(vmaxu)
        lgnorm = lgnrmu(vmaxu)
        tstu = psi (vmaxu, xu, alpha, lgnorm)
        xl = al ∗ dexp(−betal∗(rmax−rel))
        alpha = alphavl(vmaxl)
        lgnorm = lgnrml(vmaxl)
        tstl = psi (vmaxl, xl, alpha, lgnorm)
        write (∗,1180) tstu, tstl
        rsave = rmax
        go to 170
   180  rmax = rsave
   190  write (∗,1200)
  1200  format ('␣increment␣in␣r␣=␣', $)
        read (∗,∗,err=190) dr
        npts = idnint((rmax−rmin)/dr) + 1
        if (prnfil.ne.'␣')  then
           open (10, file=prnfil, status='unknown')
           lun = 10
```

```fortran
        else
            lun = 0
        endif
        write (lun,1000)
        write (lun,1090) reu, rel
 1090   format (6x, '             re =', 1pg17.10, 3x, 1pg17.10)
        write (lun,1100) betau, betal
 1100   format (6x, '            beta =', 1pg17.10, 3x, 1pg17.10)
        write (lun,1110) gammau, gammal
 1110   format (6x, '           gamma =', 1pg17.10, 3x, 1pg17.10)
        write (lun,1120) weu, wel
 1120   format (6x, '              we =', 1pg17.10, 3x, 1pg17.10)
        write (lun,1130) wexeu, wexel
 1130   format (6x, '            wexe =', 1pg17.10, 3x, 1pg17.10)
        write (lun,1140) Beu, Bel
 1140   format (6x, '              Be =', 1pg17.10, 3x, 1pg17.10)
        write (lun,1150) muu, mul
 1150   format (6x, '   reduced mass =', 1pg17.10, 3x, 1pg17.10)
        write (lun,1210) rmin, rmax
 1210   format (6x, '           r-min =', 1pg11.4, 2x, 'r-max =', 1pg11.4)
        write (lun,1220) dr
 1220   format (6x,'          delta r ='1pg11.4)
        write (lun,1230) npts
 1230   format (6x,'number of points =',i4)
        allocate(q(0:vmaxu,0:vmaxl), r1(0:vmaxu,0:vmaxl), r2(0:vmaxu,0:vmaxl), r3(0:vmaxu,0:vmaxl))
        r0 = dble(idint(50.0d0*(reu+rel))) / 100.0d0
        do 220 i=0, vmaxu
            do 210 j=0, vmaxl
                qs = 0d0
                r1s = 0d0
                r2s = 0d0
                r3s = 0d0
                do k=1, npts
                    r = rmin + (k-1)*dr
                    xu = au * dexp(-betau*(r-reu))
                    alpha = alphavu(i)
                    lgnorm = lgnrmu(i)
                    yu = psi (i, xu, alpha, lgnorm)
                    xl = al * dexp(-betal*(r-rel))
                    alpha = alphavl(j)
                    lgnorm = lgnrml(j)
                    yl = psi (j, xl, alpha, lgnorm)
                    y = yu * yl
                    qs = qs + y
                    x = r - r0
                    y = y * x
                    r1s = r1s + y
                    y = y * x
```

```fortran
                     r2s = r2s + y
                     y = y * x
                     r3s = r3s + y
                enddo
                qs = qs * dr
                r1(i,j) = r1s * dr / qs
                r2(i,j) = r2s * dr / qs
                r3(i,j) = r3s * dr / qs
                q(i,j) = qs * qs
                nv = i - 1
                mv = j - 1
  210       continue
  220   continue
        call prnfcf (vmaxu, vmaxl, r0, lun)
        if (lun.ne.0)   close (lun)
!       De = weu*weu / (4d0*wexeu)
        if (fcffil.ne.' ')   then
           open (unit=11, file=fcffil)
           do i=0, vmaxu
              do j=0, vmaxl
                  write (11,2000) i, j, q(i,j), r1(i,j), r2(i,j), r3(i,j)
              end do
           end do
           close (11)
        endif
 2000  format (1x, i3, ",", i3,   4(",", 1x,1pg14.7))
        end

        subroutine prnfcf (vmaxu, vmaxl, r0, lun)
        use DeclaredStuff
        implicit none
        integer*4 vmaxu, vmaxl, lun
!        real(8) q, r1, r2, r3
!        common / block1 / q(0:100,0:100), r1(0:100,0:100), r2(0:100,0:100),
!       c r3(0:100,0:100)
        real(8) r0, sum
        integer*4 i, j, jmin, jmax
        write (lun,1000) r0
 1000  format (/, 6x, 'r0 =', 1pg12.5,/)
        jmin = 0
        jmax = 4
   10  if (jmax.gt.vmaxl)   jmax = vmaxl
        write (lun,1010) (j, j=jmin, jmax)
        do 30 i=0, vmaxu
           write (lun,1020) i, (q(i,j), j=jmin, jmax)
           write (lun,1030) (r1(i,j), j=jmin, jmax)
           write (lun,1030) (r2(i,j), j=jmin, jmax)
           write (lun,1030) (r3(i,j), j=jmin, jmax)
```

I-5

```
  30  continue
      if (jmax.eq.vmaxl) goto 40
      jmin = jmin + 5
      jmax = jmax + 5
      goto 10
1010  format (/, 5x, 'v'' ', 4x, 'v"=', i3, 7x, 'v"=', i3, 7x,&
             & 'v"=', i3, 7x, 'v"=', i3, 7x, 'v"=', i3)
1020  format (2x, i4, 5(3x,1pg11.4))
1030  format (6x, 5(3x,1pg11.4))
  40  write (lun,1040)
1040  format (/, 6x, 'Emission sums')
      do 60 i=0, vmaxu
         sum = 0d0
         do 50 j=0, vmaxl
            sum = sum + q(i,j)
  50     continue
         write (lun,1050) i, sum
  60  continue
1050  format (6x, i5, 2x, 1pg22.15)
      write (lun,1060)
1060  format (/, 6x, 'Absorption sums')
      do 80 j=0, vmaxl
         sum = 0d0
         do 70 i=0, vmaxu
            sum = sum + q(i,j)
  70     continue
         write (lun,1050) j, sum
  80  continue
      return
      end
```

I.2 MorseSubs.for

This section list subroutines for the main program MorseFCF that computes Franck–Condon factors and the first three *r*-centroids.

```
      subroutine const(a, b, lgnorm, beta, we, wexe, Be, re, mu, gamma,
     c vmax)
!     July 8, 2011
!     James O. Hornkohl
!     Compute some constants needed for Morse eigenfunctions.
      implicit real*8 (a-h, o-z)
      real*8 h, c, Avog, pi, hbar, x
      real*8 a, b, lgnorm, beta, we, wexe, be, re, mu, gamma
      integer k, v, vmax
      dimension b(0:100), lgnorm(0:100)
      real*8 dlgama
```

```fortran
      h = 6.6260693d-27
      c = 2.99792458d+10
      Avog = 6.0221415d+23
      pi = dacos(-1d0)
      hbar = h / (2d0*pi)
      beta = 1d-08 * sqrt(4d0 * pi * c * (mu/Avog) * wexe
     c  / hbar)
!     Compute equilibrium internuclear distance
      gamma = 1d+16 * hbar * Avog / (4d0 * pi * c * mu)
      if (Be.ne.0d0)  then
         re = sqrt(gamma/Be)
      else
         Be = gamma / (re*re)
      end if
      a = we / wexe
!     Compute logarithm of normalization factor.
      do v=0, vmax
!     b(v) is the constant alpha in the Laguerre polynomial.
         b(v) = a - 2d0*v - 1d0
!     lgnorm(v) is the logarithm of the normalization factor for the
!     Morse eigenfunctions.
         lgnorm(v) = dlog(beta)
         if (v.lt.2) go to 10
         do k=2, v
            lgnorm(v) = lgnorm(v) + dlog(1d0*k)
         enddo
10       lgnorm(v) = lgnorm(v) + dlog(b(v))
         x = b(v) + v + 1d0
         lgnorm(v) = lgnorm(v) - dlgama(x)
         lgnorm(v) = lgnorm(v) / 2d0
      enddo
      return
      end


      real*8 function psi (v, x, alpha, lgnorm)
!     December 28, 2011
!     Compute eigenfunction for Morse oscillator.  Subroutine const
!     must be called once before calls to here are made.
!     The vibrational quantum number is n-1.
      implicit none
      real*8 x, alpha, lgnorm, laguer
      integer k, kmax, v
      psi = dexp(lgnorm+alpha*dlog(x)/2d0-x/2d0) * laguer(v, x, alpha)
      return
      end

      real*8 function laguer (n, x, alpha)
!     December 28, 2011
```

```fortran
!      The degree of the Laguerre polynomial is n-1.
       implicit none
       real*8 x, alpha
       integer n, k, kmax
       real*8 poly(0:100)
       poly(0) = 1d0
       poly(1) = alpha + 1d0 - x
       if (n.lt.2) go to 20
       kmax = n - 1
       do 10 k=1, kmax
           poly(k+1) = ((2*k+alpha+1d0-x) * poly(k)  -  (k+alpha) *
     c      poly(k-1) ) / (k + 1)
   10 continue
   20 laguer = poly(n)
       return
       end


       real*8 FUNCTION DLGAMA (X)
!                                      SPECIFICATIONS FOR ARGUMENTS
       real*8    X
!                                      SPECIFICATIONS FOR LOCAL VARIABLES
       real*8    P1(9),Q1(8),P2(9),Q2(8),P3(9),Q3(8),P4(7)
       INTEGER             IER,J
       real*8    BIG1,XINF,PI,
     *                     Y,T,R,SIGN,A,B,TOP,DEN,EPS
       LOGICAL             MFLAG
!                                      COEFFICIENTS FOR MINIMAX
!                                      APPROXIMATION TO LN(GAMMA(X)),
!                                      0.5 .LE. X .LE. 1.5
       DATA             P1(1)/6.304933722864032D02/,
     *                  P1(2)/1.389482659233250D02/,
     *                  P1(3)/-2.331861065739548D03/,
     *                  P1(4)/-2.651470392943388D03/,
     *                  P1(5)/-8.953073589022869D02/,
     *                  P1(6)/-9.229503102917111D01/,
     *                  P1(7)/-1.940352203312667D00/,
     *                  P1(8)/4.368019694395194D00/,
     *                  P1(9)/1.279153645893113D02/
       DATA             Q1(1)/6.689575153359349D02/,
     *                  Q1(2)/2.419887329355996D03/,
     *                  Q1(3)/3.354196974608081D03/,
     *                  Q1(4)/1.860416170944268D03/,
     *                  Q1(5)/3.944307810159532D02/,
     *                  Q1(6)/2.682132440551618D01/,
     *                  Q1(7)/3.440812622259858D-01/,
     *                  Q1(8)/5.948212550303777D01/
!                                      COEFFICIENTS FOR MINIMAX
!                                      APPROXIMATION TO LN(GAMMA(X)),
```

```
!                             1.5 .LE. X .LE. 4.0
      DATA               P2(1)/1.071722590306920D04/,
      *                  P2(2)/6.527047912184606D04/,
      *                  P2(3)/1.176398389569621D05/,
      *                  P2(4)/-9.726314581896472D03/,
      *                  P2(5)/-1.266094622188023D05/,
      *                  P2(6)/-5.393468741199669D04/,
      *                  P2(7)/-3.895916159676326D03/,
      *                  P2(8)/5.397392180667399D00/,
      *                  P2(9)/5.334390026324024D02/
      DATA               Q2(1)/5.314589562326176D03/,
      *                  Q2(2)/5.493654949398033D04/,
      *                  Q2(3)/2.205757574602192D05/,
      *                  Q2(4)/3.602313576600391D05/,
      *                  Q2(5)/2.273446951911101D05/,
      *                  Q2(6)/4.560612434396495D04/,
      *                  Q2(7)/1.702062439974796D03/,
      *                  Q2(8)/1.670328399370593D02/
!                             COEFFICIENTS FOR MINIMAX
!                             APPROXIMATION TO LN(GAMMA(X)),
!                             4.0 .LE. X .LE. 12.0
      DATA               P3(1)/-6.114039864945718D07/,
      *                  P3(2)/-5.588132821261888D08/,
      *                  P3(3)/-9.078970022444525D08/,
      *                  P3(4)/3.662935130796460D09/,
      *                  P3(5)/4.658700336821218D09/,
      *                  P3(6)/-4.570725249206307D09/,
      *                  P3(7)/-2.220833171087439D09/,
      *                  P3(8)/-1.474322990113017D04/,
      *                  P3(9)/-1.959850795570400D06/
      DATA               Q3(1)/-5.636057205056241D05/,
      *                  Q3(2)/-2.691827587118628D07/,
      *                  Q3(3)/-4.411606716771217D08/,
      *                  Q3(4)/-2.774890551941383D09/,
      *                  Q3(5)/-6.579874397740792D09/,
      *                  Q3(6)/-4.980644951174248D09/,
      *                  Q3(7)/-6.677373781427094D08/,
      *                  Q3(8)/-2.722530175870899D03/
!                             COEFFICIENTS FOR MINIMAX
!                             APPROXIMATION TO LN(GAMMA(X)),
!                             12.0 .LE. X
      DATA               P4(1)/8.40596949829D-04/,
      1                  P4(2)/-5.9523334141881D-04/,
      2                  P4(3)/7.9365078409227D-04/,
      *                  P4(4)/-2.777777777769526D-03/,
      *                  P4(5)/8.333333333333333D-02/,
      *                  P4(6)/9.189385332046727D-01/,
      6                  P4(7)/-1.7816839846D-03/
```

I-9

```
      DATA                  XINF/.4494232D+308/
      DATA                  EPS/.2220446050D-15/
      DATA                  PI/3.141592653589793D0/
      DATA                  BIG1/1.28118D305/
!                                      FIRST EXECUTABLE STATEMENT
      IER = 0
      MFLAG = .FALSE.
      T = X
      IF (DABS(T).LT.BIG1) GO TO 5
      IER = 129
      DLGAMA = XINF
      GO TO 9000
    5 IF (T.GT.0.0D0) GO TO 20
      IF (T.LT.0.0D0) GO TO 10
      IER = 130
      DLGAMA = XINF
      GO TO 9000
!                                 ARGUMENT IS  NEGATIVE
   10 MFLAG = .TRUE.
      T = -T
      R = DINT(T)
      SIGN = 1.0D0
      IF (DMOD(T,2.0D0).EQ.0.0D0) SIGN = -1.0D0
      R = T-R
      IF (R.NE.0.0D0) GO TO 15
      IER = 130
      DLGAMA = XINF
      GO TO 9000
!                                 ARGUMENT IS  NOT A  NEGATIVE  INTEGER
   15 R = PI/DSIN(R*PI)*SIGN
      T = T+1.0D0
      R = DLOG(DABS(R))
!                                 EVALUATE  APPROXIMATION  FOR
!                                   LN(GAMMA(T)) , T .GT. 0.0
   20 IF (T.GT.12.0D0) GO TO 60
      IF (T.GT.4.0D0) GO TO 50
      IF (T.GE.1.5D0) GO TO 40
      IF (T.GE.0.5D0) GO TO 25
!                                   0.0 .LT. T .LT. 0.5
      B = -DLOG(T)
      A = T
      T = T+1.0D0
      IF (A.GE.EPS) GO TO 30
      DLGAMA = B
      GO TO 9005
!                                   0.5 .LE. T .LT. 1.5
   25 TOP = T-0.5D0
      B = 0.0D0
```

```fortran
      A = TOP−0.5D0
   30 TOP = P1(8)*T+P1(9)
      DEN = T+Q1(8)
      DO 35 J=1,7
          TOP = TOP*T+P1(J)
          DEN = DEN*T+Q1(J)
   35 CONTINUE
      Y = (TOP/DEN)*A+B
      IF (MFLAG) Y = R−Y
      DLGAMA = Y
      GO TO 9005
!                                        1.5 .LE. T .LE. 4.0
   40 B = T−1.0D0
      TOP = P2(8)*T+P2(9)
      DEN = T+Q2(8)
      A = B−1.0D0
      DO 45 J=1,7
          TOP = TOP*T+P2(J)
          DEN = DEN*T+Q2(J)
   45 CONTINUE
      Y = (TOP/DEN)*A
      IF (MFLAG) Y = R−Y
      DLGAMA = Y
      GO TO 9005
!                                        4.0 .LT. T .LE. 12.0
   50 TOP = P3(8)*T+P3(9)
      DEN = T+Q3(8)
      DO 55 J=1,7
          TOP = TOP*T+P3(J)
          DEN = DEN*T+Q3(J)
   55 CONTINUE
      Y = TOP/DEN
      IF (MFLAG) Y = R−Y
      DLGAMA = Y
      GO TO 9005
!                                        12.0 .LT. X .LT. BIG1
   60 TOP = DLOG(T)
      TOP = T*(TOP−1.0D0)−.5D0*TOP
      T = 1.0D0/T
      Y = TOP
      IF (T.LT.EPS) GO TO 70
      B = T*T
      A = P4(7)
      DO 65 J = 1,5
          A = A*B+P4(J)
   65 CONTINUE
      Y = A*T+P4(6)+TOP
   70 IF (MFLAG) Y = R−Y
```

```
      DLGAMA = Y
      GO TO 9005
9000  CONTINUE
      write (*,'("␣Error␣in␣DLGAMA")')
9005  RETURN
      END
```

Reference

[1] Parigger C G, Woods A C, Keszler A, Nemes L and Hornkohl J O 2012 *AIP Conf. Proc.* **1464** 628

Quantum Mechanics of the Diatomic Molecule (Second Edition)

Christian G Parigger and James O Hornkohl

Appendix J

Boltzmann equilibrium spectrum (BESP) and Nelder–Mead temperature (NMT) scripts

J.1 BESP.m

The script BESP.m is designed following the FORTRAN/Windows 7 version [1]. The individual diatomic molecular data files for selected transitions are concatenated to only show wave numbers, upper-term values, and line strengths; see table 15.5. Adjustments of input parameters for MATLAB [2] are rather straightforward, equally, for generalizing the script for automatic input by converting the script to a function. Individual lines are computed using Gaussian profiles [1]. For the generation of a spectrum, only one temperature is needed for equilibrium computation. Conversely, as one infers temperature from a measured spectrum, a modified Boltzmann plot [3] is constructed for the determination of the equilibrium temperature. A Gaussian line shape is selected to model the spectrometer/intensifier transfer function profile. However, one usually considers a natural linewidth for electronic state-to-state transitions, and a Gaussian line shape (equation (J.1)) for Doppler broadening [4], viz.

$$\Delta\lambda = 7.16 \times 10^{-7}\lambda \ \sqrt{\frac{T}{M}}, \tag{J.1}$$

leading to Voigt line shapes. Here, $\Delta\lambda$ is the full width at half maximum, λ the wavelength, T is the temperature, and M is the molecular weight. For example, with $\lambda = 306$ nm, T = 3.5 kK, and M = 17 (OH), $\Delta\lambda = 0.0031$ nm. The spectral resolution, $\delta\lambda$, for the OH emission spectra-fitting, discussed in this appendix, amounts to $\delta\lambda = 0.33$ nm. Consequently, a Gaussian line shape is considered instead of a Voigt line shape for fitting of the OH data in the appendix, but the communicated MATLAB scripts can be adjusted for Voigt profiles, which is important for cases when individual electronic state-to-state molecular transitions/resonances are investigated. Equally, when investigating individual transitions/

resonances, asymmetric molecular line shapes can be implemented in the scripts. There is usually a volley of lines for electronic transitions of a diatomic molecules, e.g. OH [6] in excess of 3kK, within a wavelength bin and for an experimental spectral resolution of the order of 0.33 nm.

The program BESP.m receives input from the LSFs that contain relative line strengths. The output is generated in graphical format, and the program is slightly adjusted for the generation of the spectra illustrated in figures 15.1–15.9. However, figure 15.6 is generated with the BESP.m script given below.

```
% BESP.m
%
% Calculates diatomic specta using line strength data files constructed for
    selected transitions.
% The program is designed using a previous FORTRAN/Windows7 implementation
    including private communications
% with James O. Hornkohl and David M Surmick.
%
% David M. Surmick, 04—27—2016; edited by Christian G. Parigger 11—27—2022.

% input paramters, output: WL_exp (N—1 x 1 array), I (intensity)
wl_min=300; wl_max=325; T=3530; FWHM=0.35; N=10001; norm=1; x='OH—lsf.txt';

% generate wavelengths/wavelength—bins for computation akin to an experiment
nSpec=N—1; delWL=(wl_max—wl_min)/(nSpec); WL_exp=linspace(wl_min,wl_max,nSpec)
    ; WL_exp=WL_exp';

% constants in MKS units (Boltzmann factor bfac in cgs units)
h=6.62606957e—34; c=2.99792458e8; kb=1.3806488e—23; bFac=(100*h*c)/kb; gFac=2*
    sqrt(log(2));

% read line strength file
[p]=load(x); WN=p(:,1); Tu=p(:,2); S=p(:,3);

% convert vacuum wavenumber to air wavelength: CGP 11—27—2022
%a0=2.72643e—4; a1=1.2288; a2=3.555e4; r=1+a0+(a1./(WN.*WN))+(a2./(WN.*WN.*WN
    .*WN));
k0=238.0185;k1=5792105;k2=57.362;k3=167917;r=(1+k1./(1d8*k0—(WN.*WN))+k3./(1d8
    *k2—(WN.*WN)));WL=1.e7./(r.*WN);

% get LSF table wavelengths that most closely match the wavelength—bins
A=find(WL>wl_min & WL<wl_max); WLk=WL(A);
```

```matlab
% get term values and line strengths at WLk in the range wl_min to wl_max
Sk=S(A); Tuk=Tu(A); TuMin=min(Tuk);

% calculate peak intensities and initialize peak_k calculation
peak=-4*log(WLk)+log(Sk)-(bFac/T)*(Tuk-TuMin); peak_k=zeros(nSpec,1); peakMax
    =-1;
for i=1:length(peak);
    if peak(i) > peakMax; peakMax=peak(i); end;
    if peak(i) ~= 0; peak_k(i)=peak(i)-peakMax; end;
end; peak_k=exp(peak_k);

% get wavelength-bin positions that most closely matches line strength table
    wavelengths
n0=zeros(length(WLk),1); for i=1:length(WLk); [~,n0(i)]=min(abs(WL_exp-WLk(i))
    ); end;

% calculate spectrum using Gaussian profiles for peaks, and for wavelength
    dependent FWHM
I=zeros(nSpec,1); FWHMk=(FWHM*WLk)/wl_max;
for i=1:length(WLk); deln=round(FWHM/delWL,0); nMin=n0(i)-deln;
    if nMin < 1; nMin=1; end; nMax=n0(i)+deln;
    if nMax > nSpec; nMax=nSpec; end;
    for j=nMin:nMax;  u=abs(gFac*(WL_exp(j)-WLk(i))/FWHMk(i));
        if u <=9.21;  I(j)=I(j)+peak_k(i)*exp(-u*u); end;
    end;
end; I=norm*I/max(I);

%Display graphical output
figure; plot(WL_exp,I,'LineWidth',1.5); set(gca,'FontWeight','bold','FontSize'
    ,20,'TickLength',[0.02, 0.02]);
LimitsX=xlim; LimitsY=ylim; title('   ','HorizontalAlignment','left','Position
    ', [LimitsX(1)-4, LimitsY(2)]);
xlabel('wavelength (nm)','FontSize',24,'FontWeight','bold');
ylabel('intensity (a.u.)','FontSize',24,'FontWeight','bold');
```

J.2 NMT.m

```
% NMT.m
%
% Fits measured diatomic specta using line strength data files constructed for
    selected transitions.
% The program is designed using a previous FORTRAN/Windows7 implementation
   including private communications
% with James O. Hornkohl and David M Surmick.
%
% inputs: WL_exp — exerimental wavelengths (n x 1 array)
%         Dat    — experimental spextrum (n x 1 array)
%         FWHM   — measured spectral resolution, seed for varried FWHM or
%                  fixed
%         T      — temperature seed for fitting
%         tol    — tolerance of Nelder—Mead fit
%         x      — name of line strength file for calculating theory spectra
%         FIT    — enter 1 for fitting linear offset and temperature
%                  enter 2 for fitting linear offset, temperature, and FWHM
%
% outputs: profile — matrix containing experimental wavelengths, measured
%                    spectrum, fitted spectrum, fitted baseline offset
%                    (n x 4 matrix)
%           vals   — array containing fitted paramters (3x1 or 4x1 array),
%                    temperature is always last entry
%
% sub—functions: FitSpec, FitSpec1, SynthSpec
%
% Example call: [I,v]=NMT(x,y1,0.15,3000,1e—8,'OH—LSF.txt',2);
%
% David M. Surmick, 04—28—2016, edited by Christian G Parigger 11—27—2022

function [profile,vals] = NMT (WL_exp,Dat,FWHM,T,tol,x,FIT)
tic % start code timer

% global variables
global bFac gFac WLk Tuk TuMin Sk n0 nSpec fwhm delWL temp wl_max;

% constants in MKS units (Boltzmann factor bfac in cgs units)
h=6.62606957e—34; c=2.99792458e8; kb=1.3806488e—23; bFac=(100*h*c)/kb; gFac=2*
    sqrt(log(2));

%load experimental data, here an OH spectrum 100 microsecond time delay in air
    breakdown.
xexp='OH100micros.dat';data=load(xexp);WL_exp=data(:,1);Dat=data(:,2);nSpec=
    length(Dat);

% input paramters
T=2000; FWHM=0.3; x='OH—LSF.txt'; temp=T; fwhm=FWHM; wl_min=min(WL_exp);
    wl_max=max(WL_exp); delWL=(wl_max—wl_min)/(nSpec);

% read rpovided LSF file
ZZ=readtable(x); WN=ZZ.Var1; Tu=ZZ.Var2; S=ZZ.Var3;

% convert vacuum wavenumber to air wavelength: CGP 11—27—2022
% a0=2.72643e—4; a1=1.2288; a2=3.555e4; r=1+a0+(a1./(WN.*WN))+(a2./(WN.*WN.*WN
```

```matlab
    .*WN));
k0=238.0185;k1=5792105;k2=57.362;k3=167917;WLoffset=0;r=(1+k1./(1e8*k0—(WN.*WN
    ))+k3./(1e8*k2—(WN.*WN)));
WLoffset=0;if(xexp=='OH100micros.dat'); WLoffset=—0.05;end;WL=1.e7./(r.*WN)+
    WLoffset;

% get LSF table wavelengths in experimental range
A=find(WL>wl_min & WL<wl_max); WLk=WL(A);

% get Term Values and LineStrengths at WLk
Sk=S(A); Tuk=Tu(A); TuMin=min(Tuk);

% get exerpimenal wavelength positions that most closely matches line strength
     table wavelengths
n0=zeros(length(WLk),1); for i=1:length(WLk);  [~,n0(i)]=min(abs(WL_exp—WLk(i)
    )); end;

% normalize data
%Dat=Dat/max(Dat);

% Fitting with Nelder—Mead parameters including two cases options
tol=1.e—6; FIT=2; options=optimset('TolX',tol,'MaxIter',1e8,'MaxFunEvals',1e8)
    ;
switch FIT
    case 1 % fit offset, temperature
        theta=ones(3,1);
        theta(3)=T; % temperature seed
        vals=fminsearch(@(x) FitSpec(x,WL_exp,Dat),theta,options);
        bkg=vals(1)+vals(2)*WL_exp; % calculate fitted offset
        [I,bkg1]=SynthSpec(WL_exp,vals(3),FWHM,Dat,bkg); % calculate fit
    case 2 % fit offset, fwhm, temperature
        theta=ones(4,1);
        theta(3)=FWHM; % fwhm seed
        theta(4)=T; % temperature seed
        vals=fminsearch(@(x) FitSpec1(x,WL_exp,Dat),theta,options);
        bkg=vals(1)+vals(2)*WL_exp; % calculate fitted offset
        [I,bkg1]=SynthSpec(WL_exp,vals(4),vals(3),Dat,bkg); % calculate fit
end

% Visualize Fit
fname=regexprep(x,'—LSF.txt','—fit:');
figure
switch FIT
    case 1
        plot(WL_exp,Dat,'o',WL_exp,I,WL_exp,bkg1,'LineWidth',1.5)
        legend('experiment','fit','base line')
        set(gca,'FontWeight','bold','FontSize',16,'TickLength',[0.02, 0.02]);
        val3=round(vals(3),3, 'significant')
```

```matlab
            title([num2str(fname),'T=',num2str(vals(3)),'K ,FWHM=',num2str(FWHM),'
                nm'])
            xlabel('wavelength (nm)')
            ylabel('intensity (a.u.)')
        case 2
            plot(WL_exp,Dat,'o',WL_exp,I,WL_exp,bkg1,'LineWidth',1.5)
            legend('experiment','fit','base line')
            set(gca,'FontWeight','bold','FontSize',20,'TickLength',[0.02, 0.02]);
            round(vals(4),3,'significant'); round(vals(3),2,'significant');
            val4=round(vals(4),3, 'significant'); val3=round(vals(3),2, '
                significant');
            title([num2str(fname),' T=',num2str(val4),' K, FWHM=',num2str(val3),'
                nm'])
            xlabel('wavelength (nm)','Fontsize',24,'FontWeight','bold')
            ylabel('intensity (a.u.)','Fontsize',24,'FontWeight','bold')
end


toc % end code timer


end % main function

% temperature, offset fit function
function [err] = FitSpec (p,WL_exp,Dat);
global fwhm;
bkg=p(1)+p(2)*WL_exp; [F,~]=SynthSpec(WL_exp,p(3),fwhm,Dat,bkg); c=F\Dat; z=F*
    c; err=norm(z-Dat);
end % fit spec


% temperature, fwhm, offset fit function
function [err] = FitSpec1 (p,WL_exp,Dat);
bkg=p(1)+p(2)*WL_exp; [F,~]=SynthSpec(WL_exp,p(4),p(3),Dat,bkg); c=F\Dat; z=F*
    c; err=norm(z-Dat);
end % fit spec 1


% calculate synthetic spectrum for fit
function [I1,bkg1] = SynthSpec (WL_exp,T,FWHM,Dat,bkg);
global bFac gFac WLk Tuk TuMin Sk n0 nSpec delWL wl_max;
FWHMk=(FWHM*WLk)/wl_max; % wavelength dependent FWHM


% Calculate Peak Intensities
peak=-4*log(WLk)+log(Sk)-(bFac/T)*(Tuk-TuMin); peak_k=exp(peak);


% calculate synthetic spectrum
I=zeros(nSpec,1); % initialize synthetic spectrum output
for i=1:length(WLk); deln=round(2.5*FWHMk(i)/delWL); nMin=n0(i)-deln;
    if nMin < 1; nMin=1; end;
    nMax=n0(i)+deln;
    if nMax > nSpec; nMax=nSpec; end;
```

```
    for j=nMin:nMax; u=abs(gFac*(WLk(i)—WL_exp(j))/FWHMk(i)); I(j)=I(j)+peak_k
        (i)*exp(—u*u); end;
end % synthetic spectrum loop

% normailze data to measured spectrum
I=I/max(I); I=I+bkg; sxy=sum(Dat.*I); syy=sum(I.*I); nf= sxy/syy; I1=I*nf;
    bkg1=bkg*nf;
end % SynthSpec
```

References

[1] Parigger C G, Woods A C, Surmick D M, Gautam G, Witte M J and Hornkohl J O 2015 *Spectrochim. Acta* B **107** 132

[2] *MATLAB Release R2022a Update 5* (MA: Natick)

[3] Parigger C G and Hornkohl J O 2020 *Quantum Mechanics of the Diatomic Molecule with Applications* (Bristol: IOP Publishing)

[4] Corney A 1977 *Atomic and Laser Spectroscopy* (Oxford: Clarendon)

[5] Parigger C G 2022 *Foundations* **2** 934

[6] Parigger C G 2023 *Foundations* **3** 1

Quantum Mechanics of the Diatomic Molecule (Second Edition)

Christian G Parigger and James O Hornkohl

Appendix K

Abel-inversion scripts

K.1 Abel-inversion programs

The Abel integral inversion algorithm utilizes function expansion techniques [1]. Chebyshev polynomials accomplish minimization of the maximum error [2]. The advantages of the expansion techniques include direct inversion of recorded, sensitivity corrected, and wavelength calibrated time-resolved data. A summary and detailed discussion of numerical inversion of the Abel integral is communicated in [3]. The published Matlab code [4, 5] is selected to accomplish analysis of spatially- (along the slit-height) and wavelength-resolved images. A typical adapted MATLAB [5] script, MixAnalysis.m, shows the implementation for analysis of CO_2: N_2 1:1 mixed gas. The Chebyshev expansion is computed using Expansion.m

The adaptation includes provision for correction of a slight asymmetry in the otherwise spherically symmetric expansion for specific time delays. The Matlab script CGPimage.m generates graphical output that is also included in this appendix. The MixAnalysis.m script includes lines for preparation of the plotting routines that have been available. However, the CGPimage.m script applies simple MATLAB display methods.

K.1.1 MixAnalysis.m

```matlab
function [ f_rec , X ] = abel_inversion(h,R,upf,plot_results,lsq_solve)
upfin=15;%8;%was 12 initially; nspectra=256; nwavel=1001;
midpoint=138;%8_8mix%145;%128;%139;%87;
npoints=80;%8_8_mix%73;%60; ninvertedspectra=2*npoints—1;
dr=1024./nspectra*13.6/1000.; %0.0544=4*0.0136
R=npoints*dr;                          % radius
X=(0:dr:R—dr)';          % spatial coordinates
ndim=length(X);
nsymmetric=1; %=1 for symmetric, =0 for asymmetric
nfilestart=1;%8_8mix%16;
nfileend=21;%8_8mix%21;
nlambda(1)=385;%660; nlambda(2)=490; nlambda(3)=438; nlambda(4)=414;
for i=1:1
nlam=nlambda(i)
for nfile=nfilestart:nfileend%:13
fnamein=sprintf('%02dabelc%03d.dat',nfile,nlam);

if nsymmetric == 1
    fnameout=sprintf('%02dabelc%03d_symmetric.dat',nfile,nlam);
    fnameout3D=sprintf('%02dabelc%03d_symmetric3D.dat',nfile,nlam);
else
    fnameout=sprintf('%02dabelc%03d_asymmetric.dat',nfile,nlam);
    fnameout3D=sprintf('%02dabelc%03d_asymmetric3D.dat',nfile,nlam);
end
fileID=fopen(fnamein,'r');%'08abelc.dat','r');
tline=fgetl(fileID); formatSpec='%f %f %f'; sizeDor=[3 Inf];
D=fscanf(fileID,formatSpec,sizeDor);
fclose(fileID);
D=D'; L=D(:,[1]); Warr=L(1:nwavel);%L(1:1001); H=D(:,[2]); Val =D(:,[3]);
for j=1:nspectra %256
    for i=1:nwavel %1001
        Arr(i,j)=Val(i+1001*(j—1));
    end
end
Arr=Arr';

yarr=zeros(length(X),1); garrR=zeros(length(X),1); garrL=zeros(length(X),1);
f_rec_l=zeros(length(X),1); f_rec_r=zeros(length(X),1);

%jwave=86;
for jwave=1:1001

    for k=1:ndim
        yarr0(k,1)=1./2.*(Arr(k—1+midpoint,jwave)+Arr(midpoint—k+1,jwave));
        if (yarr0(k,1) < 0.0001)
            yarr0(k,1)=0.0001;
        end
        garrR(k,1)=Arr(k—1+midpoint,jwave);%/yarr0(k,1);
        garrL(k,1)=Arr(midpoint—k+1,jwave);%/yarr0(k,1);
    end
garrL=garrL.\yarr0;
garrR=garrR.\yarr0;
for c=1:length(X)
 h(c,1)=yarr0(c,1);%Arr(c+66,jwave);
```

```matlab
end
%
if ~exist('h', 'var') || isempty(h)
    [X,h,R]=generate_test_data;
    plot_results=1;
else
    plot_results=0;
    X=linspace(0,R—0.1,length(h))';
end

% default value for number of expansion elements
if ~exist('upf', 'var'); upf=upfin; end;

% avoiding problems if flags are not given in input
if ~exist('plot_results', 'var'); plot_results=0; end;
if ~exist('lsq_solve', 'var'); lsq_solve=0; end;

%% calculate series expansions fn and corresponding integrals hn

[fn,hn] = compute_expansion( X,upf,R );

%% solve equation system A*L=B for the amplitudes A
if lsq_solve ~= 1

    B = zeros(1,upf+1); L = zeros(upf+1,upf+1);   %create arrays

    for k=1:upf+1

        for l=1:upf+1
            L(l,k)=2.*sum(hn(:,k).*hn(:,l));
        end

        B(k)=sum(h(:).*hn(:,k));
    end

    A=B/L;

else

    x0=1*ones(upf+1,1);       % guess some initial values for optimisation
    A=solve_lsq(h,hn,x0);     % solve for amplitudes A
end

%% final stage: calculate the resulting distribution profile

% create vector for resulting reconstructed distribution
f_rec=zeros(length(h),1);
```

```matlab
% special case for n=0 (where f_0(r) = 1)
f_rec = f_rec + A(1)*1;

% iterate eq. (1) for n=1:upf
for c=1:upf+1
    f_rec = f_rec + A(c).*fn(:,c);
end

for c=1:ndim
    f_rec_r(c,1)=f_rec(c,1)*garrR(c,1);
    f_rec_l(ndim-c+1,1)=f_rec(c,1)*garrL(c,1);
end

for c=1:ndim
     f_rec_all(c,1)=f_rec_l(c,1);
     h_all(c,1)=h(ndim-c+1,1);
     x_all(c,1)=-X(ndim-c+1);
     f_rec_all(ndim+c-1,1)=f_rec_r(c,1);
     h_all(ndim+c-1,1)=h(c,1);
     x_all(ndim+c-1,1)=X(c,1);
     g_all(ndim+c-1,1)=garrR(c,1);
     g_all(c,1)=garrL(ndim-c+1,1);
     inp_all(ndim-c+1,1)=garrR(c,1)*yarr0(c,1);
     inp_all(ndim+c-1,1)=garrL(c,1)*yarr0(c,1);
     f_rec_sym(ndim+c-1,1)=f_rec(c,1);
     f_rec_sym(ndim-c+1,1)=f_rec(c,1);
end

%jwave loop
fileID=fopen(fnameout,'a');%'08abelc_symmetric.dat','a');
if nsymmetric == 1
    fprintf(fileID,'%f %f ',Warr(jwave),f_rec_sym);
else
    fprintf(fileID,'%f %f ',Warr(jwave),f_rec_all);
end
fprintf(fileID,'\n');
fclose(fileID);

if plot_results==1
    figure; % normalized profiles for better comparison
    set(gca,'linewidth',1.5,'fontsize',16);
    plot(x_all,f_rec_all,'g','Linewidth',1.5);
    hold on; plot(x_all,inp_all,'r','Linewidth',1.5);
    grid on; box on;
    title(sprintf('number of cos-expansions: %i',upf))
    legend('Abel reconstructed profile','measured profile','Location','South')

    figure; % normalized profiles for better comparison
```

```matlab
        set(gca,'linewidth',1.5,'fontsize',16);
        plot(x_all,f_rec_sym,'g','Linewidth',1.5);
        hold on; plot(x_all,h_all,'k','Linewidth',1.5);
        grid on; box on;
        title(sprintf('wavelength position: %i',jwave))
        legend('Abel reconstructed profile','symmetrized profile','Location','
            South')

    end

end
%prepare for 3D plot of Abel—inverted data
fileID=fopen(fnameout,'r'); formats='%f';
jspectra=(ndim—1)*2+1; sizeResult=[jspectra+1 nwavel];
Result=fscanf(fileID,formats,sizeResult);
fclose(fileID)
Result=Result';
fileID3D=fopen(fnameout3D,'a')
fprintf(fileID3D,'Zone f=point i=%d j=%d\n',nwavel,jspectra);
        for jdummy=2:jspectra+1
          wave=Result(:,[1]);
          waveout=wave(1:nwavel);
          waveout=waveout';
          spectrum=Result(:,[jdummy]);
          spectrumout=spectrum(1:nwavel);
          spectrumout=spectrumout';
          for iout=1:nwavel
              x=waveout(iout);
              y=(jdummy—(ndim+1))*dr;
              z=spectrumout(iout);
              fprintf(fileID3D,'%f %f %f \n',x,y,z);
              %fprintf(fileID3D,'\n');
          end
        end
fclose(fileID3D);
end
end
```

K.1.2 Expansion.m

```matlab
function [ fn,hn ] = compute_expansion( X,upf,R )
% COMPUTE_EXPANSION calculates the Fourier series expansion terms, on which
% the Abel inversion algorithm [1] is based.
%
% Details: The unknown distribution f(r) is expanded as
%           f(r) = sum_{n=lof}^{upf} (A_n * f_n(r))               (1)
% where the lower frequency is set to 1 and the upper frequency upf is
% important for noise—filtering. f_n(r) is a set of cos—functions:
%           f_n(r) = 1 — (—1)^n*cos(n*pi*r/R)  and f_0(r) = 1      (2)
% For the Abel inversion, the integrals h_n have to be calculated
%           h_n(x) = int_x^R f_n(r) * r / sqrt(r^2—x^2) dr          (3)
%
%   [1] G. Pretzler, Z. Naturforsch. 46a, 639 (1991)
%
%                                      written by C. Killer, Sept. 2013


% allocate matrices for f_n and h_n — rows are x—values,
% columns are the number of expansion elements (n+1 since we start with n=0)
fn=zeros(length(X),upf+1);
hn=zeros(length(X),upf+1);


% special case: first column for n=0, where f_0(r)=1;
fn(:,1)=1;
for c=1:length(X);
    x=X(c);

    % evaluation of (3)
    fun=@(r) r./sqrt(r.^2—x.^2);
    hn(c,1) = integral(fun,x,R);
end


% all the other columns
for n=1:upf
    for c=1:length(X)
        x=X(c);

        % evaluation of (2)
        fn(c,n+1) = (1 — (—1)^n*cos(n*pi*x/R));

        % evaluation of (3)
        fun=@(r) (1 — (—1)^n*cos(n*pi*r/R)).*r./sqrt(r.^2—x.^2);
        hn(c,n+1) = integral(fun,x,R);
    end
end

% remove the next comment to plot the integrals
% figure; plot(hn); title('cos—expansion integrals h_n(x)')
```

K.2 Display of wavelength calibrated and sensitivity corrected data

```
clear
pixelsize=0.0136; numberofspectra=256; initialdelay=200; delaystep=250;
    ngatestep=125;
for nfile=01:06
  fnamein=sprintf('%02dabelc385.dat',nfile);
  fileID=fopen(fnamein,'r');
  tline=fgetl(fileID); narrsize = sscanf(tline, 'Zone I=%d J= %d');
  narrlambda = narrsize(1); narrspectr = narrsize(2);
  nwavel=narrlambda; nspectra=narrspectr;
  formatSpec='%f %f %f'; sizeD=[3 Inf]; D=fscanf(fileID,formatSpec,sizeD);
  fclose(fileID);
  D=D';L=D(:,[1]);Warr=L(1:nwavel);%L(1:1001);H=D(:,[2]);
    for ii=1:numberofspectra
      Harr(ii)=ii*pixelsize*4.;
    end
  Val =D(:,[3]);
  for j=1:nspectra %256
    for i=1:nwavel %1001
      Arr(i,j)=Val(i+nwavel*(j—1));
    end
  end
  figure
  xdummylow=Warr(1); ximage=linspace(xdummylow,xdummyhig,nwavel);
  ydummy=(nspectra—1)*pixelsize*4;
  nlow=61; nhig=211; ylow=nlow/nspectra*ydummy; yhig=nhig/nspectra*ydummy;
  yimage=linspace(ylow,yhig,nspectra);
  clims=[0 500000];
  imagesc(ximage,yimage,Arr(1:nwavel,nlow:nhig)');%,clims);%, clims);
  colormap jet;
  axis([380 390 ylow yhig]);
  set(gca,'YDir','normal');
  set(gca,'TickDir','out');
  set(gca,'Fontsize',15,'Fontweight','bold');
  xlabel ('wavelength (nm)', 'Fontsize',20, 'Fontweight', 'bold');
  ylabel ('slit height (mm)', 'Fontsize',20,'Fontweight', 'bold');
  nfiledelay=initialdelay+(nfile—1)*delaystep;
  fname=sprintf('Filter #%d: %d ns delay, %d ns gate.',nfile,nfiledelay,
      ngatestep);
  title (fname, 'Fontsize',22,'Fontweight','bold');
end
```

Figure K.1 displays typical wavelength calibrated and detector sensitivity corrected data. The images illustrate the spectra recorded along the slit-direction.
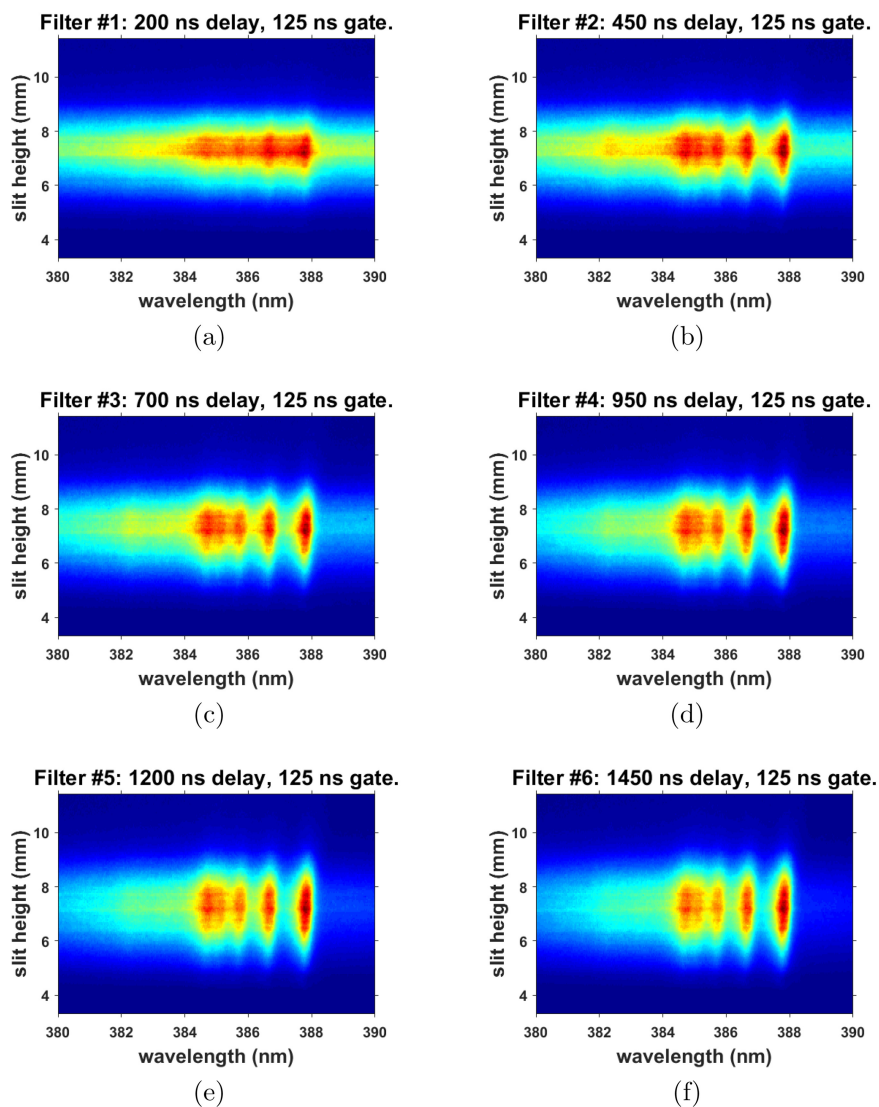
Filter #1: 200 ns delay, 125 ns gate.

(a)

Filter #2: 450 ns delay, 125 ns gate.

(b)

Filter #3: 700 ns delay, 125 ns gate.

(c)

Filter #4: 950 ns delay, 125 ns gate.

(d)

Filter #5: 1200 ns delay, 125 ns gate.

(e)

Filter #6: 1450 ns delay, 125 ns gate.

(f)

Figure K.1. Typical captured, wavelength calibrated, and sensitivity corrected CN spectra—1:1 molar CO_2:N_2 gaseous mixture held at atmospheric pressure and recorded with a CN spectra cut-on filter. Time delay: (a) 200 ns; (b) 450 ns; (c) 700 ns; (d) 950 ns; (e) 1200 ns; and (f) 1450 ns. Reprinted with permission from [6].

K.3 Display of Abel inverted data

```
clear;
pixelsize=0.0136; numberofspectra=256; initialdelay=200; delaystep=250;
    ngatestep=125;

for nfile=01:06
fnamein=sprintf('%02dabelc385_symmetric3D.dat',nfile);
  fileID=fopen(fnamein,'r');
    tline=fgetl(fileID); narrsize = sscanf(tline, 'Zone f=point i=%d j=%d');
    narrlambda = narrsize(1); narrspectr = narrsize(2);
    nwavel=narrlambda; nspectra=narrspectr;
    formatSpec='%f %f %f'; sizeD=[3 Inf]; D=fscanf(fileID,formatSpec,sizeD);
  fclose(fileID);
  D=D';L=D(:,[1]);Warr=L(1:nwavel);%L(1:1001); H=D(:,[2]);
  for ii=1:numberofspectra
    Harr(ii)=ii*pixelsize*4.;
  end
  Val =D(:,[3]);
    for j=1:nspectra %256
      for i=1:nwavel %1001
        Arr(i,j)=Val(i+nwavel*(j—1));
      end
    end
  figure
    xdummylow=Warr(1);%370.3000;xdummyhig=Warr(nwavel);%393.3547;
    ximage=linspace(xdummylow,xdummyhig,nwavel);
    ydummy=(nspectra—1)/2*pixelsize*4;%0.0544;%/2*0.0544/2;
    yimage=linspace(—ydummy,ydummy,nspectra);
    clims=[0, 250000];
    imagesc(ximage,yimage,Arr');%,clims); colormap jet;
    axis([380 390 —ydummy*0.8 ydummy*0.8]);
    set(gca,'YDir','normal');
    set(gca,'TickDir','out');
    set(gca,'Fontsize',15,'Fontweight','bold');
    xlabel ('wavelength (nm)', 'Fontsize',20, 'Fontweight', 'bold');
    ylabel ('radius (mm)', 'Fontsize',20,'Fontweight', 'bold');
    nfiledelay=initialdelay+(nfile—1)*delaystep;
    fname=sprintf('filter #%d: %d ns delay, %d ns gate.',nfile,nfiledelay,
        ngatestep);
    title (fname, 'Fontsize',22,'Fontweight','bold');
end
```

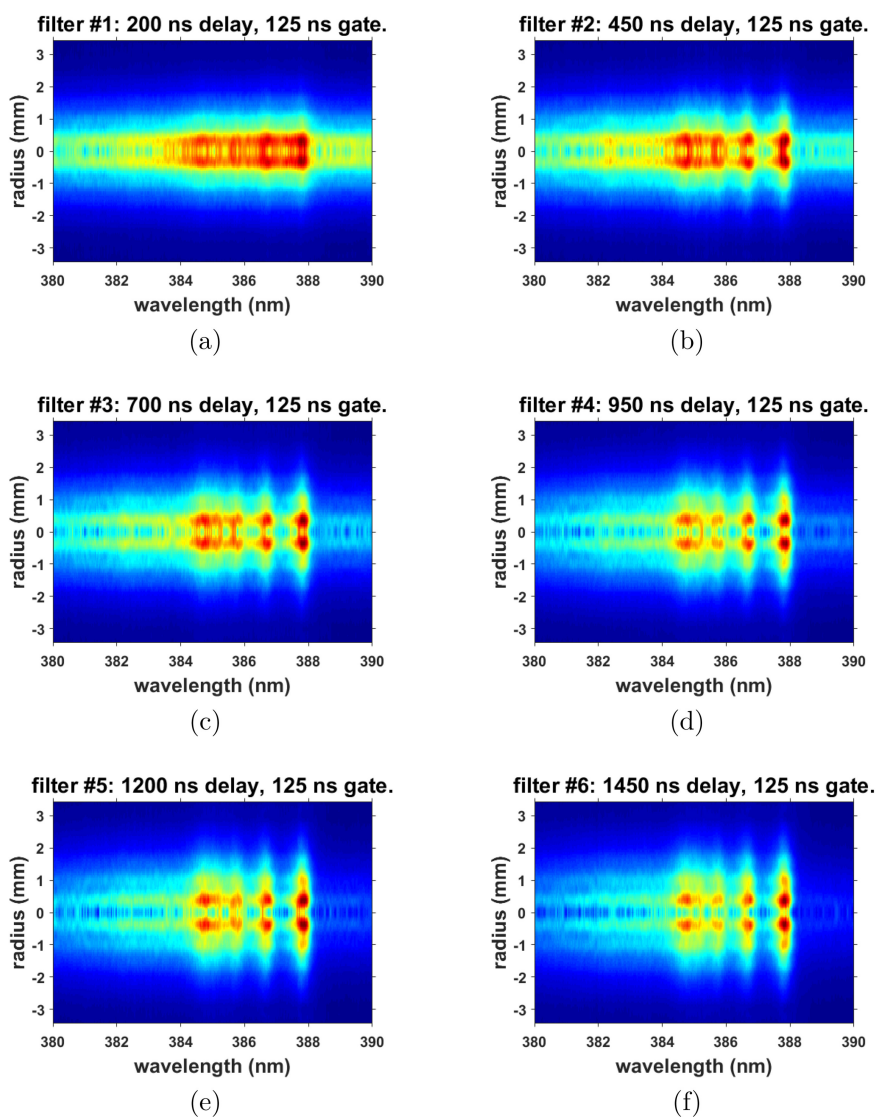Figure K.2 displays typical output of the Abel inverted data.

Figure K.2. Typical Abel inverted CN spectra—1:1 molar CO_2:N_2 gaseous mixture held at atmospheric pressure and recorded with a CN spectra cut-on filter. Time delay: (a) 200 ns; (b) 450 ns; (c) 700 ns; (d) 950 ns; (e) 1200 ns; and (f) 1450 ns. Reprinted with permission from [6].

References

[1] Pretzler G and Naturforsch Z 1991 *Z. Naturforsch* **46a** 639

[2] Arfken G B, Weber H J and Harris F E 2012 *Mathematical Methods for Physicists, A Comprehensive Guide* 7th edn (New York: Academic)

[3] Pretzler G, Jäger H, Neger T, Philipp H and Woisetschläger J 1992 *Z. Naturforsch.* A **47** 955

[4] Killer C 2014 http://www.mathworks.com/matlabcentral/fileexchange/43639-abel-inversion-algorithm.

[5] *MATLAB Release R2022a Update 5* (MA: Natick)

[6] Helstern C M 2020 Laser-induced breakdown spectroscopy and plasmas containing cyanide *PhD Dissertation* (University of Tennessee)

Quantum Mechanics of the Diatomic Molecule (Second Edition)

Christian G Parigger and James O Hornkohl

Appendix L

LIBS: 2018 to 2023 publications that include C.G.P.

L.1 Introduction

The physics activities and works by the author C.G.P. led to his inclusion in the most recent 2023 Stanford University career list of the World's Top 2% Scientists [1]. This communication summarizes research on the subject of laser-induced transient micro-plasma diagnoses and selected publications during the years 2018 to 2023. Time-resolved spectroscopy elucidates plasma dynamics and species distributions that are generally of value in analytical chemistry. The contents of the summarized work include aspects of electron density, and atomic and molecular distributions. Applications extend from analyses of laboratory to stellar plasma. Of particular interest is the spectroscopy of the hydrogen Balmer series and several diatomic molecules. In most of the publications, nominal nanosecond radiation from table-top laser devices is employed for the generation of the micro-plasma, and spatio-temporal experimental methods capture phenomena that occur at well-above hypersonic, supersonic, and subsonic plasma and gas expansion speeds.

This research-summary addresses recent 2018 to 2023 investigations [2] that were primarily conducted at the Center for Laser Applications at The University of Tennessee Space Institute. However, a few selected publications with international collaborators are also included. The author, Dr Christian Parigger, has been engaged in laser-plasma research at the University of Tennessee from 1987 to 2023. Recent publications in Multidisciplinary Digital Publishing Institute (MDPI) journals Atoms, Molecules, Foundations, and Symmetry encompass various research aspects. The 21 MDPI articles referenced in this summary reflect scientific, open-access, and peer-reviewed engagements. Various conference contributions, including in the *Journal of Physics: Conference Series*, further portray recent research associated with the biannual and well-established International Conferences on Spectral Line Shapes (ICSLS). The transition from previous archived journals such as Applied Optics, Optics Letters, Spectrochimica Acta

Part A and/or Part B, and Journal of Quantitative Spectroscopy and Radiative Transfer to peer-reviewed open-access journals is in accord with worldwide transition to open-access viz. access-for-everyone. In addition, the moderated Cornell University https://arxiv.org and MDPI https://www.preprints.org preprint servers also convey aspects of research. And, of course, the Auburn University electronic International Review of Atomic and Molecular Physics (IRAMP) journal https://www.auburn.edu/cosam/departments/phyiscs/iramp/index.htm communicates peer-reviewed research activities.

L.2 Summary

L.2.1 Laser-plasma atomic and molecular spectroscopy

Hydrogen and selected diatomic emission spectroscopy includes analysis of laboratory and stellar astrophysical plasma, e.g., from white dwarfs [3–8]. These works include self-absorption assessments. Expansion dynamics at hypersonic, supersonic, and subsonic are usually measured with spatio-temporal spectroscopy [9–17]. Fundamental aspects of diatomic molecular spectroscopy [18] lead to consistent data analyses without invoking the concept of reversed angular momentum—the Nelder–Mead temperature (NMT) program and the Boltzmann equilibrium spectra program (BESP) are freely available [19] as clear-text scripts with data files. Plasma diagnosis is elaborated with selected diatomic molecules, including comparisons of the published database with other readily available databases for OH, CN, C_2, and AlO [19–25]. In addition, the collaboration with the University of Prayagraj (formerly Allahabad), India, on meteorite and gypsum laser-induced breakdown spectroscopy (LIBS) [26, 27] and on medical applications that include gallstone and pointed gourd leaves analyses has been elaborated [28, 29]. Collaborations with the University of Cairo include research on plasma involving silver nano-particles [30–32]. Recent collaborations with the Chemical Research Center in Hungary focus on microwave plasma methylidyne (CH) cavity ring-down spectroscopy [33].

L.2.2 Molecular spectroscopy chapter and e-book

The two fundamental works in 2020 are a book chapter [34] on molecular LIBS and an e-book on diatomic spectroscopy [35]. The former communicates molecular spectroscopy and applications to plasma, combustion, and astrophysics analyses. Primary interests include plasma in gases; however, the book chapter [34] includes laser ablation, including the coauthors' work on laser-ablation molecular isotopic spectrometry (LAMIS). Diatomic molecules include cyanide (CN), aluminum monoxide (AlO), titanium monoxide (TiO), Swan bands of C_2, and the hydroxyl radical (OH). Aspects of spherical aberrations from focusing with a single lens are elaborated, and Abel inversion techniques are discussed for determination of spatial molecular distribution. The latter derives diatomic spectroscopy transition strengths [35] employing the Wigner–Witmer diatomic eigenfunction. The diatomic line strength is composed of electronic, vibrational, and rotational transition terms, including Franck–Condon, Hönl–London and r-centroid factors.

L.3 Discussion

Both atomic and molecular species can be readily discerned from comparisons of measured and computed atomic line shapes and molecular band appearances. Several of the investigations elucidate experimental spatially- and temporally-resolved LIBS records' analysis details. The molecular emission spectroscopy comparisons require accurate databases. The established and well-tested databases for selected electronic, vibrational, and rotational diatomic transitions and the associated analysis programs are now published for applications in LIBS research [19]. The 2018 to 2023 summary shows a research focus in 2022 to 2023 on molecular diagnosis by comparing accurate line strengths predictions [19–23] with those from readily available other corresponding databases [36, 37], including ExoMol [37]. Future applications are envisioned to include laser-induced hydrogen-based combustion—analysis of hydrogen emission lines and OH molecular bands are expected to benefit from the research publications communicated in this summary.

References

[1] Ioannidis J P A 2023 *October 2023 data-update for: Updated science-wide author databases of standardized citation indicators,* Elsevier Data Repository, Electronic data https://ecebm.com/2023/10/04/stanford-university-names-worlds-top-2-scientists-2023/

[2] Parigger C G 2023 *Int. Rev. At. Mol. Phys.* **14** 89

[3] Parigger C G, Drake K A, Helstern C M and Gautam G 2018 *Atoms* **6** 36

[4] Parigger C G 2020 *Contrib. Astronom. Observat. Skalnaté Pleso* **50** 1

[5] Parigger C G, Helstern C M, Gautam G and Drake D A 2019 *J. Phys.: Conf. Ser.* **1289** 012001

[6] Parigger C G, Helstern C M and Gautam G 2019 *Atoms* **7** 63

[7] Surmick D M and Parigger C G 2019 *Atoms* **7** 101

[8] Parigger C G, Sherbini A M E L and Splinter R 2019 *J. Phys.: Conf. Ser.* **1253** 012001

[9] Gautam G and Parigger C G 2018 *Atoms* **6** 46

[10] Parigger C G 2019 *Atoms* **7** 61

[11] Parigger C G, Helstern C M and Gautam G 2020 *Symmetry* **12** 2116

[12] Parigger C G, Helstern C M and Gautam G 2019 *Atoms* **7** 74

[13] Helstern C M and Parigger C G 2019 *J. Phys.: Conf. Ser.* **1289** 012016

[14] Parigger C G and Helstern C M 2023 *J. Phys.: Conf. Ser.* **2439** 012003

[15] Surmick D M, Dagel D J and Parigger C G 2019 *Atoms* **7** 86

[16] Parigger C G, Helstern C M, Jordan B S, Surmick D M and Splinter R 2020 *Molecules* **25** 615

[17] Parigger C G 2020 *Spectrochim. Acta* B **179** 106122

[18] Parigger C G 2021 *Foundations* **1** 208

[19] Parigger C G 2023 *Foundations* **3** 1

[20] Parigger C G 2022 *Foundations* **2** 934

[21] Parigger C G 2023 *Atoms* **11** 62

[22] Parigger C G 2023 *Preprints* **2023** 2023050423

[23] Parigger C G 2023 *Preprints* **2023** 2023041258

[24] Parigger C G, Helstern C M, Jordan B S, Surmick D M and Splinter R 2020 *Molecules* **25** 988

[25] Parigger C G and Helstern C M 2023 *J. Phys.: Conf. Ser.* **2439** 012004

[26] Rai A K, Pati J K, Parigger C G, Dubey S, Rai A K, Bhagabaty B, Mazumdar A C and Duorah K 2020 *Molecules* **25** 984

[27] Rai A K, Pati J K, Parigger C G and Rai A K 2019 *Atoms* **7** 72

[28] Pathak A K, Rai N K, Kumar R, Rai P K, Rai A K and Parigger C G 2018 *Atoms* **6** 42

[29] Kumar T, Rai P K, Rai A K, Rai N K, Rai A K, Parigger C G, Watal G and Yadav S 2022 *Foundations* **2** 981

[30] Sherbini A M E L, Sherbini A E E L and Parigger C G 2018 *Atoms* **6** 44

[31] Sherbini1 A M E L, Sherbini A E E L, Parigger C G and Sherbini T M E L 2019 *J. Phys.: Conf. Ser.* **1289** 012002

[32] Sherbini A M E L, Farash A H E L, Sherbini T M E L and Parigger C G 2019 *Atoms* **7** 73

[33] Nemes L and Parigger C G 2023 *Foundations* **3** 16

[34] Parigger C G, Surmick D M, Helstern C M, Gautam G, Bol'shakov A A and Russo R 2020 Molecular laser-induced breakdown spectroscopy *Laser Induced Breakdown Spectroscopy* ed J P Singh and S N Thakur 2nd edn (New York: Elsevier)

[35] Parigger C G and Hornkohl J O 2020 *Quantum Mechanics of the Diatomic Molecule with Applications* (Bristol: IOP Publishing)

[36] McKemmish L K 2021 *WIREs Comput. Mol. Sci.* **11** e1520

[37] Tennyson J *et al* 2020 *J. Quant. Spectrosc. Radiat. Transf.* **255** 107228